PREPARATION OF ACTIVATED CARBON FROM BIOMASS AND ITS APPLICATION IN GAS ADSORPTION

A Thesis submitted by

Shan Liu

For the award of

Doctor of Philosophy

Faculty of Health, Engineering and Sciences

University of Southern Queensland

Toowoomba, QLD 4350, Australia

2017

Abstract

Biomass is an abundantly available and sustainable resource, which is widely utilized as precursor for producing activated carbons.

In this thesis, hemp hurd and retted hemp hurd, the by-products of hemp fibre industry, were used as precursors for the preparation of activated carbon by chemical activation with $ZnCl_2$ and physical activation with CO_2. Then, activated carbons were prepared from bamboo fibre and hemp fibre in the similar conditions for comparison. The influence of the carbonization temperature and the impregnation ratio was studied on morphology, porosity, chemical property, and activation mechanism of the activated carbons. The gas capture performance of the synthesized activated carbons was evaluated in CO_2 adsorption.

Key findings include an understanding of the structure, morphology, and characteristics of hemp hurd and retted hemp hurd, and the influence of retting process on the obtained activated carbons. In addition, a systematic comparison of the effect of $ZnCl_2$ chemical activation and CO_2 physical activation on the properties of activated carbons, and a comprehensive review of the activated carbons derived from hemp hurd, retted hemp hurd, bamboo fibre, and hemp fibre was realised. The effect of carbonization temperature and the impregnation ratio, and the influence of precursor on activated carbon properties was also analysed.

Experimental results showed that hemp hurd possesses a unique structure, which consists of two types of macropore channels of different sizes. Activated carbons from hemp hurd after HCl washing retains the original appearance of the hemp hurd with increased porosity of the inner walls. $ZnCl_2$ activation was deemed

advantageous for synthesis of high surface area of porous carbon from biomass, and the derived activated carbons using this method exhibited larger surface areas compared with those using the CO_2 activation. The pore development was strongly dependent on the impregnation ratio of activation reagent and the subsequent carbonization temperature. HCl washing further increased the porosity of activated carbon. Activated carbons from retted hemp hurd and bamboo fibre were highly microporous materials. Activated carbons from hemp fibre possessed mixtures of micropores and mesopores. The optimized Brunauer-Emmett-Teller (BET) specific surface area of the activated carbon from retted hemp hurd reached 1781 m^2/g and total pore volume reached 1.023 cm^3/g. Activated carbon from retted hemp hurd by $ZnCl_2$ activation showed the highest CO_2 adsorption capacity of 142 cm^3/g STP at 273 K.

This thesis contributes to the field of biomass-based activated carbon production and application in gas adsorption. This investigation reinforces the understanding of activation mechanisms as well, and the potential of obtained activated carbons and the future work are discussed.

Certification of Thesis

This Thesis is entirely the work of (Student name) Shan Liu except where otherwise acknowledged. The work is original and has not previously been submitted for any other award, except where acknowledged.

Principal Supervisor: Prof Hao Wang

Associate Supervisor: Dr Venkata Sankaranand Chevali

Student and supervisors signatures of endorsement are held at the University.

Acknowledgements

I would firstly like to acknowledge and thank my supervisor Prof. Hao Wang for his constant, valuable support. He taught me the value of hard work. Without him, I may never have gotten to where I am today. I would like to thank Dr. Venkata S. Chevali and Dr. Lei Ge for their contribution and support towards my research. I would also like to thank Prof. John Zhu for introducing me to gas adsorption application and Prof. Zhengping Fang for encouraging me to enrol in this Ph.D. program.

I would like to acknowledge the financial support received from the University of Southern Queensland for conducting the background work for this research. The support of the School of Chemical Engineering of The University of Queensland is also highly appreciated. I would like to thank Phil Warner, managing director of Ecofibre Industries Operations Pty Ltd, Australia who kindly provided the raw biomass materials for this research. I would also like to thank my colleagues at the Centre for Future Materials for their moral, technical, and financial support. I also would like to thank all the people who create a research-conductive atmosphere in the lab oratories.

I would also like to thank my family for their unending love and support, without which I could not have managed to complete my thesis. I would like to thank my husband, Yunbo Song, for waiting up many late nights for my arrival after working late on my thesis and for helping to cheer me up and encourage me to continue with the research.

Table of Contents

List of Figures

List of Tables

CHAPTER 1 INTRODUCTION

1.1 Background

Carbon materials have been used since prehistoric times, dating back to the ancient Egyptians who used chars to purify water (Azargohar & Dalai, 2009), and even today, the worldwide demand of activated carbon is steadily increasing. Activated carbon removes non-carbon impurities and the oxidation on the carbon surface. The main feature common to all activated carbon is a basic structure similar to graphite. Activated carbon by definition is an amorphous solid with a large internal surface area and pore volume (Jodeh, Abdelwahab, Jaradat, Warad, & Jodeh, 2016). Activated carbon is a reproducible adsorbent, a carbon-containing substance with highly developed porosity, large specific surface area, good adsorption capacity, thermal stability, and high surface reactivity (Babel & Kurniawan, 2003). These unique characteristics make activated carbon very versatile materials, which have been studied as adsorbents, catalysts and catalyst supports for different purposes (Angın, Köse, & Selengil, 2013; De, Azargohar, Dalai, & Shewchuk, 2013; Dias, Alvim-Ferraz, Almeida, Rivera-Utrilla, & Sánchez-Polo, 2007).

Activated carbons can be prepared from a variety of precursors with high carbon content and low levels of inorganic compounds by physical and/or chemical activation methods. The physicochemical properties of activated carbon by chemical activation are strongly dependent upon the nature of precursor and pyrolysis conditions (e.g., carbonization temperatures and $ZnCl_2$ impregnation rate). It is possible to obtain activated carbon with different pore textures by varying the activation conditions, therefore optimizing their production for a specific purpose (Dias et al., 2007).

Activated carbon is relatively expensive and its cost depends on the precursor, activation method, and process conditions (Angın, Altintig, & Köse, 2013; Downie, Munroe, Cowie, Van Zwieten, & Lau, 2012; Erdem, Orhan, Şahin, & Aydın, 2016; Rodríguez-Reinoso, Molina-Sabio, & González, 1994; Uçar, Erdem, Tay, & Karagöz, 2008). However, the commercially activated carbons are very expensive, and their cost limits their usage.

To reduce the cost of the activated carbon, biomass as precursor is receiving increased attention (Erdem et al., 2016). Agricultural biomass is abundant and renewable, with high lignocellulosic content, hence promising as precursors for low-cost activated carbons (Dias et al., 2007; Erdem et al., 2016). Moreover, biomass-derived activated carbons possess a high surface area, a complex pore structure, hydrophobic graphene layers, enriched heteroatoms, and various oxygen-containing functional groups in the carbon network particularly accessed by chemical activation, rendering advanced applications in environmental protection, energy conversion and storage devices, and biosensing (Madhu et al., 2016). Recycling the bio-waste natural fibre to produce useful end products like activated carbon would clearly be an appropriate solution, and of potential benefit to the industry (Dias et al., 2007).

Lignocellulosic biomass is commonly used as the precursor of activated carbon because of two important characteristics, (1) low inorganic materials content, and (2) relatively high volatile content. The former characteristic results in producing activated carbon with low ash content and the latter characteristic helps to control the production process (Uçar et al., 2008). The bio-waste can be converted into activated carbon through pyrolysis under controlled conditions with or without a chemical activating agent (Xu, Gao, Jin, & Yue, 2016). The critical factors for activated carbon

application are the specific surface area, pore volume, and pore size distribution, which are largely determined by the precursor.

The useful hemp fibres produced from the fibre production process is typically only about 25 wt. % consequently a high proportion of waste. The waste is hemp hurd. Hemp hurd have a unique structure and connected pore geometry, which is a desirable characteristic for the adsorption of the obtained activated carbons.

In the preliminary experiment, hemp hurd showed a unique microstructure. The production of activated carbon from hovel biomass wastes is the subject of our investigation. There are still few works on the preparation of high-surface-area activated carbons using hemp hurd. Today, the relationship of hemp hurd structure and properties is not completely understood. With a few exceptions, there are no studies that draw definitive conclusions on structure-property relationships of hemp hurd and activated carbons, based on systematic research. In thesis body-of-work, activated carbons were produced from hemp hurd, retted hemp hurd using different activation temperatures and impregnation ratios, and were compared with activated carbon from bamboo fibre and hemp fibre as controls.

1.2 Aim and objectives of the research

The aim of this thesis was to study was multifaceted. Firstly, the morphology and properties variance of hemp hurd and retted hemp hurd and the influence of retting process was studied. In addition, the effect of physical activation and chemical activation and their mechanisms was investigated along with understanding the effect of activation temperature and impregnation ratio with respect to different precursors. In addition, the effect of structure, and process conditions on corresponding resultant

porous structure of activated carbon and the relationship of porous structure and its corresponding adsorption capacities was elucidated.

The objective of this study is to use biomass materials including hemp hurd, retted hemp hurd, bamboo fibre, and hemp fibre, which have unique microstructures as precursors to produce activated carbon. The obtained activated carbons were targeted for gas adsorption. The adsorption capacities are related to the pore size, pore shape and pore surface chemistry. The final activated carbon produced have surface areas and adsorption capacities comparable with those produced from conventional sources, and to retain a relatively high yield was expected to realize the potential of biomass. The effects of various process parameters on the pyrolysis stage of producing activated carbon are studied. The effects of physical and chemical activating conditions on the active carbon properties from different precursors are also discussed.

The main research questions addressed are as follows:

- What are the specific morphology and properties of hemp hurd and retted hemp hurd, and what is the effect of retting process?
- How do the yield, specific surface area, pore volume, pore size, and CO_2 adsorption capacity of activated carbons derived from different precursors by physical activation using CO_2 compare to those produced using chemical activation with $ZnCl_2$?
- What are the effects of activation temperature and impregnation ratio on the yield, specific surface area, pore volume, pore size, and CO_2

adsorption capacity of activated carbons, and the effect of different precursors?

1.3 Outline of the manuscript

Chapter 1 provides an introduction, aim of the research, the scope, objectives, and outline of this thesis.

Chapter 2 provides the literature review relevant to the research background, including the state-of-the-art, production, and application of activated carbon and the research gap of this area.

Chapter 3 presents the precursors used to conduct the study followed by the methodology to prepare and optimize activated carbons, and to characterise raw materials and the obtained activated carbons.

Chapter 4 focuses on the morphology and property difference of hemp hurd and retted hemp hurd, yield, morphology, surface areas and porosity, CO_2 adsorption capacity of activated carbon from hemp hurd and retted hemp hurd, to investigate the influence of retting process.

Chapter 5 concentrates on the properties and CO_2 adsorption capacity of activated carbons derived from hemp hurd, retted hemp hurd and bamboo fibre by CO_2 activation and $ZnCl_2$ activation, to investigate the effect of physical activation and chemical activation.

Chapter 6 highlights the properties and CO_2 adsorption capacity of activated carbons derived from retted hemp hurd, bamboo fibre, and hemp fibre by $ZnCl_2$ activation

with different activation temperature and impregnation ratio. The effect of these precursors on the CO_2 adsorption capacity is also compared.

Chapter 7 presents the conclusions and proposals for future work.

CHAPTER 2 LITERATURE REVIEW

2.1 Activated carbon

Activated carbons are the porous materials with developed pore structure, high internal surface area, and high adsorption capacity (B. Liu, Gu, & Zhou, 2016). Activated carbons have vast applications, including filtration and purification, catalysts, hydrogen storage, and supercapacitors (Xu et al., 2016). Figure 1 shows the activated carbon adsorption mechanism ("Supplemental Material: ELGA Lab activated carbon,"). Specifically, they are used in sewage treatment, for removing the organic and inorganic pollutants from industry, air purification, bleaching industry, improving noble metals and energy & storage, and catalytic reaction (Altintig & Kirkil, 2016; B. Liu et al., 2016; Williams & Reed, 2003).

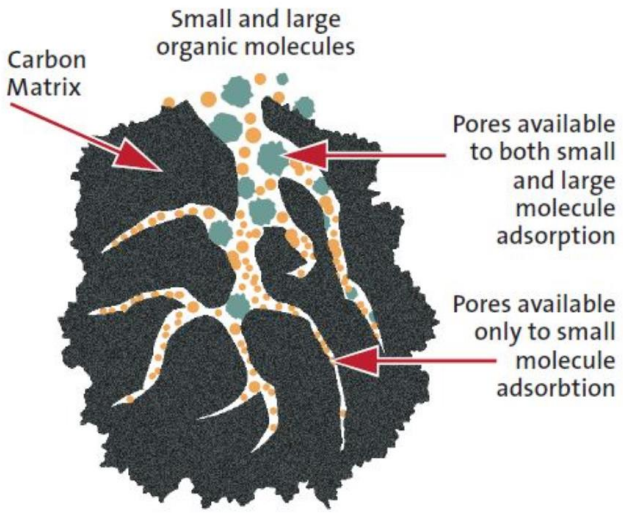

Figure 1. Diagram of activated carbon adsorption mechanism ("Supplemental Material: ELGA Lab activated carbon,").

In addition to the specific surface area and porosity, mechanical properties are also key considerations for activated carbons. Mechanical strength can be regarded as the resistance to abrasion or attrition during its use. A variety of tests are available for the

evaluation of the mechanical strength of granular activated carbon. The most common test method is Hardness number, followed by the abrasion number. Different mechanical strength test methods measure different aspects of strength and can therefore mathematically not be correlated to one another. In these tests, the change in particle size distribution or the amount of fines produced is determined (Cukierman, 2013; J. Lin & Zhao, 2016; Lozano-Castelló, Cazorla-Amorós, Linares-Solano, & Quinn, 2002; Memming, Tolle, & Wierenga, 1986; Salleh, Yusop, & Rosdi).

2.1.1 Activated carbon introduction

Activated carbon has played an important role in the environmental applications, chemical, pharmaceutical, and food industries (Erdem et al., 2016). However, because of their high production costs, activated carbons are often more expensive than other adsorbents, and the high production cost of activated carbon restricts its utilization (Dias et al., 2007; Xu et al., 2016).

The precursors for preparing activated carbons include petroleum coke, fertilizer waste, waste rubber tire, charcoal, bone-char, polymers, and biomass (Juana M. Rosas, Bedia, Rodríguez-Mirasol, & Cordero, 2008). Almost all carbon-containing organic materials can be considered as precursors of activated carbon (Uçar et al., 2008). By controlling the activation conditions and temperatures, these materials are activated into a crude form of graphite with amorphous, highly porous structure (Xu et al., 2016). Coal, asphalt, and petroleum coke are still the major sources for the preparation of activated carbons, but these are non-renewable resources, and hence contribute to high cost in the preparation of activated carbons (B. Liu et al., 2016). Most carbon nanomaterials are synthesized from precursors based on the fossil fuels,

which are eventually destined to be depleted. The cost of these raw materials is also expected to keep on increasing, hence there is a need to find cost-effective renewable precursors (Yang, Liu, Li, Zhang, & Hao, 2012).

2.1.2 Activated carbon from biomass

The demand for renewable and environmentally friendly energy is becoming critical because of the pollution of environment, global warming, and depletion of fossil oil reserves (Yang et al., 2011). Recent technology and policies relating to greenhouse gas emissions and energy security have triggered interest in using thermochemical conversion technologies to process forest biomass (Anderson et al., 2007; Ioannidou & Zabaniotou, 2013). Thermochemical conversion occurs at broad ranges of pressures, temperatures, heating rates, oxidation conditions, and residence times. Pyrolysis of biomass at 200-300 °C produces a devolatilized, hydrophobic high-carbon content product often referred to as torrefied wood. Lower moisture content, higher energy density, hydrophobicity, resistance to decay, and homogenous particle size distribution make torrefied wood more efficient to transport and storage than raw biomass (Anderson et al., 2007; Ioannidou & Zabaniotou, 2013).

Recycling biomass waste to produce useful end products are clearly beneficial for the industry (McHenry, 2009). The conversion of biomass to a long-lived, soil-based carbon species results in a long-term carbon sink, as the biomass removes atmospheric CO_2 through photosynthesis. Unlike fossil fuels, biomass is a renewable source of carbon and used to produce bio-char that can release energy with virtually no sulphur or mercury, and negligible nitrogen and ash. Thus, producing bio-char from farm wood-waste is one promising method of achieving greater levels of certainty and flexibility for integrating carbon sequestration and renewable energy

generation into conventional agricultural production (McHenry, 2009). Currently, biomass is undoubtedly the cost-optimal raw material for producing activated carbons (Yang, Wang, Li, & Hong, 2014).

Biomass is used for the production of high adsorption capacity and low ash content activated carbon (Anderson et al., 2007; Ioannidou & Zabaniotou, 2013). Activated carbons from biomaterials such as Hazelnut shell, coconut husk, corn stalks, soybean hulls, palm shell were often used to adsorb anionic species (Xu et al., 2016). The major advantages for sorption of anionic species include: (1) unique chemical composition, (2) abundance, (3) renewability, and (4) cost-effectiveness. Some biomass-derived carbons are endowed with superior performance through doping and modification (Yang et al., 2014).

There are currently many studies on the use of biomass to produce activated carbon. Most of these studies focus on the use of waste materials of considerable rigidity, such as the shells and/or stones of fruits, or from the production of cereals (Dias et al., 2007). In recent years, substantial amount of research was carried out on the efforts to obtain low cost activated carbons (Tay, Ucar, & Karagöz, 2009). The use of bio-materials, such as wood and fibres, shells, husks, bagasse, and stones, shown in Figure 2, as renewable precursors for low-cost activated carbon production is being widely studied (Azargohar & Dalai, 2009; Dias et al., 2007; Gottipati & Mishra, 2016; Hameed, Tan, & Ahmad, 2009; Hong, Choi, Kim, & Lee, 2016; Juana M. Rosas et al., 2008; Xu et al., 2016). Hemp is one of the most productive and useful plants known. A few studies explored hemp application as precursors for activated carbon.

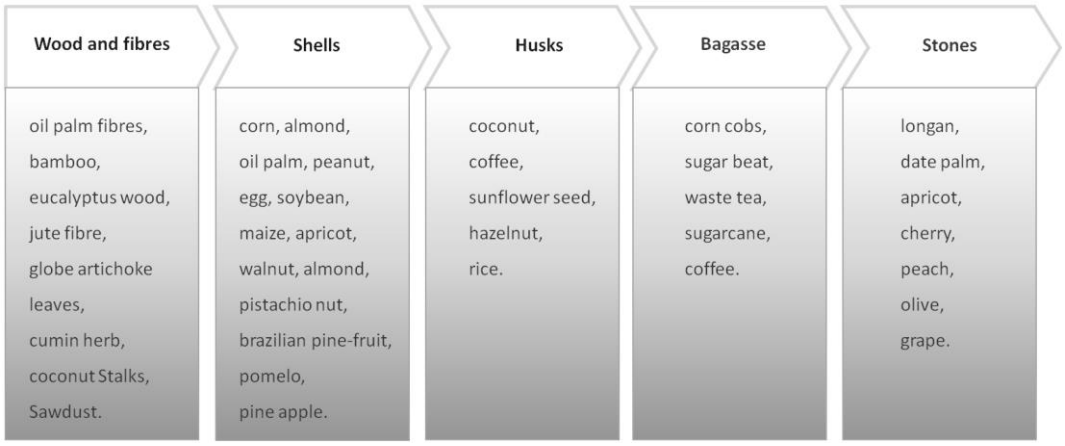

Figure 2. Bio-materials as precursors for low-cost activated carbon production.

2.1.3 Activated carbon from hemp

Hemp has been cultivated for centuries since it grows quickly without any special requirements for climate, pesticides, or fertilizer in most locations, with only moderate water requirement, becoming a valuable and environmentally friendly crop (J. M. Rosas, Bedia, Rodríguez-Mirasol, & Cordero, 2009).

Hemp is an energy crop with several advantages. Hemp is rich in leafage and produces a high amount of biomass due to its high growth rate (50 cm/month). Hemp exhibits many salient features like low feedstock cost, high biomass content, high land use efficiency, higher dry matter yield, low nutrients requirement and can improve soil health with organic matter. Hemp yield depends largely on the environmental conditions. For example, hemp yield is about 20 t per hectare in high temperate areas such as Italy and the United Kingdom. Hemp production in Germany approached about 1600 m^3 per hectare. Late maturing hemp is also capable to have high yield under cold climate conditions in Eastern Europe, Canada and the USA (Nelson, 1999; Rehman, Rashid, Saif, Mahmood, & Han, 2013).

Hemp fibre usually separated from the woody core by mechanical means or by retting. Retting is a process in which pectineus substances that bind together elemental bast fibres become degraded. This progression is completed by microorganisms present on the stems or by acid/bases or special enzymes. A fibre crop of hemp is harvested in the early flowering stage, and retting of the fibre is usually done in the field, requiring several weeks (Cherney & Small, 2016; Nelson, 1999; J. M. Rosas et al., 2009).

The two traditional retting methods are field retting and water retting. Field retting is inexpensive and mechanized. It is accomplished by leaving hemp stalks on the ground for several weeks. Length of the retting depends on the moisture and air temperature. Warm weather with intermittent precipitation maintaining moisture accelerates the pectin degradation. Water retting is labour- and capital-intensive. Hemp stems are immersed in water (rivers, ponds, or tanks) and monitored frequently. Water retting produces more uniform and high-quality fibre (Cherney & Small, 2016).

Hemp is currently regarded as a key industrial source of paper, textiles, building materials, food, yarns, twine, industrial and marine rope, nets, sailcloth, canvas, medicine, paint, detergent, varnish, oil, ink, fuel, and in the plastics industry (H. Wang et al., 2013; Williams & Reed, 2003; Yang et al., 2011). Hemp is especially utilised in novel research fields such as biodiesel production from hempseed oil and textiles production from hemp stems. Due to the increasing demand for hemp fibre, and the development of technologies for hemp fibre processing led to substantial increase in the cultivated area of hemp (Yang et al., 2012).

Hemp seed is an important feedstock for oil, and hemp bast provide fibres for the textile industry. Hemp fibre has also been used as a precursor for activated carbon, which exhibits potential for water purification and supercapacitors (Yang et al., 2014). The outer portion of the hemp hurd contains long fibres that provide the strength and quality to the crop. The inner portion of the stem contains the hurd, which is used for paper and building materials (Juana M. Rosas et al., 2008).

In all natural cellulosic fibres, the most important part is the plant cell wall. The cell wall of hemp is constituted by cellulose, hemicellulose, pectin and lignin. Hemp stems consist of about 65% hemp hurd and 35% bast fibres, and the core fibres consist of 40-48% cellulose, 18-24% hemicellulose and 21-24% lignin, and the bast fibres are 57-77% cellulose, 9-14% hemicellulose and 5-9% lignin (Yang et al., 2011). The properties of each constituent contribute to the overall properties of the fibre. The smallest building element of the cellulose skeleton is the elementary fibril. The fibril can be about 5-10 nm in diameter and from 100 nm to several micrometres in length in different source.

As schematically illustrated in Figure 3, the wall of a hollow hemp fibre (10-30 μm in diameter) is mainly composed of three layers. The internal and outer layers are mainly composed of hemicellulose and lignin while the middle layer is comprised of primarily crystalline cellulose. The middle layer makes up more than 85% of the total wall thickness, is itself a layered structure that are 10-30 nm in diameter consisting of microfibrils.

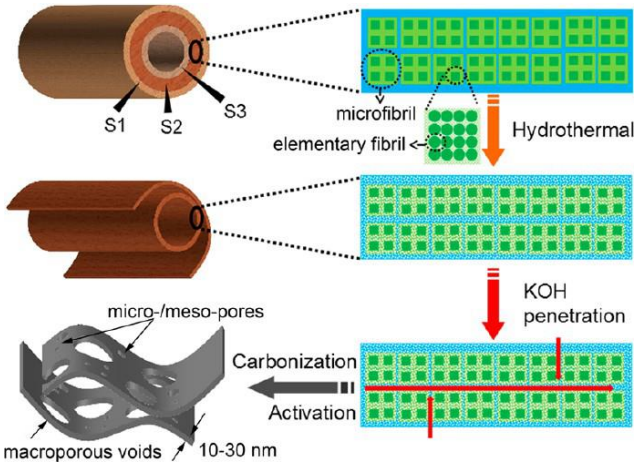

Figure 3. A synthesis process of carbon nanosheets form hemp which has three different structural layers (H. Wang et al., 2013).

Hemp fibre extraction generates an extensive amount of solid residues, which are incinerated under most situations, and hence present an environmental problem in terms of adequate disposal (Yang et al., 2011). Specifically, the hemp processing industry generates a residue that represents 50-55% of the treated material (Juana M. Rosas et al., 2008; J. M. Rosas et al., 2009). Development of recycling processes of such biomass is generating great interest, and the production of activated carbons could be an appropriate solution (Juana M. Rosas et al., 2008; J. M. Rosas et al., 2009).

In the processing of hemp fibres, the hempseed, hemp bast and hemp stem become underutilized by-products. The hemp seed and hemp bast can be used in the production of biodiesel and activated carbon fibres, respectively, while the hemp hurd is of little use. The woody core often accounts for 70% of the hemp hurd (Yang et al., 2012). Yet as a by-product, it is of little use and necessitates further development (Yang et al., 2012). Hemp and hemp by-products are often useful for

the production of activated carbon, and present the advantage of the potential revalorization of a low-cost and easily processed material.

The pore structure and pore size distribution of an activated carbon is largely determined by the nature of the precursor. The activation of carbonaceous materials with significant proportion of fibrous structures like cellulose and hemicellulose is relatively easier, however, lignin presents a challenger because of a less robust and more labile nature of cellulose and hemicellulose as compared to lignin (Yang et al., 2011).

Table 1 summarizes the cellulose, hemicellulose and lignin content of cellulose-containing bio-materials (Thakur & Thakur, 2014). The use of hemp hurd to produce activated carbon is very feasible and presents the advantage of the potential revalorization of a biomass material (J. M. Rosas et al., 2009).

Table 1. The cellulose, hemicellulose and lignin content of some typical cellulose-containing bio-materials (Thakur & Thakur, 2014).

Sample	Composition (%)			
	Cellulose	Hemicellulose	Lignin	Extract
Hardwood	43-47	25-35	16-24	2-8
Softwood	40-44	25-29	25-31	1-5
Bagasse	40	30	20	10
Corn cobs	45	35	15	5
Corn stalks	35	25	35	5
Cotton	95	2	1	0.4
Retted flax	71	21	2	6
Flax	63	12	3	13
Hemp	70	22	6	2
Ramie	76	17	1	6
Wheat straw	30	50	15	5

Hemp-derived activated carbon monolith was prepared with surface area of 1500 m^2/g by phosphoric acid activation (J. M. Rosas et al., 2009). The carbonization temperature and the impregnation ratio strongly affected the properties of the activated carbon. The residual phosphates and/or polyphosphates on the surface of activated carbon causes comparable adsorption capacities of water vapour as on silica gel. However, the mesoporosity and low surface area of this activated carbon limited its gas adsorption capacity (Yang et al., 2011). Activated carbon fibrous was prepared from hemp fibres by phosphoric acid activation. The influence of the activation temperature and the impregnation ratio on the porous structure and surface

chemistry of activated carbon fibrous were analysed. Activated carbons presents a high oxidation resistance attributing to the existence of $CePO_3$ and CeP, blocking the active carbon sites for the oxidation reaction (Yang et al., 2011).

However, there are still few works on the preparation of high surface activated carbon by using hemp hurd and its related applications (J. M. Rosas et al., 2009). Like other biomass, the carbonization of hemp stems can generate a reducing atmosphere, which is worth exploiting during material preparation (Yang et al., 2014). As a consequence, the utilization of hemp hurd to produce activated carbons not only make considerable economic benefit to meet the increasing demand of activated carbons in the application areas such as food, environment, chemistry, and energy, but also make contribution to the mechanism study of carbonaceous materials derived from agricultural wastes (Yang et al., 2012).

2.2 Process of activated carbon production

All activated carbons bear a porous structure, with small percentage of chemically bonded heteroatoms (mainly oxygen and hydrogen). In addition, activated carbon may contain up to about 20 wt.% of mineral matter, which is usually shown as ash content (Dąbrowski, Podkościelny, Hubicki, & Barczak, 2005). Activated carbons are classified into powder activated carbon, granular activated carbon, fibrous activated carbon, and clothe activated carbon according to their size and shape.

Each type of activated carbon has specific applications, advantages, and disadvantages because of their different precursors, the extent of chemical activation, and the physicochemical characteristics (Du et al., 2016; Erdem et al., 2016; Kamandari, Hashemipour Rafsanjani, Najjarzadeh, & Eksiri, 2015; Namasivayam &

Sangeetha, 2006b; Özhan, Şahin, Küçük, & Saka, 2014; Şencan, Karaboyacı, & Kılıç, 2015; Yu, Tu, & Luo, 2015).

Activated carbon powder (includes particles < 0.177 mm) is obtained when small particles compose the raw material, like wood sawdust. Activated carbon powder is mixed with the liquid to be treated and afterwards disposed. Activated carbon powder adsorption is very effective because of its small particle size, however, and for the same reasons, settling and removal tend to be slower than using granular activated carbon (Dias et al., 2007). Granular activated carbon normally includes particles retained in an 80-mesh sieve (0.177 mm), as it can be prepared from hard material, such as coconut shells. Granular activated carbon is commonly used as column filler for gas or liquid treatments and can be regenerated after use. Fibrous activated carbon show a mono-dispersed pore size distribution, it can be prepared from homogeneous polymeric raw materials. Their thin fibre shape enhances intra-particle adsorption and improved contact efficiency between the aqueous media and the adsorbent. Clothe activated carbon were initially developed in the early 1970s, using as precursors phenolic or viscose rayon. Clothe activated carbon are considered to be excellent adsorbents because of their low-pressure drop during process, high contact efficiency and flexibility. Although many kinds of adsorbents were already prepared and tested in aqueous-phase treatments, granular activated carbon and powder activated carbon are still the most widely used (Dias et al., 2007; Ioannidou & Zabaniotou, 2007, 2013).

There are two main steps for the preparation and manufacture of activated carbon: (1) the carbonization of the carbonaceous raw material below 800 °C, where the carbonaceous source materials are heated, decomposed and converted to carbonized material in the absence of air, and (2) the activation of the carbonized product, which

increases the surface area of the carbonized material (Ioannidou & Zabaniotou, 2007; Jodeh et al., 2016).

2.2.1 Carbonization

The process of carbonization is conversion of organic materials into carbon or a carbon-containing residue through pyrolysis. During carbonization, after non-carbonaceous elements such as hydrogen and oxygen are eliminated, and a biochar with high carbon content is obtained. The process of pyrolysis is performed in the absence of oxygen to avoid combustion. The sample starts to develop an internal porous structure, lower than that developed afterwards during the activation process (Ioannidou & Zabaniotou, 2007).

2.2.2 Activation

Activated carbon texture includes a wide range of pores that can be classified according to their pore width in: micropores (< 2 nm), mesopores (2-50 nm), and macropores (> 50 nm). Carbonization as a stand-alone process is not sufficient for efficient preparation of biomass as an adsorbent. To increase its adsorption capacity, the pore network should be developed during activated carbon preparation by the application of adequate physical or chemical treatments (Dias et al., 2007; Ma, Wang, Wang, Sun, & Wang, 2015).

Activated carbons are commercially produced by activation (Williams & Reed, 2004). Many researchers employed physical and chemical activation methods for improving activated carbon properties such as total pore volume, mesoporous volume, and specific surface area (Ahmadpour & Do, 1997; Daffalla, Mukhtar, &

Shaharun, 2012; Gañán-Gómez, Macías-García, Díaz-Díez, González-García, & Sabio-Rey, 2006; Hayashi, Kazehaya, Muroyama, & Watkinson, 2000; Olivares-Marín, Fernández-González, Macías-García, & Gómez-Serrano, 2006).

Physical activation involves pyrolysis of the source material to produce a char followed by the partial gasification of carbonaceous materials in oxidizing gases such as steam, CO_2, or a combination of these (Hong et al., 2016). Precursors are first carbonized followed by activation step with oxidising gases such as air, CO_2 or steam at high temperature in the range of 600-1000 °C (Kong et al., 2016; Rincón-Silva, Moreno-Piraján, & Giraldo, 2016). This activation method creates small pores but it requires high-pressure steam.

In chemical treatment, precursors are carbonized and activated together at temperatures between 400 and 900 °C under a N_2 atmosphere (Kong et al., 2016). Chemical activation involves impregnation with a chemical agent (Williams & Reed, 2004).

2.2.2.1 Physical activation process

Physical activation is the development of porosity by gasification with an oxidizing agent at relatively high temperatures (Uçar et al., 2008). Physical activation comprises carbonization of the raw material in an inert atmosphere followed by partial gasification of the resulting char with nitrogen, steam, air, CO_2 or mixtures of the above (Dąbrowski et al., 2005; Xu et al., 2016).

The physical activation of biomass can be a one-step or two-step process. In the one-step procedure, all samples are thermally treated for 0-2 h at the final temperature (200 °C up to 900 °C) under gas flow. In the two-stage process, the biomass is first

carbonized at high temperatures under an inert atmosphere, and then the charred biomass reacts with the activating agents (steam, air and CO_2) under heating for a certain retention time (Xu et al., 2016). The appropriate temperature is 350-550 °C if air is used and it is 800-1100 °C if steam or CO_2 is used (Altintig & Kirkil, 2016). After one or two-stage activation, the structure of biomass becomes mesoporous and microporous, forming the biomass based activated carbons (Xu et al., 2016). To optimize preparation process, the parameters optimized are time of carbonization, temperature, and CO_2/steam flow rate.

During carbonization, the material is pyrolysed to remove non-carbon elements, and then activation occurs, at temperatures ranging from 700 °C to 1100 °C, using gases that open and develop the porosity of the carbonized material (Dias et al., 2007). Further gasification result in a decrease in micropore volume for the case of CO_2. The mass burn-off increased continuously when steam was added for partial gasification. The process enlarged the micropores and their size shift towards mesopores (Dąbrowski et al., 2005).

From literature, bio-based activated carbons obtained by physical activation exhibited lower sorption capacities for anionic pollutants as compared with those prepared by chemical activation (Xu et al., 2016). The physical activation method was found to be more suitable for preparing activated carbon for odour reduction, while the chemical process was used for decolourization of wastewater treatment (Jutakridsada, Prajaksud, Kuboonya-Aruk, Theerakulpisut, & Kamwilaisak, 2016).

Activated carbons were prepared from rubber-seed shell by physical activation with steam. The microstructure of rubber-seed shell and the obtained activated carbons are shown in the Figure 4. Carbon activated at 820 °C retains canal structure for the raw

material. The surface in carbon activated at 850 °C shows that the canal structure has been partly broken which means the activation process happened. A most well-developed porous structure was further increased in activating temperature at 880 °C (Xu et al., 2016). This is a typical example of the activated carbon formation during the heating process by physical activation process.

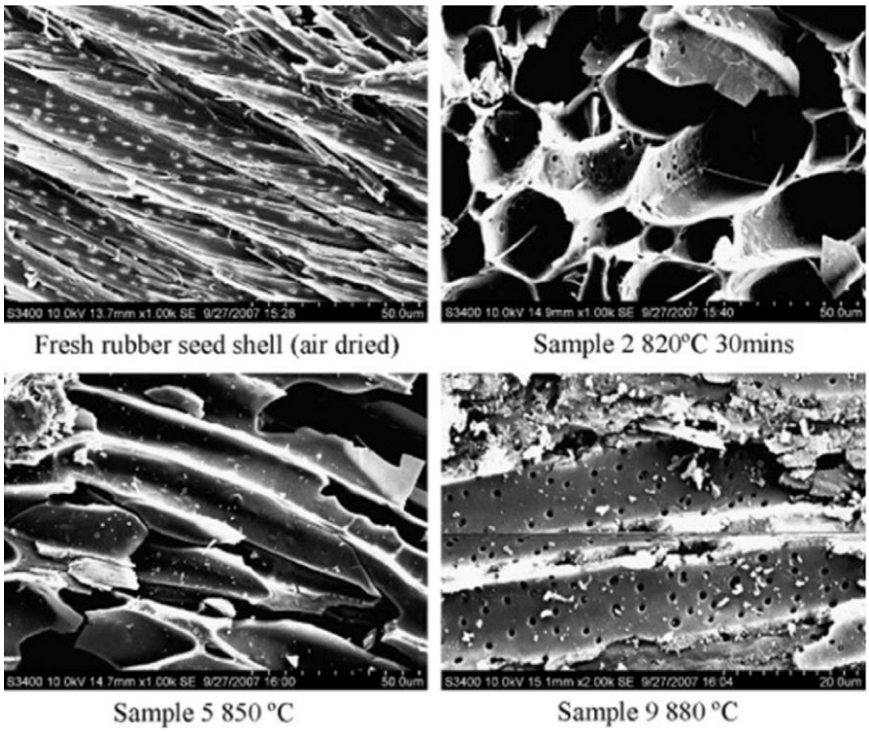

Figure 4. Morphologies of activated carbons by physical activation at 820 °C, 850 °C and 880 °C (Xu et al., 2016).

2.2.2.2 Chemical activation process

Chemical activation involves a pre-treatment scheme where the biomass is impregnated with appropriate chemicals before the activating reaction. Impregnation leads to an increase in carbonization ability, and therefore, forming desired pore structure on network of biomass. The processes are carried out by impregnation of biomass with the activating chemicals in solid or liquid form. The commonly used

chemicals for chemical activation of biomass materials include NaOH, KOH, K_2CO_3, Na_2CO_3, $AlCl_3$, H_3PO_4, H_2SO_4 and $ZnCl_2$ (Bamufleh, 2009; Fortier, Westreich, Selig, Zelenietz, & Dahn, 2008; J. Liu et al., 2014; Mohammadi, Hamidian, & Moeinadini, 2014; Namasivayam & Sangeetha, 2004, 2005; Uçar, Erdem, Tay, & Karagöz, 2009; T. Wang, Tan, & Liang, 2009; Xu et al., 2016; Z. Zhu, Li, Yan, Liu, & Zhang, 2007; Zyoud, Nassar, El-Hamouz, & Hilal, 2015).

Carbonization and activation processes occur simultaneously with the existence of an activation chemical (Altintig & Kirkil, 2016). The inorganic components from the agents used can cause environmental contamination and corrosion of equipment, so additional washing steps are necessary (Hong et al., 2016). These activation chemicals are dehydrating agents that influence pyrolytic decomposition, and inhibit formation of tar (Erdem et al., 2016). Activated carbons with desirable surface properties and pore structure were extensively prepared by chemical activation.

The development of porosity in activated carbon mainly depends on various process parameters involved in the preparation such as precursor used, and type of chemical agent used for the activation (Gottipati & Mishra, 2016). To optimize preparation, carbonization temperature, time of impregnation and impregnation ratio of chemical agents are adjusted. Activated carbon characteristics strongly depend on both the raw material and the activation process (Dias et al., 2007).

KOH only produces a widening of micropore, $ZnCl_2$ additionally develops small mesoporosity, and H_3PO_4 leads to a more heterogeneous pore size distribution. Chemical activation of bio-chars can generate significant effects on their properties. For example, H_3PO_4 has been used as activation agent to prepare activated carbon by biomass. H_3PO_4 activation has led to an enhancement of porosity, a relative higher

carbon yield, and the formation of P-containing functional structures on treated activated carbon. KOH has also been used in the production of activated carbon when either coal or char was used as a precursor. The pores within such chars were suggested to create more available sites for KOH-based reactions, which resulted in activated carbons with a higher surface area after KOH activation (Y. Lin, Munroe, Joseph, Henderson, & Ziolkowski, 2012).

In cellulose pyrolysis, an organic compound with six-carbon ring known as levoglucosan is produced resulting in the formation of tar. Some pores of the obtained carbons are filled or blocked with tars, which hinders its adsorption capability. In chemical activation process, activating agents act as dehydrating agents to inhibit the formation of tar during pyrolytic decomposition, and to increase carbon yield (Xu et al., 2016). Chemical activation is carried out if the raw material is wood. Dehydration of cellulosic material occurs during pyrolysis, which results into charring and aromatization of the carbon skeleton, and the creation of the porous structure (Dąbrowski et al., 2005).

Many researchers have prepared activated carbon from biomass by different activation methods (Erdem et al., 2016). In particular, $ZnCl_2$ is an effective activator causing higher yield of the activated carbon, with greater capacity for gas adsorption and liquid contaminant removal (Jutakridsada et al., 2016). $ZnCl_2$ melt is found to be a superior medium for carbonization because it is weakly corrosive and environmentally friendly, and also is well compatible with the biomass (Kong et al., 2016). $ZnCl_2$ solution is also well compatible with the biomass (Bamufleh, 2009; Fortier et al., 2008; Kong et al., 2016; J. Liu et al., 2014; Mohammadi et al., 2014; Namasivayam & Sangeetha, 2004, 2005; Uçar et al., 2009; T. Wang et al., 2009; Z. Zhu et al., 2007; Zyoud et al., 2015).

Activated carbons from pistachio-nut shell were prepared by chemical activation of with $ZnCl_2$ under nitrogen and vacuum atmosphere. The activated carbons prepared under vacuum condition slightly better results in terms of Brunauer-Emmett-Teller (BET) surface area and pore volume than those produced under nitrogen atmosphere (Azargohar & Dalai, 2009). Activated carbons were prepared from peach stones by $ZnCl_2$ activation. The main factor affecting the surface area and the micropore size distribution was the amount of $ZnCl_2$ introduced. Partial gasification in CO_2 of the carbons developed the surface area and porosity (Azargohar & Dalai, 2009).

Chemical activation has many advantages over physical activation, including (1) the lower carbonization temperature, is compensated by the interaction between the chemicals and the carbon skeleton, (2) yield tends to be greater in chemical activation since char burn off is not required, (3) shorter treatment time, and (4) activated carbons with higher surface area and higher porosity (Dąbrowski et al., 2005; Kong et al., 2016; Tay et al., 2009). However, the unfavourable aspects in chemical activation include high autogenic pressure at elevated temperature, high solubility of oxygen, the activating agent cost, and the need to perform an additional washing stage to remove the chemical agent, and corrosion potential of the activating agents in solution. The activating agents are more expensive and additional neutralization stage is also necessary (Dias et al., 2007; Kong et al., 2016) (Härmas et al., 2016).

2.3 Adsorption theories

Activated carbons widely applied in adsorption. Figure 5 is a schematic view of four stages of the adsorption process (Lowell, Shields, Thomas, & Thommes, 2012). The N_2 isotherms were used to determine the BET specific surface area and Langmuir

specific surface area; total pore volumes; micropore volumes using the t-plot method and mesopore volumes from the Barrett-Joyner-Halenda (BJH) method (Barrett, Joyner, & Halenda, 1951; Lippens, Linsen, & Boer, 1964; Marsh, 1987; Reed & Matsumoto, 1993; Rouquerol, Rouquerol, Sing, Llewellyn, & Maurin, 2013; Walton & Snurr, 2007).

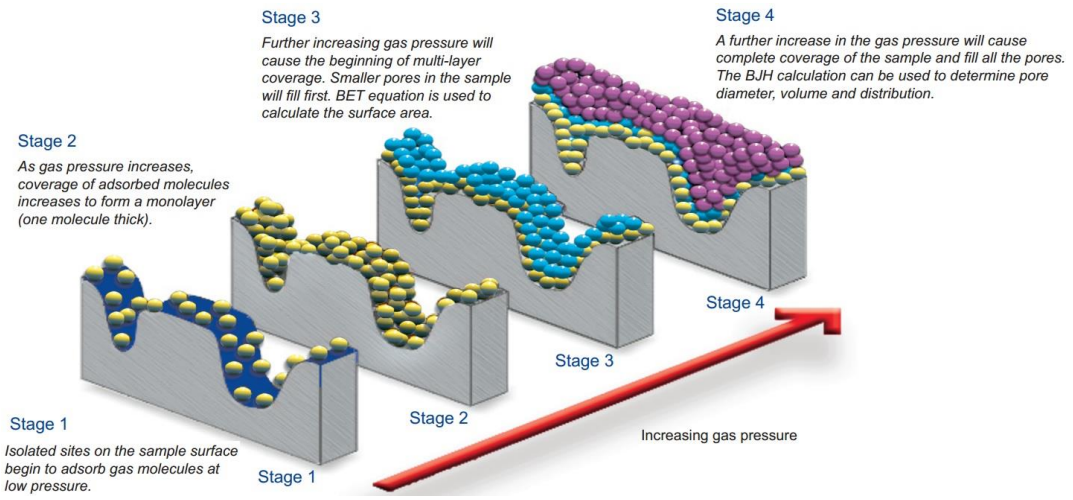

Figure 5. The four stages of the adsorption process (Lowell et al., 2012).

Langmuir method determines surface area based on monolayer coverage of the solid surface by the adsorptive. Its limitation is that it describes the formation of a monolayer. Langmuir method sometimes also be successfully applied to Type I isotherms (pure micropore material) but the reason for plateau is micropore filling (Lippens et al., 1964; Marsh, 1987; Rouquerol et al., 2013).

BET method is a method to obtain the specific surface area of microporous materials, which is the most famous gas sorption model although BET method does not take micropore filling into account ("Supplemental Material: Surface area Analysis Using BET,"). For such samples, the linear BET curve range is usually at relative pressures < 0.1, in contrast to the classical BET range, which extends over relative pressures

between 0.05-0.3. BET method is widely accepted and easy to apply despite its inability to accurately measure the true surface area of microporous materials (Barrett et al., 1951; Lippens et al., 1964; Marsh, 1987; Rouquerol et al., 2013; Walton & Snurr, 2007).

BJH method uses the Kelvin model of pore filling, to calculate pore size distributions from experimental isotherms. Kelvin equation predicts pressure at which adsorptive will spontaneously condense and evaporate in a cylindrical pore of a given size. Condensation occurs in pores that already have some multilayer on the walls ("Supplemental Material: Surface area Analysis Using BET,"). Therefore, the pore size is calculated from the Kelvin equation and the selected statistical thickness equation. It underestimates small to medium mesopores severely, so it only applies to the mesopore and small macropore size range (Barrett et al., 1951; Lippens et al., 1964; Marsh, 1987; Rouquerol et al., 2013).

T-Plot method is used to determine the external surface area and micropore volume of microporous materials. T-Plot method assumes that in a certain isotherm region, the micropores are already filled-up, and the adsorption in larger pores occurs according to some simple equation, which can characteristic for a large class of solids ("Supplemental Material: A Practical Guide to Isotherms of Adsortion on Heterogeneous Surfaces,"). T-Plot method is suitable for a flat surface in a narrow pressure range just above complete filling of micropores, but below vapour condensation in mesopores. T-Plot method should approximate adsorption in mesopores and macropores. It is based on standard isotherms and thickness curves which describe the statistical thickness of the film of adsorptive on a nonporous reference surface ("Supplemental Material: Surface Area and Pore Size Distribution,"). Multi-layer formation is to calculate a layer “thickness, t” as a

function of increasing relative pressure (P/Po). The t-curve is compared with the experimental isotherm in the form of a t-plot. That is, experimental volume adsorbed is plotted versus statistical thickness for each experimental P/Po value. The linear range lies between monolayer and capillary condensation. The slope of the t-plot is equal to the external area. Mesopores, macropores and the outside surface are able to form a multilayer, which contribute further to the adsorption process. It is recommended to initially select P/Po range 0.2-0.5, and subsequently adjust it to find the best linear plot (Barrett et al., 1951; Lippens et al., 1964; Marsh, 1987; Rouquerol et al., 2013).

The Langmuir model (Lippens et al., 1964; Marsh, 1987; Reed & Matsumoto, 1993; Rouquerol et al., 2013) is based on many assumptions, including monolayer adsorption, localized adsorption (occur on specific sites), and constant heat of adsorption. Langmuir model is independent of the amount of material adsorbed. Based on kinetic model of adsorption-desorption process, at equilibrium, $k_A P\,(N - n) = k_D n$, where k_A, k_D are the rate constants, P is the pressure of the adsorbate, N is the total number of adsorption sites, n is the number of occupied sites.

The equilibrium constant is:

$$K_{eq} = \frac{k_A}{k_D} \tag{1}$$

$$K_{eq} = \frac{n}{p(N-n)} = \exp\frac{-\Delta H^0}{RT} \tag{2}$$

$\triangle H^0$: heat of adsorption at temperature, T and standard pressure, P_{ST}

The fraction of the adsorption sites occupied is:

$$q = \frac{n}{N} \tag{3}$$

Eq. (1) can be written as:

$$q = \frac{K_{eq} P}{1 + K_{eq} P} \tag{4}$$

or

$$q = \frac{P}{P + K_{eq}^{-1}} = \frac{P}{P + P_{st} \exp\left(\frac{\Delta H^0}{R}\right)} \tag{5}$$

Eq. (2) can be rearranged to a linearized form as:

$$n^{-1} = N^{-1} + \left(K_{eq} N P\right)^{-1} \tag{6}$$

or

$$p/V = p/V_m + 1/\left(aV_m\right) \tag{7}$$

A plot of n^{-1} versus P^{-1} should be linear with K_{eq} as the slope and N as the intercept. If the plot is not linear, then the Langmuir model cannot fit the adsorption process.

BET model (Barrett et al., 1951; Lippens et al., 1964; Marsh, 1987; Rouquerol et al., 2013; Walton & Snurr, 2007) is an analysis technique for the measurement of the specific surface area of materials. It explains the physical adsorption of gas molecules on a solid surface. The concept of the theory is an extension of the Langmuir theory, which is a theory with the following assumptions including

multilayer adsorption, and that the adsorption of first layer has a heat of adsorption, ΔH_A, whereas the subsequent layers are controlled by heat of condensation, ΔH_L.

The linearized form of BET equation is:

$$\frac{P}{V(P_0 - P)} = \frac{l}{V_m C} + \frac{(C-1)P}{V_m C P_0} \tag{8}$$

(V: volume of adsorbed vapour at STP, V_m: monolayer capacity at STP, P: partial pressure of the adsorbate, P_0: saturation vapour pressure of the adsorbate)

$$C \approx \exp\left[\left(\Delta H_A - \Delta H_L\right)/RT\right] \tag{9}$$

BET was developed primarily to describe the Type II isotherm, i.e., in N_2, Ar on polar surface, $C \approx 100$. It reduces to the Langmuir isotherm at low pressure and monolayer coverage ($\Delta H_A >> \Delta H_L$), at such situation $P_0 >> P$, $C \sim (C\text{-}1)$, where first adsorption is less exothermic ($\Delta H_A < \Delta H_L$), $C < 1$, describes a Type III isotherm.

The method of Barrett-Joyner-Halenda (BJH) was designed for wide-pore adsorbents with a wide pore size distribution. However, it can be successfully applied to virtually all types of porous materials. BJH model assumed that pores have a cylindrical shape and pore radius is equal to the sum of the Kelvin radius and the thickness of the film adsorbed on the pore wall ("Supplemental Material: BJH,").

In general, the desorption isotherm in the pressure range (0.4-0.967) P/P_0*) is used for BJH calculations. P/P_0* is the ratio of partial pressure of the adsorbed substance to saturated vapour pressure of the adsorbed gas ("Supplemental Material: BJH,").

2.4 Applications of activated carbon

Activated carbons have pertinent applications in a wide variety of different fields such as adsorption, aqueous-phase treatment, and supercapacitors. Figure 6 shows the main applications of activated carbon ("Supplemental Material: Tam Dinh Co. Ltd,"). Activation of suitable precursors results in formation of highly porous activated carbons whose large surface areas dictate their performance as adsorbents. The tailored porosity and pore size distribution have strengthened the usefulness of activated carbons for more demanding applications, such as catalysis/electro-catalysis, separation of multi-sized molecules, energy storage in capacitors, electrodes and Li-ion batteries (Jain, Balasubramanian, & Srinivasan, 2016).

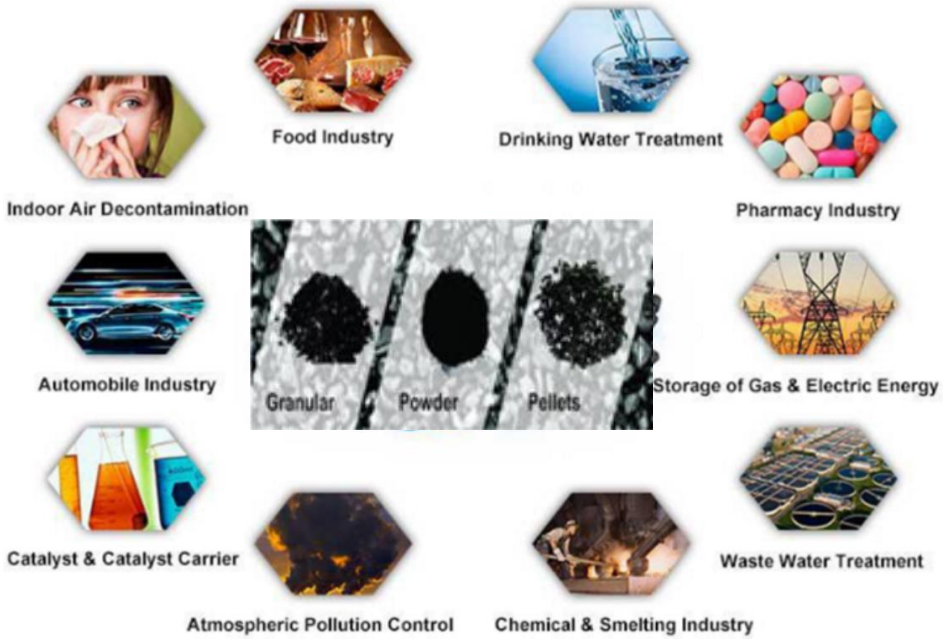

Figure 6. Diagram of applications of activated carbon ("Supplemental Material: Tam Dinh Co. Ltd,").

2.4.1 Application in gas adsorption

Sorption is an efficient physico-chemical treatment process for removing various anionic pollutants from aqueous solutions. Due to the chemical properties of these anionic adsorbates, selective sorption utilizing mineral oxides, clays, activated carbons and exchange resins, has generated interest. Although many kinds of sorbents have been produced for this purpose, activated carbons and exchange resins are still the two most common sorption materials used because of their extensive applications in waters (Xu et al., 2016).

The major methods for removal of toxic substances include membrane filtration, chemical precipitation, ion exchange, and adsorption on activated carbon and silica. However, some of these methods are costly. Researchers studied the use of low-cost adsorbents for removal of toxic substances from wastewater (Arampatzidou & Deliyanni, 2016; dos Reis, Adebayo, Lima, Sampaio, & Prola, 2016).

Activated carbon can effectively adsorb contaminants through the van der Waals force, electrostatic attraction, or chemical bonds between surface functional groups and adsorbate. However, the adsorption process primarily achieves phase transfer only and not transformation of some toxic pollutants into nontoxic or low toxic substances. Hence, to synthesize functionalized and reactive activated carbons combining both adsorption and detoxification for environmental remediation is needed (Altintig & Kirkil, 2016; Yang et al., 2014).

Activated carbons can adsorb molecules from both liquid and gas phases (Altintig & Kirkil, 2016; dos Reis et al., 2016). Figure 7 illustrates the diagram of high-performance canister systems for vehicle emissions using activated carbon

("Supplemental Material: Kuraray Chemical Co., Ltd."). Its advantages are non-toxic, cost-effective, flexible, ease of operation and design, and insensitivity to toxic pollutants. Granular activated carbon was used for adsorption of gases and vapours, which powder activated carbon was used for purification of liquids (Karimnezhad, Haghighi, & Fatehifar, 2014). Activated carbons have the ability to display different functional groups that affect their chemical nature, which is an important characteristic that allows for interactions with molecules of interest (Vargas, Giraldo, & Moreno-Piraján, 2016). For example, the surface modified activated carbons were prepared by impregnating with the cationic surfactants or metal ions (Xu et al., 2016).

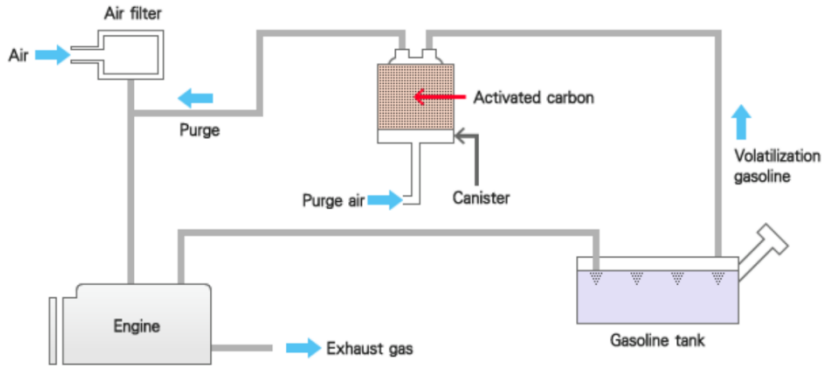

Figure 7. Diagram of high-performance canister systems for vehicle emissions using activated carbon ("Supplemental Material: Kuraray Chemical Co., Ltd.,").

Activated carbons were used to adsorb CO_2. The international panel on climate change predicts that the atmosphere may contain up to 570 ppm CO_2 which can increase the global temperature of around 1.9 °C and can increase of mean sea level about 38 m by the year 2100 (Abang, Janaun, Anisuzzaman, & Ikhwan, 2016). Increase in CO_2 emissions is inevitable because of the high demand for fossil fuels, which are crucial energy sources (Hong et al., 2016; Kongnoo, Intharapat, Worathanakul, & Phalakornkule, 2016). CO_2 is also a major component in biogas.

CO_2 separation from biogas, followed by CO_2 capture and storage can reduce risks of machinery and instruments deterioration and can help to decrease the CO_2 concentration in the atmosphere (Kongnoo et al., 2016).

Several methods were suggested to reduce the CO_2 emission, to reduce energy intensity, to reduce carbon intensity and to enhance the sequestration of CO_2. The carbon, which has a pore size less than 1 nm, is very suitable for CO_2 capture under ambient conditions. The activated carbons which impregnates sterically hindered amines had superior adsorption performance (Abang et al., 2016).

Several technologies have been developed to capture the CO_2. Current CO_2 capture methods include absorption by aqueous solutions, adsorption by solid materials, and membrane separation. Among these approaches, adsorption is advantageous owing to the low energy consumption and easy regeneration of the adsorbent, without the production of unfavourable by-products or polluted sorbents (Kongnoo et al., 2016). Commercial adsorbents such as metal-organic frameworks and zeolites have high CO_2 adsorption capacities, however, the adsorption abilities of these highly hydrophilic materials dramatically decline in the presence of water. In contrast, activated carbon is hydrophobic and exhibits high surface area and excellent thermal and chemical stability. It can be easily prepared and has a relatively low cost (Hong et al., 2016; Kongnoo et al., 2016).

Adsorption is a physicochemical process based on mass transfer of a substance (adsorbate) in aqueous solution to a solid substrate (adsorbent) (Dos Santos, Felsner, Almeida, & Justi, 2016). Adsorption process depends on the pore size and the type of activation of carbon. When the pollutant size equals the pore size of activated carbon the adsorption efficiency increased (Jodeh et al., 2016). Activated carbon efficiency

for removing a given substance depends on both its surface chemistry and its adsorption capacity. The activated carbon adsorption capacity is usually attributed to its internal pore volume that may be distributed throughout the solid as pores ranging in width from micro pores to macropores (Jodeh et al., 2016). Recently, narrow micropore volume was linked to CO_2 adsorption at ambient temperature and pressure (Hong et al., 2016). The relationship between the CO_2 adsorption capacity and textural properties of activated carbon such as surface area and pore volume needs to be studied.

Several factors affect the adsorption process such as time, temperature, initial dye concentration, pH, ionic strength, agitation, and adsorbent dosage. Based on the study of these parameters, it is possible to find the optimum conditions for adsorption (Arampatzidou & Deliyanni, 2016). Considering that these variables do not act in the same way for different precursors, it then becomes necessary to conduct a study to evaluate the influence of variables in adsorption as well as optimize the process (Dos Santos et al., 2016).

2.4.2 Application in water treatment

Many problems worldwide associated with the lack of clean, fresh water are well known. In industrialized nations, a growing number of contaminants are entering water supplies from human activity (Gaya, Otene, & Abdullah, 2015; Karaçetin, Sivrikaya, & Imamoğlu, 2014; Namasivayam & Sangeetha, 2006c, 2008; Pezoti et al., 2014; Şencan et al., 2015). Increasingly, public health and environmental concerns drive efforts to decontaminate waters previously considered clean. More effective, lower-cost, robust methods to disinfect and decontaminate waters are needed (Bhatnagar et al., 2008; Bouchenafa-Saïb et al., 2014; Bouguettoucha, Reffas,

Chebli, Mekhalif, & Amrane, 2016; Danish et al., 2011; Martínez, Van der Bruggen, Negrin, & Luis Alconero, 2012; Namasivayam & Sangeetha, 2006a; Shannon et al., 2008; Subha & Namasivayam, 2010).

Activated carbon is an effective adsorbent for removing pollutants from liquid phases because of its high porosity, large specific surface area, and high surface activity (Babel & Kurniawan, 2003; Dias et al., 2007). However, it is still a challenge to prepare activated carbon with very specific characteristics, such as a given pore size distribution. Therefore, it is of extreme relevance to find suitable low-cost precursors that are economically viable and with better characteristics than the conventional activated carbons (Bouguettoucha et al., 2016; Chen, Zhao, Li, & Tong, 2016; Dias et al., 2007; Karaçetin et al., 2014; Martínez et al., 2012; Martins et al., 2015; Mataji & Khoshandam, 2014; Namasivayam & Sangeetha, 2006a, 2008; Pezoti Junior et al., 2014; Pezoti et al., 2014; Ramakrishnan & Namasivayam, 2011; Şahin, Saka, Ceyhan, & Baytar, 2015; Şencan et al., 2015; Subha & Namasivayam, 2010).

Activated carbons are used for the removal of phenols, phenolic compounds, heavy metals and dyes, metal ions and mercury (II) from aqueous solutions. Based on papers related with the adsorption of organic pollutants and heavy metals in activated carbon, the fundamentals regarding the adsorption of these micropollutants were discussed (Babel & Kurniawan, 2003; Dias et al., 2007; Ioannidou & Zabaniotou, 2007, 2013; Xu et al., 2016).

The adsorption process of activated carbon results from interactions between the activated carbon surface and the adsorbate. The interactions between the activated carbon surface and the adsorbate can be electrostatic or non-electrostatic. Electrostatic interactions occur if the adsorbate is an electrolyte that dissociates in

aqueous solution. The interactions can be attractive or repulsive, which depend on: (1) charge density of the activated carbon surfaces, (2) chemical characteristics of the adsorbate, and (3) ionic strength of the solution. Non-electrostatic interactions are attractive, and can include van der Waals forces, hydrophobic interactions and hydrogen bonding (Dias et al., 2007) (Bhatnagar et al., 2008; Bouchenafa-Saïb et al., 2014; Bouguettoucha et al., 2016; Karaçetin et al., 2014; Martínez et al., 2012; Namasivayam & Sangeetha, 2006a, 2006c, 2008; Pezoti et al., 2014; Şencan et al., 2015; Subha & Namasivayam, 2010).

The properties of the adsorbate that influence the adsorption of activated carbon are: (1) solubility; (2) molecular size; (3) acid dissociation constant; and (4) nature of the substituents (in the case of aromatic adsorbates) (Bhatnagar et al., 2008; Bouchenafa-Saïb et al., 2014; Bouguettoucha et al., 2016; Chen et al., 2016; Karaçetin et al., 2014; Martínez et al., 2012; Martins et al., 2015; Mataji & Khoshandam, 2014; Namasivayam & Sangeetha, 2006a, 2006c, 2008; Park et al., 2013; Pezoti Junior et al., 2014; Pezoti et al., 2014; Ramakrishnan & Namasivayam, 2011; Şahin et al., 2015; Şencan et al., 2015; Subha & Namasivayam, 2010). The solubility determines the hydrophobic interactions degree between the adsorbate and the activated carbon surface. The molecular size determines the accessibility of the adsorbate to the pores of the activated carbon. The acid dissociation constant controls the dissociation of the adsorbate (if it is an electrolyte). For aromatic adsorbate, the substituents of the aromatic rings can withdraw or release electrons, which affect the non-electrostatic interactions between the adsorbate and the activated carbon surface (Dias et al., 2007).

When the activated carbon is in contact with an aqueous solution, an electric charge is generated. This charge results from either the dissociation of the surface functional

groups of the carbon or the adsorption of ions from the solution, and strongly depends on the solution pH and on the surface characteristics of the adsorbent (Babel & Kurniawan, 2003; Dias et al., 2007; Ioannidou & Zabaniotou, 2007, 2013; Xu et al., 2016). The central issue for ion adsorption from an aqueous medium is the understanding of the mechanisms by which ionic species become attached to the carbon surface.

There are three different mechanisms by which metallic ions are removed from an aqueous solution (Bhatnagar et al., 2008; Bouchenafa-Saïb et al., 2014; Bouguettoucha et al., 2016; Chang, Wang, Pei, Yang, & Dong, 2014; Chen et al., 2016; Karaçetin et al., 2014; Martínez et al., 2012; Martins et al., 2015; Mataji & Khoshandam, 2014; Namasivayam & Sangeetha, 2006a, 2006c, 2008; Pezoti Junior et al., 2014; Pezoti et al., 2014; Ramakrishnan & Namasivayam, 2011; Şahin et al., 2015; Şencan et al., 2015; Subha & Namasivayam, 2010). The first states that the process is based on electrostatic adsorbate–adsorbent interactions being very dependent on the existence of carbon surfaces functionality, especially oxygen surfaces complexes. The second suggests that enhanced adsorption potentials may be strong enough to adsorb and retain ions. The third mechanism is based on the hard and soft acids and bases concept, a consequence of the amphoteric nature of carbon surfaces (Dias et al., 2007).

Variable heteroatoms can be found in activated carbon, which might have origin in the raw material or could be introduced during preparation or further treatments, which influence the charge, hydrophobicity, and electronic density of the activated carbon surface. The carbon surface chemistry has major influence on both, electrostatic and non-electrostatic interactions (Dias et al., 2007; Karimnezhad et al., 2014; Mahmoudi, Hamdi, Kriaa, & Srasra, 2012).

Activated carbon is used for the removal of phenols, phenolic compounds, heavy metals and dyes, metal ions and mercury (II) from aqueous solutions (Babel & Kurniawan, 2003; Dąbrowski et al., 2005; Ioannidou & Zabaniotou, 2007, 2013; Xu et al., 2016). Phenolic derivatives are common environmental contaminants. Phenols cause unpleasant taste and odour of drinking water and have negative effects on biological processes. (Arampatzidou & Deliyanni, 2016; Dąbrowski et al., 2005; Ramakrishnan & Namasivayam, 2011; Rincón-Silva et al., 2016; Subha & Namasivayam, 2010). Activated carbons adsorb arsenic and trace metals from drinking water, or used as support for noble metals or as catalysts in liquid phase reactions (Ioannidou & Zabaniotou, 2007; Xia et al., 2016). Adsorption of acid dyes from aqueous solution by activated carbons is one of the most efficient methods, like acid violet 17 from waste waters, by orange peel derived activated carbons, or acid yellow 36 by rice husk derived activated carbons (Ioannidou & Zabaniotou, 2007). Activated carbons by phosphoric acid activation are the best in the uptake of methylene blue from aqueous solution (200-400 mg/g). Activated carbons derived from rice straw by KOH activation by the two-stage method have high surface area and adsorption capacities for methylene blue and iodine (Ioannidou & Zabaniotou, 2007) (Karaçetin et al., 2014; Pezoti et al., 2014).

2.4.3 Application in electrode

The porous electrodes of commercial supercapacitors are realized from porous carbon or activated carbon, an existing and relative cheap material. The commercial supercapacitors manufacturing technology is based on carbon materials as electrodes (Du et al., 2016; Li et al., 2016; Y. Liu et al., 2016; S. Zhu et al., 2016). Figure 7 is a diagram of a supercapacitor based on carbon materials as electrodes in its charged

state (Pandolfo & Hollenkamp, 2006). Activated carbons, carbon nanofibres, carbon nanotubes, templated carbons, carbide-derived carbons, and graphene were intensively investigated for supercapacitor electrode applications. Activated carbons were successfully developed as electrodes for commercial supercapacitor devices (Chang et al., 2014; Faraji & Ani, 2015). Commercial activated carbons for supercapacitor usually possess moderate gravimetric capacitances in the range of 100-120 F/g in an organic electrolyte (Babel & Kurniawan, 2003).

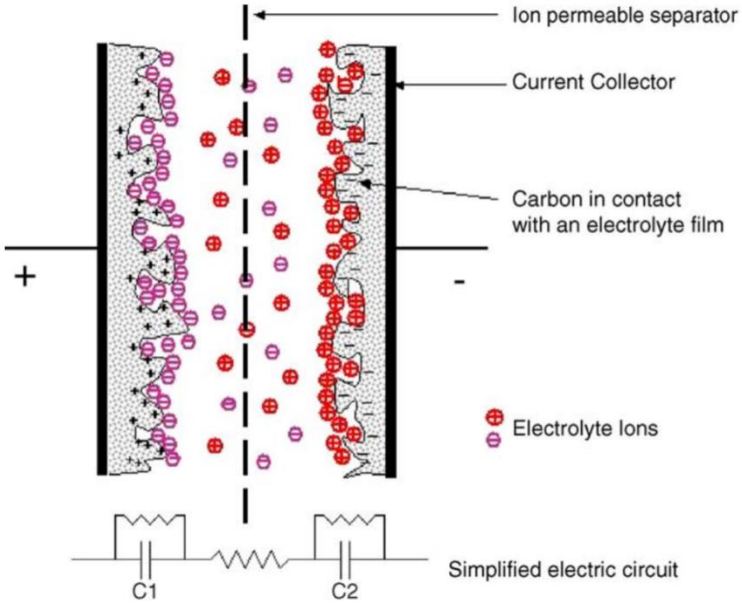

Figure 8. Diagram of a supercapacitor based on carbon materials as electrodes in its charged state (Pandolfo & Hollenkamp, 2006).

Activated carbons are promising electrode materials for supercapacitors. Hydrothermal carbonization was used to obtain spherical lyophilic materials from carbon-rich precursors (Härmas et al., 2016). A novel electrochemical flow capacitor with activated carbon slurry as electrode materials was prepared. It enables rapid charging/discharging and decoupled energy/power ratings. Figure 9 is the operation of an electrochemical flow capacitor system. In this study, slurries are charged in the

flow cell and stored in separate containers. They are pumped back to the cell for discharge (Campos et al., 2013).

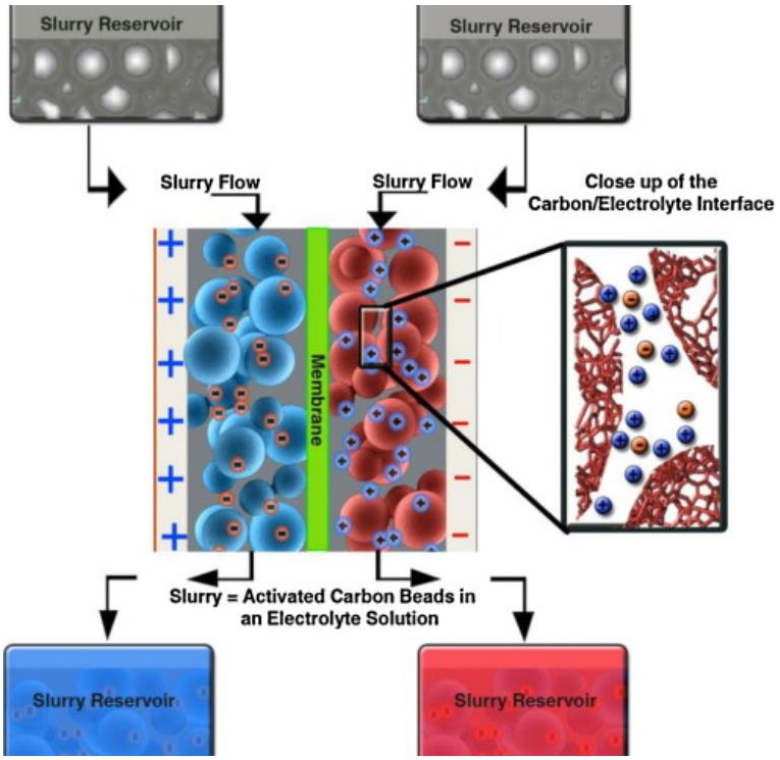

Figure 9. Schematic of the operation of an electrochemical flow capacitor system (Campos et al., 2013).

High specific capacitances of 200-300 F/g in organic electrolyte or ionic liquid were reported by using activated carbon electrodes with a given pore size distribution. However, the power characteristics of these activated carbons remain limited because of an intrinsically high fraction of microporosity, which limits pore accessibility of the electrolyte ions at high scan rates (H. Wang et al., 2013). The specific surface area of the activated carbon reach values as high as 3000 m^2/g, and significantly higher capacitance value is reached in the case of electrochemical capacitors with porous electrodes, than in the case of conventional electrolytic capacitors (Obreja, 2008).

Main performance characterization of supercapacitor electrodes consists in: the specific capacitance as a function of charge/discharge rates employing cyclic-voltammetry and constant current charging curves, reversibility, energy efficiency and conductivity, Ragone plots (Obreja, 2008). Ragone plots depict dependence of the specific energy on the specific power. The specific power is related to the electrical conductivity in the capacitor porous electrode or to the equivalent series resistance. Higher energy density or specific energy for supercapacitors is a way for performance improvement. A high specific capacitance can increase the specific energy. Electrodes of commercial supercapacitors are based on porous or activated carbon material because of its availability and lower cost (Obreja, 2008).

Activated carbon can has specific surface area as high as 3000 m^2/g, but linear variation of capacitance with the specific surface area, usually is not found in practice. Micropores with a diameter of the order of 1 nm have significant contribution to a high specific surface area, but access of electrolyte ions in such pores may be difficult. Suitable distribution of pore sizes from micropores to mesopores for a given surface area can provide high capacitance value. (Campos et al., 2013; Chang, Wang, Pei, Yang, & Dong, 105 2014; Du et al., 175 2016; Li et al., 100 2016; Madhu et al., 37; Obreja, 19; S. Zhu et al., 102 2016)

Another challenge is wettability of the pore surface by the electrolyte. The specific capacitance is dependent on the discharging current density. At high current density, significantly lower value of capacitance is exhibited in the case of activated carbon with large number of micropores. Further optimization of available activated carbons is required to obtain maximum possible specific capacitance. The addition of metallic oxides or conductive polymers in the activated carbons provides significant higher capacitance than for pure activated carbon. Hybrid or asymmetric supercapacitors

where an electrode is of activated carbon and the other electrode is based on a different material can provide significantly higher capacitance than in the case of two electrodes of pure activated carbon (Obreja, 2008).

To reduce the ion transport time is the key factor to achieving high power. The ion transport time (τ) can be expressed by the equation $\tau = l^2/d$, where l is the ion transport length and d is the ion transport coefficient. The ion transport length of carbons with open two-dimension type morphology is significantly shortened because their thin dimension. They have an intrinsic advantage over particulate type systems. (H. Wang et al., 2013).

In summary, activated carbon from biomass is a suitable electrode material for supercapacitors. Nanomaterials based on graphene or graphene hybrids are a new class of promising high rate electrode candidates. To create nanosheets with graphene-like morphology in activated carbons by biomass precursors would be a promising method to produce high-performance electrode for supercapacitors.

CHAPTER 3 METHODOLOGY

In this thesis, hemp hurd and retted hemp hurd were used as precursors for the preparation of activated carbon by chemical activation with $ZnCl_2$ and physical activation with CO_2. Then, activated carbons were prepared from bamboo fibre and hemp fibre in the similar conditions for comparison. The influence of the carbonization temperature and the impregnation ratio was studied on morphology, porosity, chemical property, and activation mechanism of the activated carbons. The yield, specific surface area, pore volume, and pore size of the activated carbons were determined. The CO_2 adsorption performance was evaluated. Figure 10 is the research plan and design.

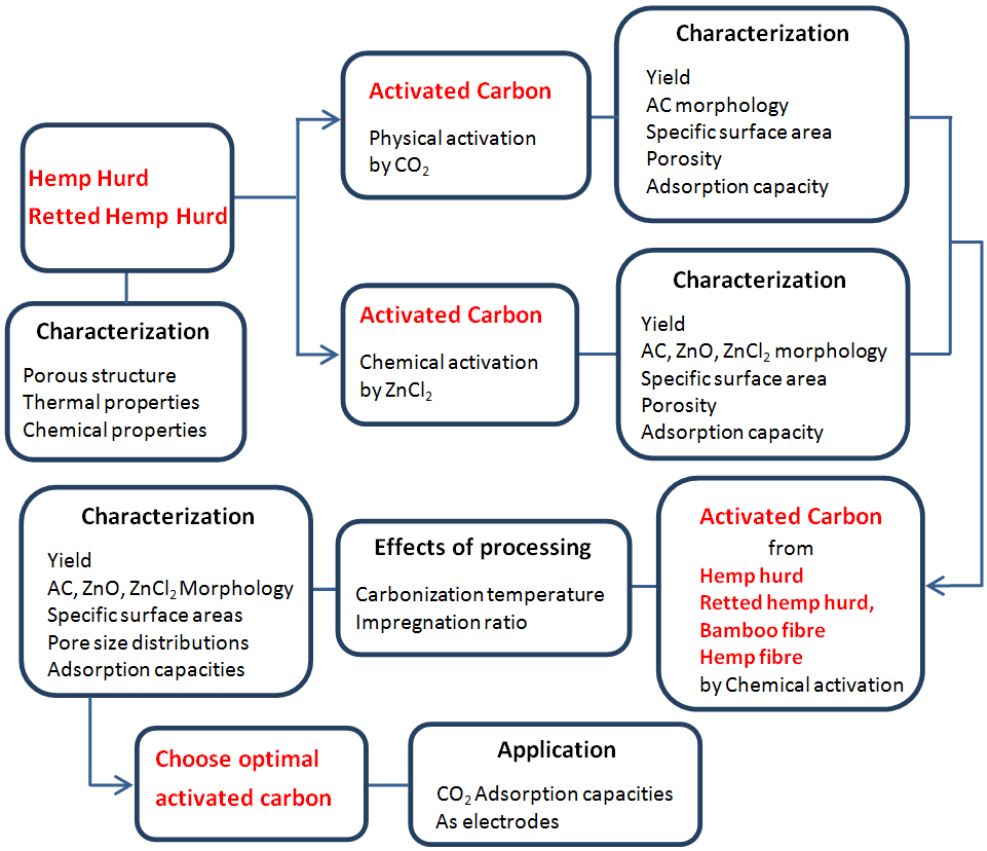

Figure 10. Research plan and design of the current body of work.

3.1 Materials

Hemp hurd, semiretted hemp hurd, retted hemp hurd, bamboo fibre, and hemp fibre were obtained from Ecofibre Industries Operations Pty Ltd, Australia. The hemp hurd and retted hemp hurd were cut into sections of about 10 mm and dried in the oven for 12 h at 100 °C before use. All chemicals used in the investigation such as $ZnCl_2$ and HCl were of analytical grade.

3.2 Preparation of activated carbon

Activated carbon is a highly porous material, which has high surface area and exhibits good adsorptive capacities. In general, high surface areas result in high adsorption capacities, but adsorption capacities are more accurately related to pore size, pore shape and pore surface chemistry (Williams & Reed, 2003). The activation process largely influences the porosity and surface chemistry of activated carbon.

There are two kinds of activation process, physical or chemical. In chemical activation, carbon precursor reacts with a chemical dehydrating reagent. After preparation of the mixture, it is heated, according to a specific heat treatment schedule, in an inert atmosphere and then the reaction product is washed to remove the activating agent (Azargohar & Dalai, 2006; Williams & Reed, 2003). Physical activation is the development of porosity by gasification with an oxidizing agent at relatively high temperatures (Uçar et al., 2008). It comprises carbonization of the raw material in an inert atmosphere followed by partial gasification of the resulting char with N_2, steam, air, CO_2 or mixtures of the above (Dąbrowski et al., 2005; Xu et al., 2016).

In this research, the biomass materials, i.e., hemp hurd, retted hemp hurd, bamboo fibre, and hemp fibre were used as the precursors of activated carbon. They were activated by physical activation using CO_2 and by chemical activation using $ZnCl_2$.

The effect of physical activation and chemical activation on the properties of derived activated carbon was compared.

3.2.1 Physical activation by CO_2

Activated carbons produced by CO_2 activation were carried out in a two-step process:

(1) The biomass was pyrolysed in a tubular furnace under the N_2 flow. The temperature was ramped from ambient temperature to 850 °C at a heating rate of 10 °C/min with retention time of 2 h. Then the reactor was cooled down naturally to 800 °C under nitrogen atmosphere. This preliminary heating process would serve to further pyrolyse the char; consequently, the influence of the original biomass pyrolysis temperature that produced the char is not significant.

(2) The reactor was kept 800 °C under the CO_2 flow with retention time of 2 h, and then cooled down naturally to the room temperature under CO_2 atmosphere. The obtained activated carbons from hemp hurd and retted hemp hurd are labelled as AC-HH-CO_2 and AC-RH-CO_2.

3.2.2 Chemical activation by $ZnCl_2$

Activated carbons produced by $ZnCl_2$ activation were carried out in three stages:

(1) In step 1, the biomass was impregnated by $ZnCl_2$ solution for 24 h (the weight ratio of $ZnCl_2$ to biomass is 2) then dried at 110 °C for 24 h.

(2) In step 2, the impregnated biomass was pyrolysed in a tubular furnace under the nitrogen flow. The temperature was ramped to 800 °C at a heating rate of 10 °C/min with retention time of 2 h. Then the reactor was cooled down naturally to the room temperature.

(3) In step 3, the obtained samples were washed in 1 mol/L HCl, rinsed by distilled water to neutral PH, and then dried in the oven at 80 °C. The obtained activated carbons from hemp hurd and retted hemp hurd are labelled as AC-HH-$ZnCl_2$ and AC-RH-$ZnCl_2$.

The experimental impregnation ratio was estimated from the following equation 10.

$$\text{Impregnation ratio} = \frac{\text{Weight of sample after impregnation} - \text{Weight of waste biomass}}{\text{Weight of waste biomass}} \quad (10)$$

3.3 Optimization of the activation process

The surface areas and adsorption capacities of activated carbon are related to the pore size, pore shape and pore surface chemistry (Williams & Reed, 2003). Optimization of the activation process can further improve the porosity and adsorption capacity of activated carbons (Park et al., 2013).

The porous structure and sorption characteristics of activated carbons are dependent on the physicochemical properties of the precursors and the activation methods. In particular, Zn morphologies and structures play a role in the formation of porous structures of activated carbons during the activation process. The physicochemical

properties of activated carbon are strongly dependent upon the nature of precursor and pyrolysis conditions (e.g. carbonization temperatures and $ZnCl_2$ impregnation rate). Thus, a study of the porosities and surface properties, and adsorption capacities of the activated carbons is essential to identify optimum pyrolysis conditions.

The $ZnCl_2$ impregnation rate to biomass was selected in the range of 2:1-4:1, and the carbonization stage was carried out in the range of 400-800 °C. The yields, specific surface areas, pore volumes, and pore sizes of the activated carbons were determined. The gas capture performance of the synthesized activated carbons was evaluated in adsorption of CO_2. The systematic study will assist in the development of value-added activated carbons from biomass, to identify optimum process to produce activated carbon, and to maximize the adsorption capacity of activated carbon.

3.4 Characterization

Scanning electron microscope (SEM) images were collected on a Hitachi TM-1000 instrument (HITACHI, Japan) at an accelerating voltage of 15 kV. The biomass used in this study, and the activated carbon obtained were observed in SEM directly without a subsequent coating.

The thermal properties were characterized using differential scanning calorimetry (DSC) on a TGA/DSC1 analyser (Mettler-Toledo, Switzerland). The samples were heated to 350 °C at 10 °C/min, and maintained for 3 min to erase thermal history, prior to cooling down to 25 °C at 25 °C/min. A second scan from 25 °C to 350 °C at 10 °C/min was performed. The samples were kept under a nitrogen flow of 20 mL/min throughout the whole process. The melting temperatures (T_m) were determined from the second scan.

X-ray photoelectron spectroscopy (XPS) was performed on a PHI-560 ESCA (Perkin Elmer) at 15 kV. The C1s peak position was set to 284.8 eV and taken as an internal standard. The contents such as carbon, hydrogen, oxygen, and nitrogen percentages of the activated carbon were measured.

Sorption isotherms of N_2 at 77 K and CO_2 at 273 K were measured with a TriStar II 3020 apparatus (Micromeritics, USA) after degassing the activated carbon at 473 K and a pressure of 10^{-5} mm-Hg for 24 h. The N_2 isotherms were used to determine the specific surface area; total pore volumes; micropore volumes and mesopore volumes. The activated carbons were degassed at 423 K for 24 h prior to high pressure adsorption measurements.

CHAPTER 4 THE INFLUENCE OF HEMP HURD RETTING PROCESS

4.1 Structure and morphology of hemp hurd

Utilizing biomass hemp hurd and retted hemp hurd to produce useful products activated carbons would bring significant economic benefit to the industry. In this thesis, hemp hurd and retted hemp hurd, by-products of hemp fibre industry, were used as precursor for the preparation of activated carbon by chemical activation with $ZnCl_2$ and physical activation with CO_2. Retting is the process of using microbes and moisture on plants to dissolve the cellular tissues and pectin surrounding the bast-fibre bundles to separate the fibres from the stem. The effect of retting process on activated carbon properties was investigated.

Figure 11 shows a schematic drawing of the cross-section of a hemp stem with structure of different layers. The outside of the stem is covered with epidermis, and the inside is made of bast fibres and hemp hurd. Each fibre bundle consists of single fibres. The hemp stem consists of approximately 20-40 wt.% of bast fibres and 60-80 wt.% of hurd (Balčiūnas, Vėjelis, Vaitkus, & Kairytė, 2013; Stevulova et al., 2014).

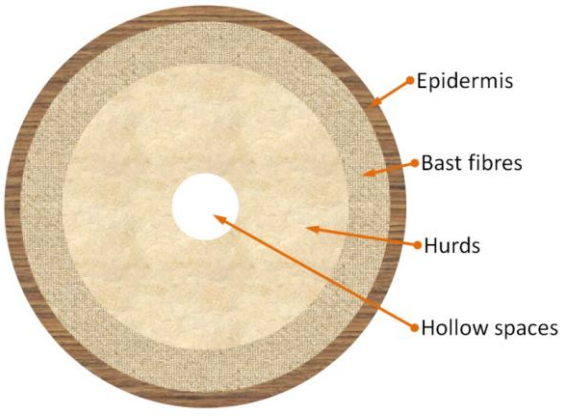

Figure 11. An illustration of a section of a mature hemp stem.

The bast fibres are 10 to 100 times longer than the hemp hurd. The hemp hurd is chemically close to wood, so it is the least valuable part of the plant. The hemp hurd consist of 40-48% cellulose, 18-24% hemicellulose, and 21-24% lignin. The bast fibres contain higher amounts of cellulose (57-77%) and content of hemicellulose (9-14%) and lignin (5-9%) is lower compared to hemp hurd (Stevulova et al., 2014).

The critical factors for the application of activated carbon are the pore structure and pore size distribution, which are largely determined by the nature of the original material. The study of micro-morphology of bamboo fibre, hemp hurd and retted hemp hurd forms the basis for the corresponding activated carbon.

The SEM images of full view of hemp hurd at different magnifications are shown in Figure 12, showing the unique structure of hemp hurd, which consists of two types of macropore channels of different sizes. The size of pores formed between the particles depends on the texture of hurds, and is about 1 mm. The inner porosity of hemp hurds consists of 15% of 70 μm sized pores, and 85% of 400 μm pores (Balčiūnas et al., 2013). Figure 12 shows that the hemp hurd consists of 20-30 μm sized pores and 40-60 μm pores.

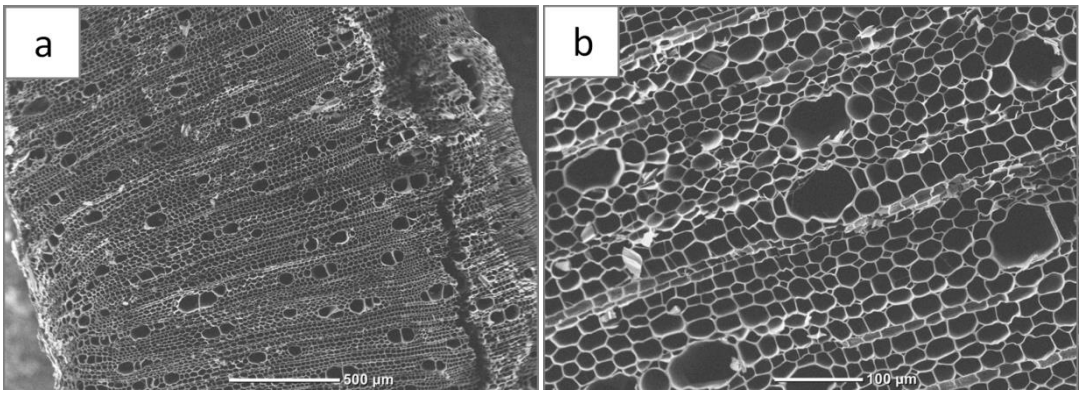

Figure 12. SEM images of hemp hurd at showing macropore channels.

Figure 13 are the SEM images of the longitudinal section of hemp hurd at different magnifications. Figure 14 are the SEM images of the cross section of hemp hurd at different magnifications. Figure 13 show that hemp hurd has a structure, which consists of two types of macropore channels of different sizes. One type is the round like or elliptic large pore channels with 40-60 μm in diameter, which is resulted from the vascular bundles. Another type of pore channel is the polygonal or round like pores with smaller diameter, 20-30 μm, which derives from the ground tissues and continuously distribute like honeycomb around the large pores. The channels are parallel to the growth direction of the hemp hurd result from water and nutrients transportation. These pore channels also have high porosity on its inner wall, leading to the formation of hierarchical pore structures and connected pore geometry.

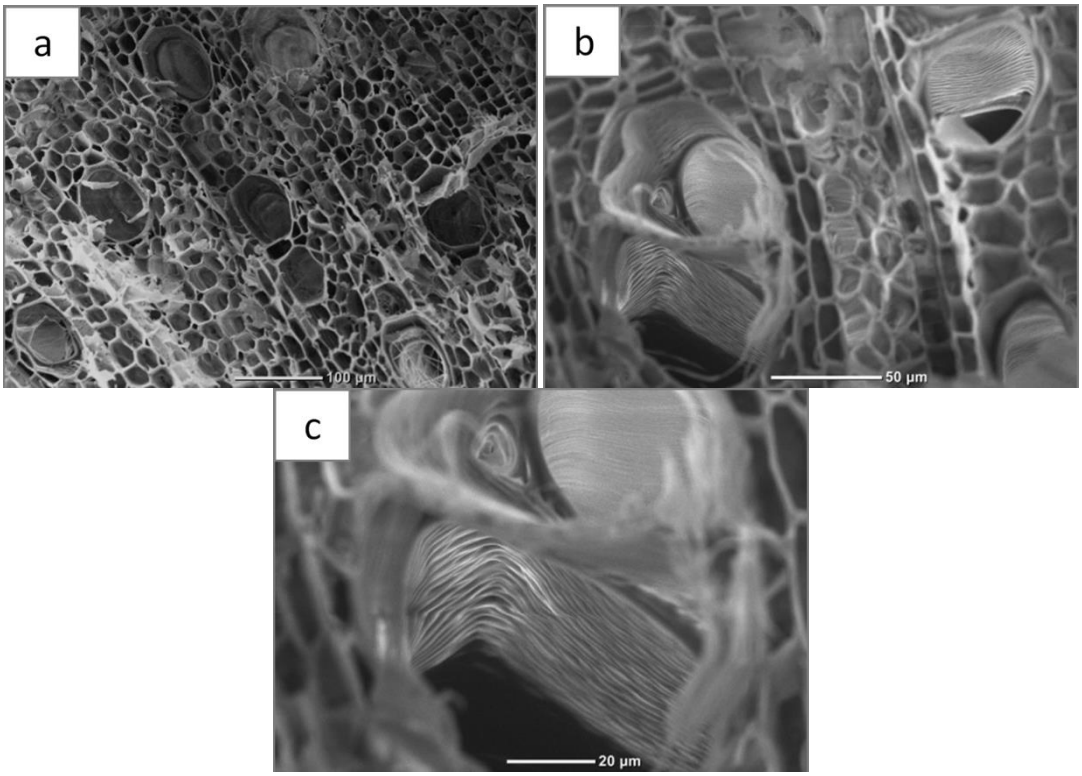

Figure 13. The longitudinal section of hemp hurd with hierarchical pore structures at different scales.

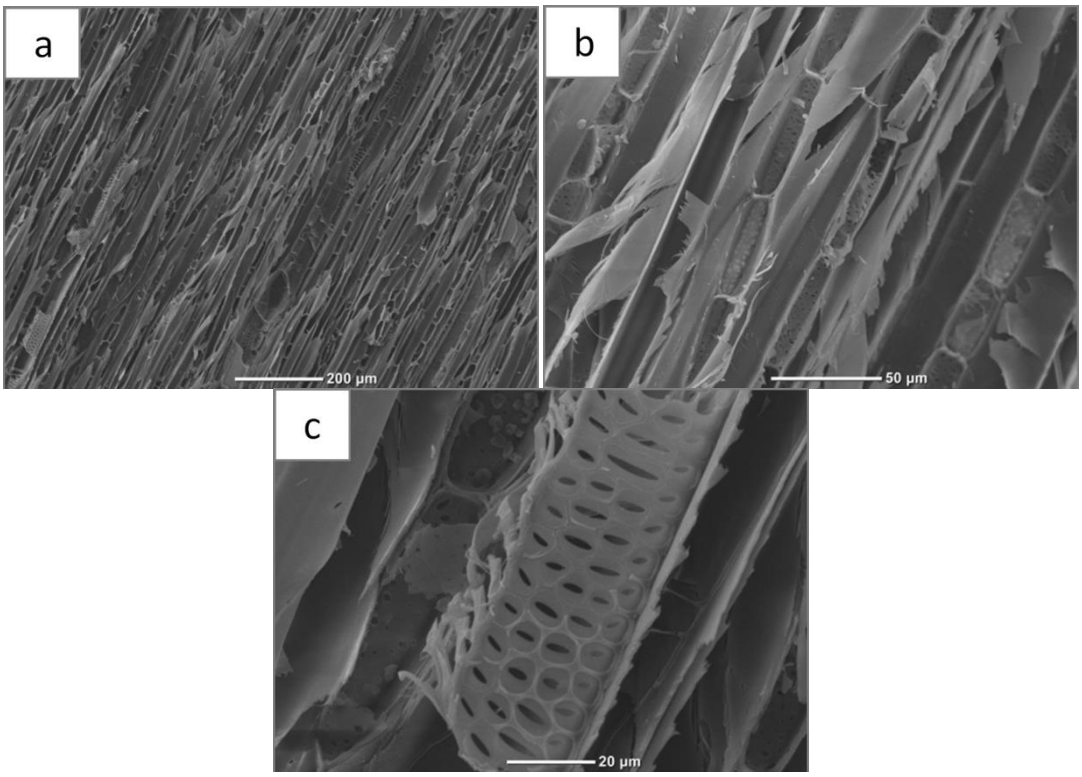

Figure 14. The cross section of hemp hurd with high porosity on its inner wall.

Figure 15 are the SEM images of the longitudinal section and cross section of hemp hurd and retted hemp hurd. It shows that hemp hurd has a structure, which consists of two types of macropore channels. These pore channels also have high porosity on its inner wall, leading to the formation of hierarchical pore structures and connected pore geometry. From Figure 15, the morphologies of the longitudinal section and cross section of retted hemp hurd are very similar with the morphologies of hemp hurd. The different is that, at the location of the large macropore channels, there are some coil like structures in both the longitudinal section and cross section of retted hemp hurd. Retting is the process to separate the fibres from hemp hurd, using microbes and moisture to dissolve the cellular tissues and pectin of the hemp bast bundles. From the morphology and location of the coil like structure, retting process corroded part of the larger pore channels and turned some of them into a coil like structure presumably.

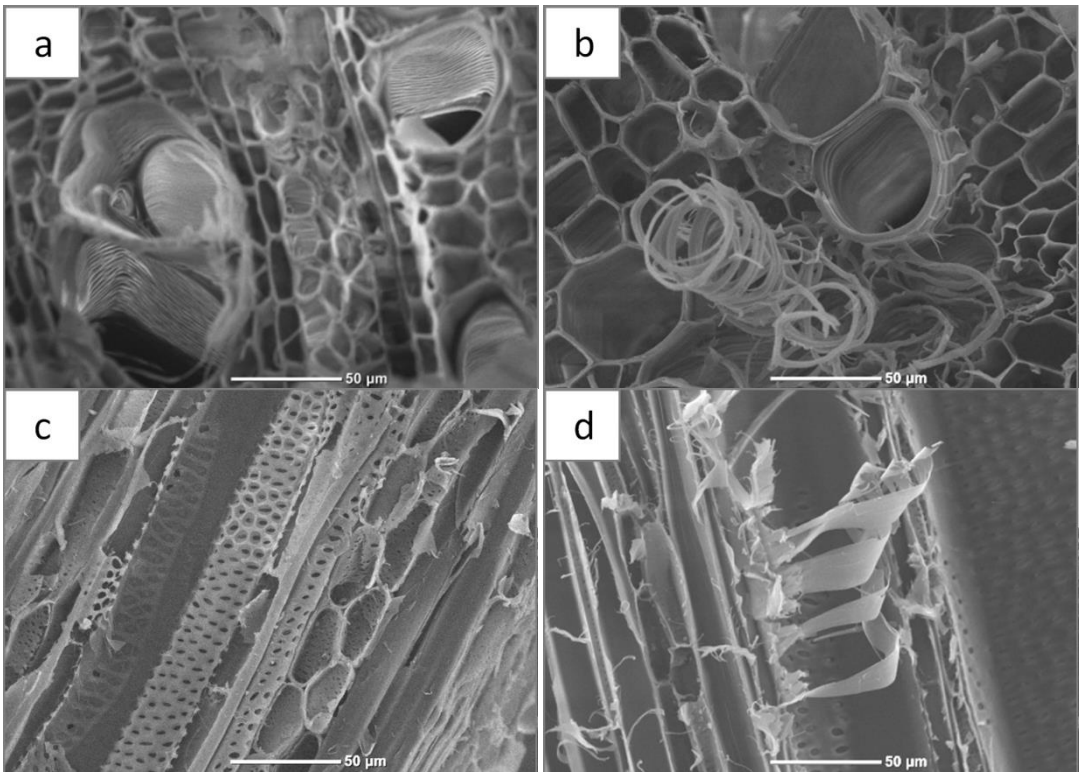

Figure 15. The longitudinal section of (a) hemp hurd with two types of channels, and (b) retted hemp hurd with two types of channels and coil like structures, and the cross section of (c) hemp hurd with pores on its inner wall, and (d) retted hemp hurd with pores and coil like structures.

4.2 Thermal properties of hemp hurd and retted hemp hurd

Figure 16 is the DSC curves of hemp hurd, semi retted hemp hurd and retted hemp hurd. It shows the endothermic peaks of hemp hurd, semi retted hemp hurd and retted hemp hurd. From the DSC curves, the initial decomposition temperature of hemp hurd is 291 °C, while the initial decomposition temperature of semi retted hemp hurd and retted hemp hurd are 298 °C and 308 °C respectively. The process of retting can effectively improve the thermal stability of hemp hurd. The thermal stability increased with increasing retting degree. Other researchers also observed

that the thermal stability of flax fibres with increasing retting degree (Martin, Mouret, Davies, & Baley, 2013; Vedoy, 2013).

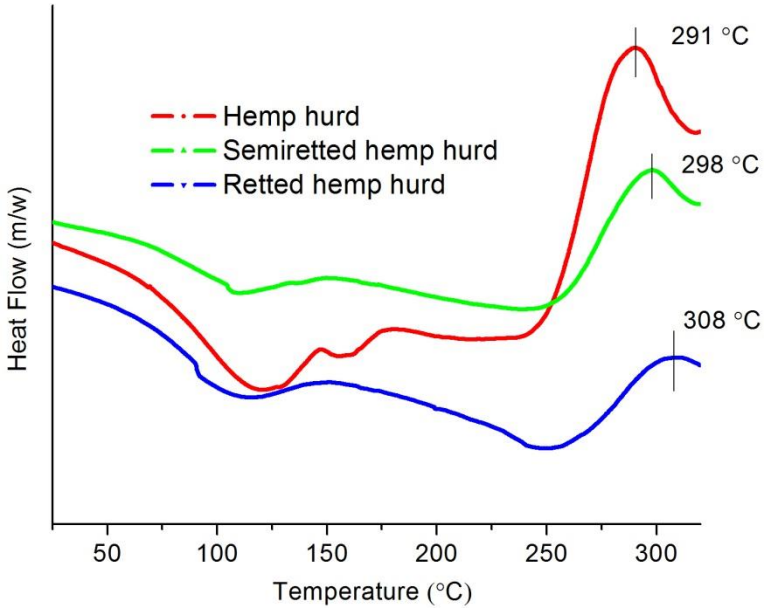

Figure 16. DSC curves of hemp hurd, semi retted hemp hurd and retted hemp hurd.

4.3 Yield of activated carbon

The yield of the activated carbon was estimated from Equation 11.

$$\text{Yield of activated carbon (wt. \%)} = \frac{\text{weight of activated carbon}}{\text{weight of waste biomass}} \times 100 \quad (11)$$

The chemical recovery (wt.%) was estimated from Equation 12:

$$\text{Chemical recovery (wt. \%)} = \frac{\{\text{sample weight (before washing)} - \text{sample weight (after washing)}\}}{\text{weight of impregnated chemical}} \times 100 \quad (12)$$

The yields of the activated carbons and the chemical recoveries in the activation process are shown in Table 2. The chemical recovery of the activated carbons produced from hemp hurd and retted hemp hurd by $ZnCl_2$ activation were around 97 wt.%. The yields of the activated carbons produced from hemp hurd and retted hemp

hurd by physical activation were lower than those of activated carbons by chemical activation. The yields of the activated carbons by $ZnCl_2$ activation with the impregnation ratio of 2:1 at 800 °C with retention time of 2 h reached around 29%, while those by CO_2 activation were about 20%. This result is similar to those obtained by other researchers. The yield of activated carbon fibre from hemp fibres under N_2 flow at 800°C without activation agent was 12.9% (J. M. Rosas et al., 2009). The yield of activated carbon monoliths from hemp stems at 800°C without activation agent was 16.6% (J. M. Rosas et al., 2009). The yields of activated carbons from hemp stems by KOH activation at 800°C with impregnation ratio of 4.5:1 with 3-4.5 h were 21.5-22.9%. It is worth noting that the yield of activated carbons reached 48.6% with 2h (Yang et al., 2012).

There are two reasons. The first reason is that some CO_2 reacted with the samples during the pyrolysis but there is no sample consumption in N_2 atmosphere by $ZnCl_2$ activation (S. Liu et al., 2017). Another reason is that the activation agent $ZnCl_2$ restricts the formation of tars during the carbonization process, thus increasing the yield of the remaining solid product (J. M. Rosas et al., 2009).

Table 2. The yields of the activated carbons by physical activation and chemical activation, and the chemical recoveries in the activation process.

Natural fibre	Activating agent	Sample	Yield (wt. %)	Chemical recovery (wt. %)*
Hemp hurd	CO_2	AC-HH-CO_2	20.7%	_
Retted hemp hurd	CO_2	AC-RH-CO_2	20.2%	_
Hemp hurd	$ZnCl_2$	AC-HH-$ZnCl_2$	30.3%	97.3%
Retted hemp hurd	$ZnCl_2$	AC-RH-$ZnCl_2$	28.6%	97.1%

*No chemical recovery for physical activation.

4.4 Morphology of precursors and the obtained activated carbons

The SEM images of raw hemp materials and activated carbons are shown in Figure 17. Figure 17 (a, b) are the full view of hemp hurd of different angles, (c, d) are the longitudinal and cross section of hemp hurd, (e, f) are the longitudinal and cross section of retted hemp hurd, and (g, h) are the obtained activated carbons AC-HH-CO_2 and AC-HH-$ZnCl_2$.

Hemp hurd and retted hemp hurd have a structure, which consists of two types of macropore channels. Retting process turned some of larger pore channels into a coil like structure (Figure 17 (a-f)). From Figure 17 (g, h), the activated carbons by both CO_2 activation and $ZnCl_2$ activation retain the original connected pore geometry of hemp hurd which consists of two types of macropore channels of different sizes. The difference of porosity and morphology of activated carbons by CO_2 activation and $ZnCl_2$ activation cannot be seen at this magnification.

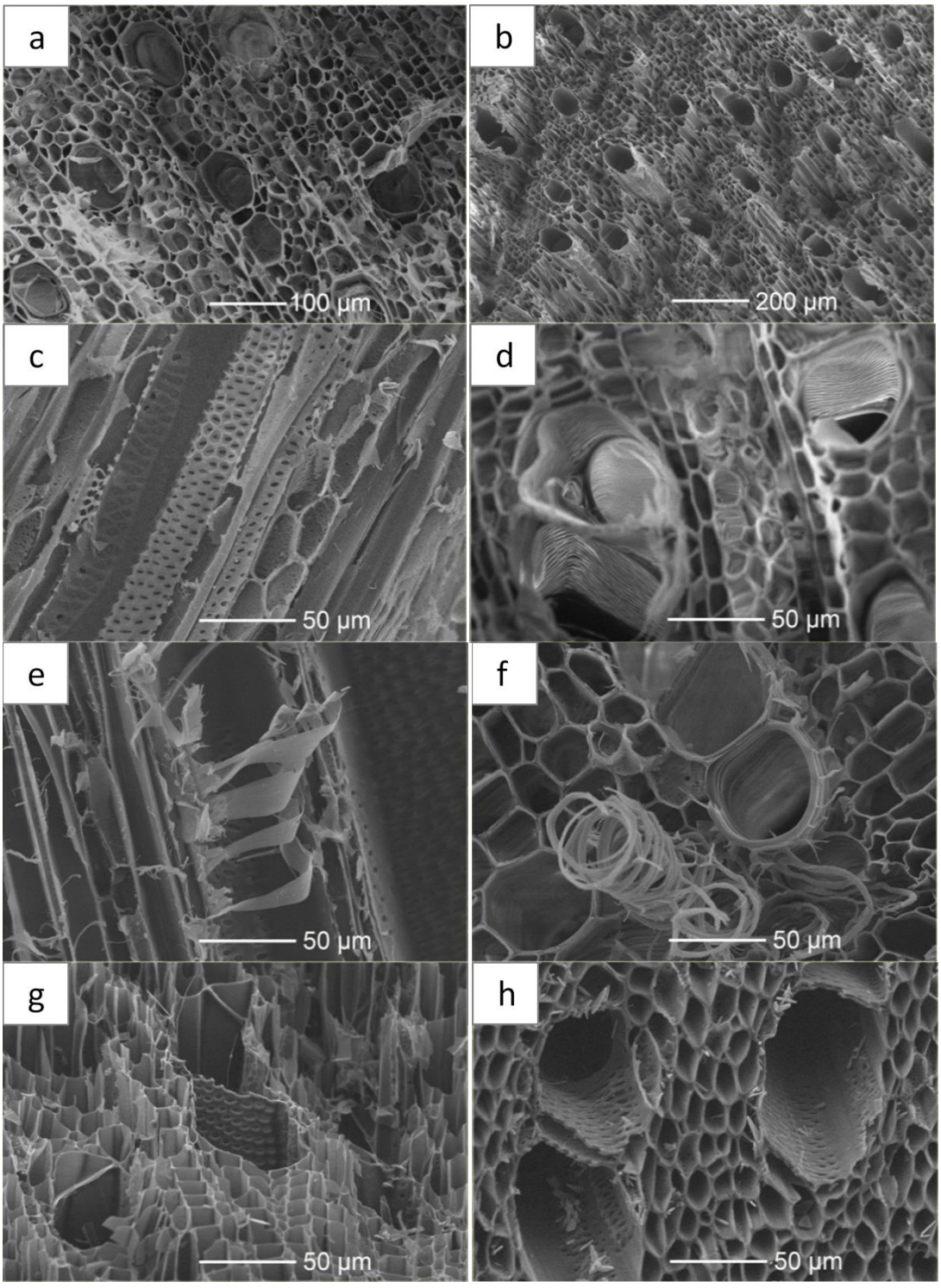

Figure 17. SEM images of (a, b) full view of hemp hurd of different angles, (c, d) the longitudinal and cross section of hemp hurd, (e, f) the longitudinal and cross section of retted hemp hurd and (g, h) the AC-HH-CO_2 and AC-HH-$ZnCl_2$.

4.5 Surface areas and porosity of activated carbon

The adsorption behaviour and pore structure of the activated carbons can be analysed using nitrogen adsorption isotherms. The shape of these isotherms can explain general properties of activated carbons. The N_2 adsorption–desorption isotherms of the activated carbons derived from hemp hurd and retted hemp hurd by CO_2 and $ZnCl_2$ activation are shown in Figure 18. The most frequently used isotherms in describing the nonlinear equilibrium are Langmuir isotherm and BET isotherm (Jodeh et al., 2016).

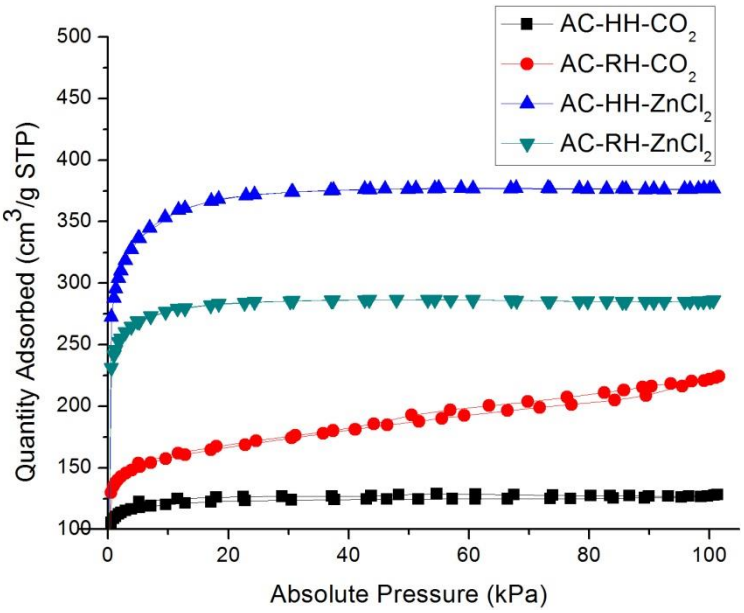

Figure 18. N_2 adsorption-desorption isotherms on activated carbons from hemp hurd and retted hemp hurd.

Table 3. Specific surface area and pore volume of the activated carbons obtained from N_2 isotherms at 77 K.

Sample	N_2 adsorption				
	S_{BET} ($m^2 \cdot g^{-1}$)	$S_{Langmuir}$ ($m^2 \cdot g^{-1}$)	V_{total} ($cm^3 \cdot g^{-1}$)	V_{micro} ($cm^3 \cdot g^{-1}$)	V_{meso} ($cm^3 \cdot g^{-1}$)
AC-HH-CO_2	489	545	0.198	0.170	0.008
AC-RH-CO_2	632	783	0.347	0.174	0.108
AC-HH-$ZnCl_2$	1431	1669	0.583	0.467	0.006
AC-RH-$ZnCl_2$	1128	1259	0.442	0.393	0.002

Figure 18 shows the adsorption and desorption of N_2 at 77 K on activated carbons. From the shape of the isotherms, it can be surmised that all activated carbons by $ZnCl_2$ activation exhibit Type I isotherms with a horizontal plateau at higher relative pressures, indicating highly microporous materials. The small hysteresis loops seen on the adsorption–desorption isotherms of the activated carbons occur because of the existence of mesopores (Demiral, Aydın Şamdan, & Demiral, 2016).

From Figure 18, the major uptake of N_2 adsorption-desorption isotherms on activated carbons from hemp hurd and retted hemp hurd can be observed at relative pressure less than 0.1. The initial part of the isotherm represents micropore filling, and a low slope of the plateau indicates multilayer adsorption on the external surface. The significant adsorption of N_2 at $P < 10$kPa is attributed to the adsorption in the micropores derived by $ZnCl_2$ activation.

The adsorption isotherms of the AC-HH-CO_2 exhibited Type I behaviour while AC-RH-CO_2 exhibited Type IV behaviour with clear Type-H3 hysteresis loops in the

relative pressure region, which demonstrated the wide mesopore distribution in the materials (Demiral et al., 2016). Type IV isotherms describe adsorption in AC-RH-CO_2 with a mixture of micropores and mesopores.

Table 3 summarizes yield, Langmuir specific surface area, BET specific surface area, pore, and pore volume of the obtained activated carbons. The calculation in Table 3 are in agreement with the conclusions. It also confirms that the mesopores volume of AC-RH-CO_2 is higher than that of other activated carbons.

4.6 CO_2 adsorption capacity of activated carbon

Figure 19 shows the adsorption of CO_2 at 273 K on activated carbon prepared from hemp hurd and retted hemp hurd by CO_2 activation and $ZnCl_2$ activation. The CO_2 adsorption capacities of activated carbons from $ZnCl_2$ activation were higher than those by CO_2 activation, which can be attributed to their higher surface areas and pore volume. AC-RH-$ZnCl_2$ showed the highest CO_2 adsorption capacities, because of their high surface functionality and morphological differences which were further explored.

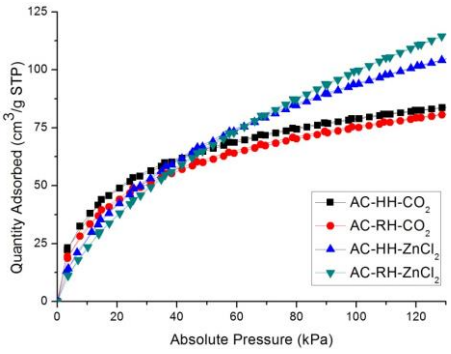

Figure 19. Adsorption of CO_2 at 273 K on activated carbon prepared from hemp hurd and retted hemp hurd by CO_2 activation and $ZnCl_2$ activation.

CHAPTER 5 THE EFFECT OF PHYSICAL ACTIVATION AND CHEMICAL ACTIVATION ON ACTIVATED CARBON PROPERTIES

The effect of physical activation and chemical activation on the properties of derived activated carbon was compared in this chapter. Bamboo is a renewable precursor for low-cost activated carbon production, is widely utilized. In this study, the biomass materials hemp hurd, retted hemp hurd and bamboo were used as the precursors of activated carbon. They were activated by physical activation and chemical activation.

Activated carbons were produced by CO_2 activation in a two-step process as the chapter 3 described. The obtained activated carbons from hemp hurd and retted hemp hurd are labelled as AC-HH-CO_2 and AC-RH-CO_2. Activated carbons produced by $ZnCl_2$ activation were carried out in three stages as the chapter 3 described. The obtained activated carbons from hemp hurd and retted hemp hurd are labelled as AC-HH- $ZnCl_2$ and AC-RH- $ZnCl_2$.

5.1 Morphology of bamboo fibre

Meisam K. Habibi and Lu (Habibi & Lu, 2014) characterised the morphology of the bamboo culm, as shown in Figure 20. Vascular bundles of bamboo along with the parenchyma ground and bamboo fibres along the (a, c) transversal direction, and (b, d) longitudinal direction are seen. In their research, bamboo fibres and parenchyma cells, comparably, possess the majority of bamboo culm whereas vessels constitute a lower fraction.

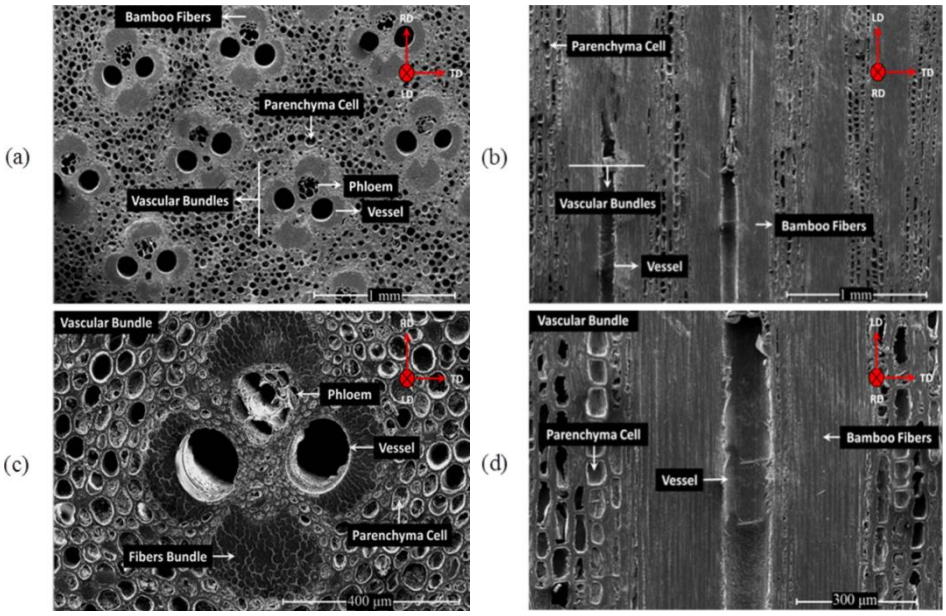

Figure 20. SEM of the bamboo culm. Zoom-in views of bamboo's vascular bundles along with the parenchyma ground and bamboo fibres along the transversal (a, c) and longitudinal (b, d) directions (Habibi & Lu, 2014).

For comparison with hemp hurd structure, the bamboo fibres construction was investigated. Figure 21 shows the SEM images of the longitudinal section of bamboo fibre at different magnifications. Many pores on its inner wall can be seen. Figure 22 shows the SEM images of the cross section of bamboo fibre. Honeycomb-like structure can be seen from this angle. When compared to bamboo fibre, hemp hurd has hierarchical pore structures and connected macropores, providing an opportunity for preparing activated carbon with low gas diffusion resistance in gas adsorption.

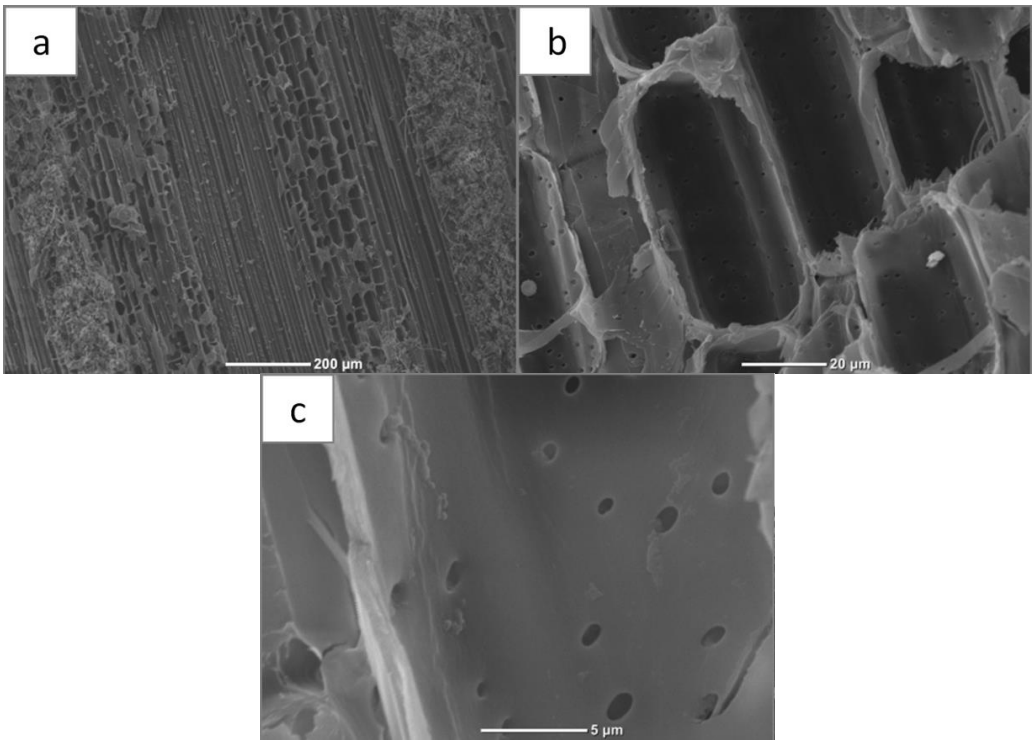

Figure 21. The longitudinal section of bamboo fibre with pores on its inner wall at different magnifications.

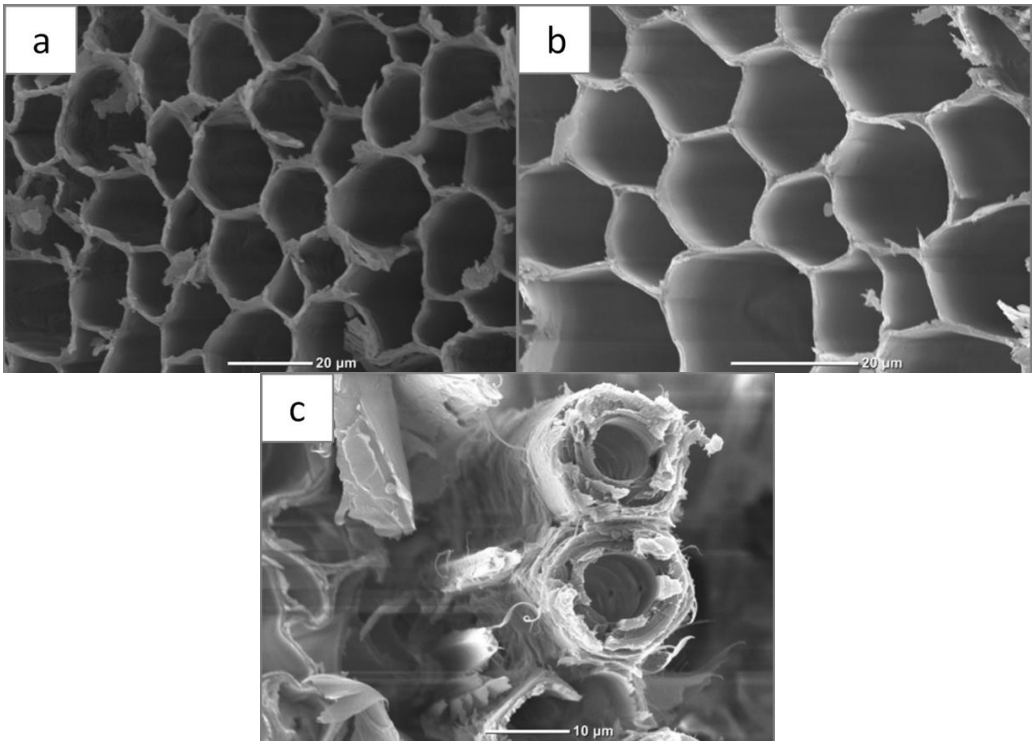

Figure 22. The cross section of bamboo fibre with honeycomb like structure at different magnifications.

5.2 Thermal properties of precursors

The thermal stability of bamboo fibre was compared with the thermal stability of hemp hurd and retted hemp hurd. Figure 23 shows the DSC thermograms of bamboo fibre, hemp hurd, and retted hemp hurd, showing the endothermic peaks of bamboo fibre, hemp hurd, and retted hemp hurd. The decomposition temperature of bamboo fibre, hemp hurd, and retted hemp hurd are 279 °C, 291 °C and 308 °C respectively. From the thermograms, the thermal stability of hemp hurd and retted hemp hurd is higher than bamboo. Since the initial decomposition temperature of them are all around 300 °C, the carbonization stage of the biomass was carried out in the range of 400-800 °C in the following experiments.

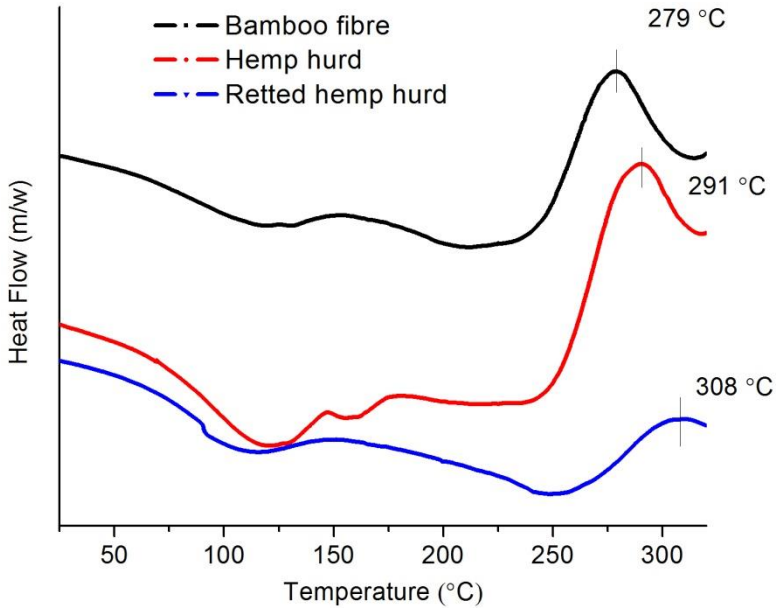

Figure 23. DSC curves of bamboo, hemp hurd and retted hemp hurd.

5.3 Yield and elemental analysis of activated carbon

The yields of the activated carbons and the chemical recoveries in the chemical activation process are shown in Table 4. The chemical recovery of the activated

carbons produced from hemp hurd, retted hemp hurd and bamboo fibre by $ZnCl_2$ activation were around 97 wt.%.

The yields of the activated carbons from hemp hurd and retted hemp hurd by $ZnCl_2$ activation reached 30%, while those by CO_2 activation were approximately 20%. The yields difference of the activated carbons from bamboo fibre produced by CO_2 activation and $ZnCl_2$ activation was small. The yields of the activated carbons from hemp hurd, retted hemp hurd and bamboo fibre by $ZnCl_2$ activation were all around 30%. The yields of the activated carbons produced by physical activation were lower than those of activated carbons produced by chemical activation. This is one of the advantages of activated carbons produced by chemical activation, which were taken into consideration in the following studies.

Table 4. The yields of the activated carbons by CO_2 activation and $ZnCl_2$ activation, and the chemical recoveries in the activation process.

Natural fibre	Activating agent	Sample	Yield (wt. %)	Chemical recovery (wt. %)
Hemp hurd	CO_2	AC-HH-CO_2	20.7%	_
Retted hemp hurd	CO_2	AC-RH-CO_2	20.2%	_
Bamboo fibre	CO_2	AC-Bamboo-CO_2	27.7%	_
Hemp hurd	$ZnCl_2$	AC-HH-$ZnCl_2$	30.3%	97.3%
Retted hemp hurd	$ZnCl_2$	AC-RH-$ZnCl_2$	28.6%	97.1%
Bamboo fibre	$ZnCl_2$	AC-Bamboo-$ZnCl_2$	29.1%	97.7%

Table 5 is the elemental analysis by XPS of the activated carbon from hemp hurd, retted hemp hurd and bamboo fibre by $ZnCl_2$ activation before and after HCl washing. As shown in Table 5, activated carbons derived from hemp hurd, retted hemp hurd and bamboo fibre by $ZnCl_2$ activation mainly consist of C, O, N, Zn and Cl. From Table 5, the Zn and Cl on the activated carbons by $ZnCl_2$ activation were removed after HCl washing and deionized water washing.

Table 5. The elemental analysis of the activated carbon from hemp hurd, retted hemp hurd and bamboo fibre by $ZnCl_2$ activation before and after HCl washing.

	AC-HH-$ZnCl_2$		AC-RH-$ZnCl_2$		AC-Bamboo-$ZnCl_2$	
Element	Before washing	After washing	Before washing	After washing	Before washing	After washing
C	94.98	96.47	95.32	94.64	93.91	95.19
O	4.08	3.24	4.21	4.44	5.25	4.04
N	0.47	0.29	0.02	0.92	0.68	0.77
Zn	0.19	0	0.18	0	0.06	0
Cl	0.27	0	0.26	0	0.10	0

5.4 Surface areas and porosity of activated carbon

The effect of the activation method of activated carbons on various porous characteristics such as surface area, pore volume, micropore volume, and mesopore volume was investigated. Table 6 and Figure 24 summarize the specific surface area and pore volume of the activated carbons derived from hemp hurd, retted hemp hurd and bamboo fibre by CO_2 activation and $ZnCl_2$ activation from the N_2 isotherms at 77 K. Specific surface area was calculated from the adsorption branch according to the BET and Langmuir method at a relative pressure in the range of the P/P_0 = (0.05-

0.35). The total pore volume was calculated by converting the amount of nitrogen adsorbed at a relative pressure of 0.995 to the volume of liquid adsorbate. Micropore volume was calculated using the t-plot method, and the mesopore volume was determined as the difference between the total pore volume and the micropore volume.

Table 6. Specific surface area and pore volume of the activated carbons by CO_2 activation and $ZnCl_2$ activation obtained from N_2 isotherms at 77 K.

Sample	N_2 adsorption				
	S_{BET} ($m^2 \cdot g^{-1}$)	$S_{Langmuir}$ ($m^2 \cdot g^{-1}$)	V_{total} ($cm^3 \cdot g^{-1}$)	V_{micro} ($cm^3 \cdot g^{-1}$)	V_{meso} ($cm^3 \cdot g^{-1}$)
AC-HH-CO_2	489	545	0.198	0.170	0.028
AC-RH-CO_2	632	783	0.347	0.174	0.173
AC-BF-CO_2	39	31	0	0	0
AC-HH-$ZnCl_2$	1431	1669	0.583	0.467	0.116
AC-RH-$ZnCl_2$	1128	1259	0.442	0.393	0.049
AC-BF-$ZnCl_2$	1213	1402	0.496	0.399	0.097

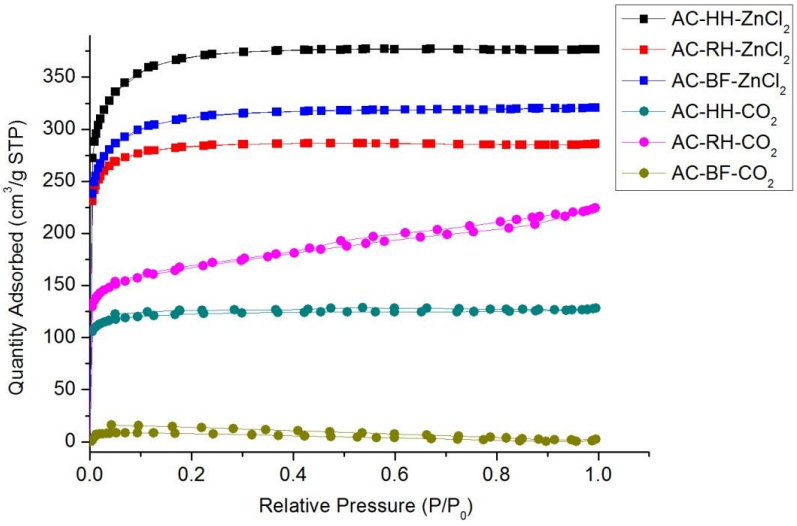

Figure 24. N_2 adsorption-desorption curves on activated carbons from hemp hurd, retted hemp hurd and bamboo fibre by CO_2 activation and $ZnCl_2$ activation.

Activation method significantly influences the specific surface area and pore volume of activated carbons. Although the surface areas of these activated carbons are different, $ZnCl_2$ activation is more beneficial for synthesis of high surface area of porous carbon from biomass, and the derived activated carbons using this method have much larger surface area compared with those using CO_2 activation. High-quality activated carbons was obtained from hemp hurd, retted hemp hurd and bamboo fibre by $ZnCl_2$ activation after HCl washing with high surface area (> 1100 m^2/g) and total pore volume (> 0.4 cm^3/g).

During CO_2 activation, porosity is developed by carbon gasification according to the reaction "$C+CO_2 \longrightarrow 2CO$". CO_2 reacts with the carbon in biomass at high temperatures.

During $ZnCl_2$ activation, $ZnCl_2$ act as a template for the pore formation. Firstly, $ZnCl_2$ can act as a dehydrating agent, catalysing the scission of glyosidic bonds and

the elimination of hydroxyl and carbonyl groups during heating. Impregnation with $ZnCl_2$ first results in degradation of the cellulosic material and on carbonization produces, dehydration that results in charring and aromatization of the carbon skeleton and creation of the pore structure. Secondly, the fused $ZnCl_2$ can react with H_2O generated from the cleavage of the biopolymer, leading to the formation of $Zn_2OCl_2.2H_2O$. Then, $ZnCl_2$ gas is generated from the decomposition of $Zn_2OCl_2.2H_2O$, and the gas diffusion developed pathways, creating the pore structure and high surface area of the obtained activated carbon after acid washing (S. Liu et al., 2017; Zhang et al., 2016).

The BET surface areas of the activated carbons by $ZnCl_2$ activation are greater than 1100 m^2/g. The obtained activated carbons exhibited comparable surface areas and pore volumes by $ZnCl_2$ activation. Although the surface areas of these carbons are different, $ZnCl_2$ activation is effective for synthesis of high surface area of porous carbon from biomass and the derived carbons using this method have much larger surface area compared with those using CO_2 activation. The $ZnCl_2$ activation provides significant contributions of micropores to the total surface area.

J.M. Rosas et al. (J. M. Rosas et al., 2009) showed that the best surface area of activated carbon derived from hemp fibre reached 1355 m^2/g in their experiment. In Table 6, the activated carbon derived from retted hemp hurd had the highest BET surface area of 1431 m^2/g, which can be considered as a competitive precursor of activated carbons.

The adsorption performance of adsorbent is highly dependent on the internal pore structure, and large specific surface area is beneficial for adsorption through

increasing the contact frequency between the adsorbates and adsorbents. Thus, the obtained activated carbons are expected to have large adsorption capacity.

5.5 CO_2 adsorption capacity of activated carbon

Figure 25 shows the CO_2 adsorption curves at 273 K on activated carbon by CO_2 activation and $ZnCl_2$ activation. A summary of the adsorption of CO_2 at 273 K on activated carbon from hemp hurd, retted hemp hurd and bamboo fibre by CO_2 activation and $ZnCl_2$ activation is provided in Table 7. Activated carbon from retted hemp hurd by $ZnCl_2$ activation has the highest CO_2 adsorption capacity among the variants investigated in this study. The adsorptions of CO_2 on activated carbon from hemp hurd, retted hemp hurd and bamboo fibre at 273 K reach 105, 116 and 108 cm^3/g STP respectively.

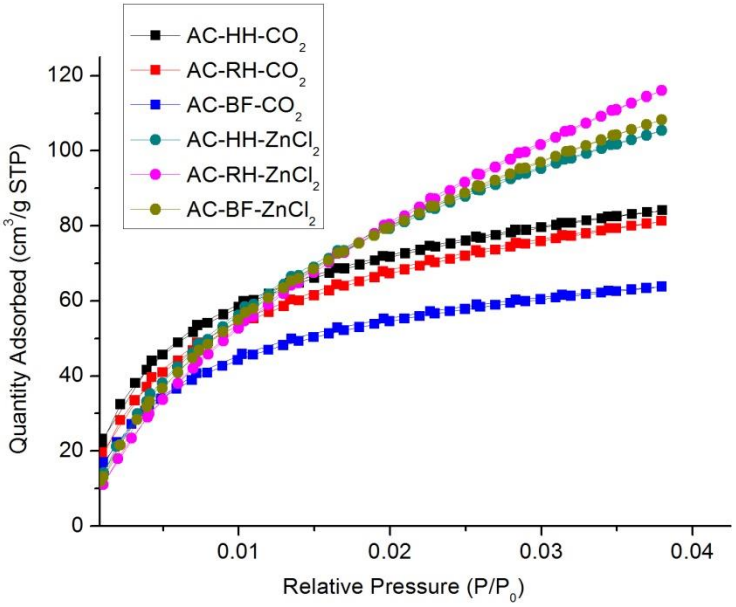

Figure 25. CO_2 adsorption at 273 K on activated carbons from hemp hurd, retted hemp hurd and bamboo fibre by CO2 activation and ZnCl2 activation.

Table 7. CO_2 adsorption at 273 K on activated carbon from hemp hurd, retted hemp hurd and bamboo by CO_2 activation and $ZnCl_2$ activation.

Sample	CO_2 adsorption (cm^3/g STP)
AC-HH-CO2	84
AC-RH-CO2	81
AC-BF-CO2	64
AC-HH-ZnCl2	105
AC-RH-ZnCl2	116
AC-BF-ZnCl2	108

The activated carbons by $ZnCl_2$ activation have much larger CO_2 adsorption capacities compared with those using CO_2 activation. This result is consistent with the comparison of yield, specific surface area and pore volume results of the activated carbons by $ZnCl_2$ activation and CO_2 activation. All the results showed that the activated carbons by $ZnCl_2$ activation are superior than those by CO_2 activation in this study. Therefore, the activated carbon by $ZnCl_2$ activation was further studied in the following chapters.

CHAPTER 6 THE EFFECT OF ACTIVATION TEMPERATURE AND IMPREGNATION RATIO ON ACTIVATED CARBON PROPERTIES

The development of porosity in activated carbon mainly depends on various process parameters involved in the preparation such as raw material used and activation method (Gottipati & Mishra, 2016). The properties of activated carbon derived from hemp hurd and retted hemp hurd by CO_2 activation are better than those by $ZnCl_2$ activation.

The properties of activated carbon derived from hemp hurd are similar with the activated carbon derived from retted hemp hurd. In industry, retted hemp hurd is more abundantly than hemp hurd. In the following experiments, retted hemp hurd was chosen as precursors to produce $ZnCl_2$-activated activated carbon. To optimize preparation, the effect of variables such as the carbonization temperature and the impregnation ratio on textural and chemical-surface properties of the activated carbons was studied. The ratio of activation agent to biomass was selected in the range of 2:1-4:1, and the carbonization stage was carried out in the range of 400-800 °C. The yields, specific surface areas, pore volumes, and pore sizes of the activated carbons were determined. The gas capture performance of the synthesized activated carbons was evaluated for CO_2 adsorption.

6.1 Morphology of precursors

To explore the reaction mechanisms of $ZnCl_2$ activation, a series of morphologies of activated carbons with the impregnation ratios of 2:1, 3:1, and 4:1 and carbonization temperatures of 400, 500, 600, 700, and 800 °C were studied. The surface morphologies of the activated carbons produced by $ZnCl_2$ activation, before and after HCl washing were examined using SEM and the corresponding micrographs are presented in this section.

Figure 26 is the SEM image of activated carbons derived from retted hemp hurd using $ZnCl_2$ activation with carbonization temperature of 400 °C at various impregnation ratios before HCl washing. Figure 26 (a, b) (c, d) (e, f) are the activated carbons with the impregnation ratio of 2:1, 3:1, and 4:1, respectively. As can be seen, at 400 °C with the impregnation ratio of 2:1, $ZnCl_2$ becomes liquid, the presence of well-dispersed droplet-like $ZnCl_2$ with an average diameter of ca. 2-8 μm on the surfaces of activated carbon are clearly indicated. At 400 °C with the impregnation ratio of 3:1, $ZnCl_2$ and ZnO co-exist in the system. The droplet-like $ZnCl_2$ and irregular ZnO flakes can be seen. At 400 °C with the impregnation ratio of 4:1, $ZnCl_2$ almost all transformed into irregular ZnO flakes.

This transformation is because the anhydrous form $ZnCl_2$ melts at around 320 °C, and remains molten below 400 °C. Above 400 °C, $ZnCl_2$ vaporizes and is partly oxidized to ZnO. ZnO is thermally stable with a melting temperature of above 1975 °C and is insoluble in both water and alcohol (Jones, Tran, Lindberg, Zhao, & Hupa, 2013).

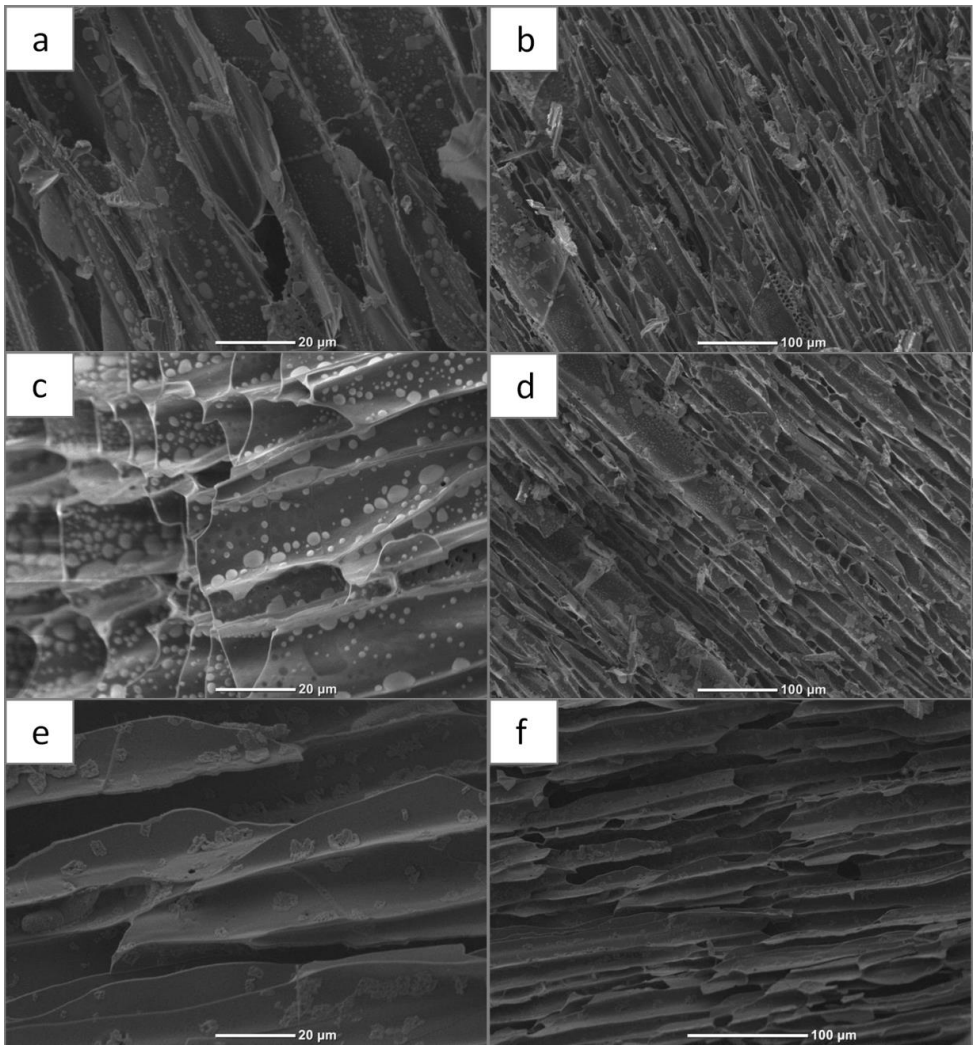

Figure 26. Activated carbon derived from retted hemp hurd in 400 °C before HCl washing, (a, b) $ZnCl_2$ impregnation ratio 2:1, (c, d) $ZnCl_2$ impregnation ratio 3:1, (e, f) ZnCl2 impregnation ratio 4:1.

$ZnCl_2$, which impregnated on the precursors, firstly results in degradation of the cellulosic part of precursors. Then on carbonization, produces dehydration that results in charring and aromatization of the carbon skeleton and creation of the pore structure (Caturla, Molina-Sabio, & Rodríguez-Reinoso, 1991). The anhydrous form of $ZnCl_2$ is highly hygroscopic, rapidly absorbing moisture from the ambient air, and transforming into one of five hydrates. Reactions involving $ZnCl_2$ and ZnO are

provided below. $ZnCl_2$ may react with oxygen according to Equation 13, or with H_2O according to Equation 14 to form ZnO.

$$ZnCl_2 + H_2O(g) \rightarrow ZnO + 2HCl(g) \quad (13)$$

$$ZnCl_2 + 1/2\ O_2(g) \rightarrow ZnO + Cl_2(g) \quad (14)$$

SEM of activated carbons derived from retted hemp hurd by $ZnCl_2$ activation with the carbonization temperature of 500 °C at various impregnation ratios before HCl washing are shown in Figure 27. Figure 27 (a, b) (c, d) (e, f) are the activated carbons with the impregnation ratio of 2:1, 3:1, and 4:1, respectively. As can be seen, at 500 °C with the impregnation ratio of 2:1, $ZnCl_2$ becomes hexagonal flaky ZnO, and there is a tendency for ZnO layers to accumulate as agglomerates. These hexagonal ZnO flaky were also reported by other researcher (Zhou, Wang, Huang, & Liu, 2008). With the impregnation ratio of 3:1 and 4:1, both droplet-like $ZnCl_2$ and irregular ZnO flaky crystals on the surfaces of activated carbon are realised.

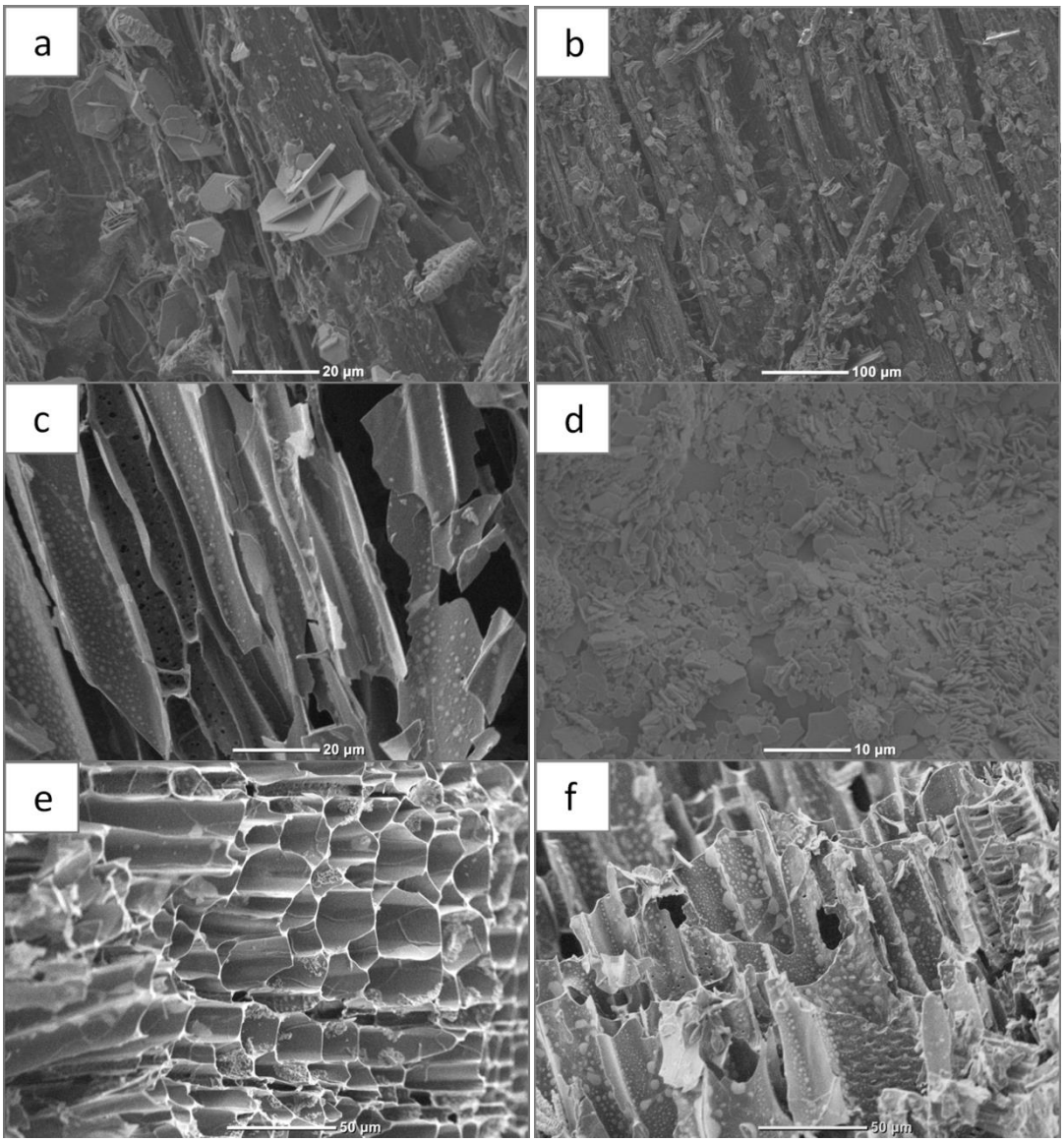

Figure 27. Activated carbon derived from retted hemp hurd in 500 °C before HCl washing (a, b) $ZnCl_2$ impregnation ratio 2:1, (c, d) $ZnCl_2$ impregnation ratio 3:1, (e, f) $ZnCl_2$ impregnation ratio 4:1.

Figure 28 shows the SEM images of activated carbons derived from retted hemp hurd by $ZnCl_2$ activation with the carbonization temperature of 600 °C at various impregnation ratios before HCl washing. Figure 28 (a, b) (c, d) (e, f) show the activated carbons with the impregnation ratio of 2:1, 3:1, 4:1, respectively. As can be seen, at 600 °C with the impregnation ratio of 2:1, ZnO becomes hexagonal pyramid and hexagonal columns, and these ZnO crystals combined to spinels. Zn possesses a

more stable oxide form, and that the volatilization of Zn could be inhibited by the formation of spinels (Jones et al., 2013). At 600 °C with the impregnation ratio of 3:1, some of the ZnO becomes irregular flakes, and remaining regular ZnO flakes tend to form stacking clusters. At 600 °C with the impregnation ratio of 4:1, ZnO assumes flakes and hexagonal columnar structure.

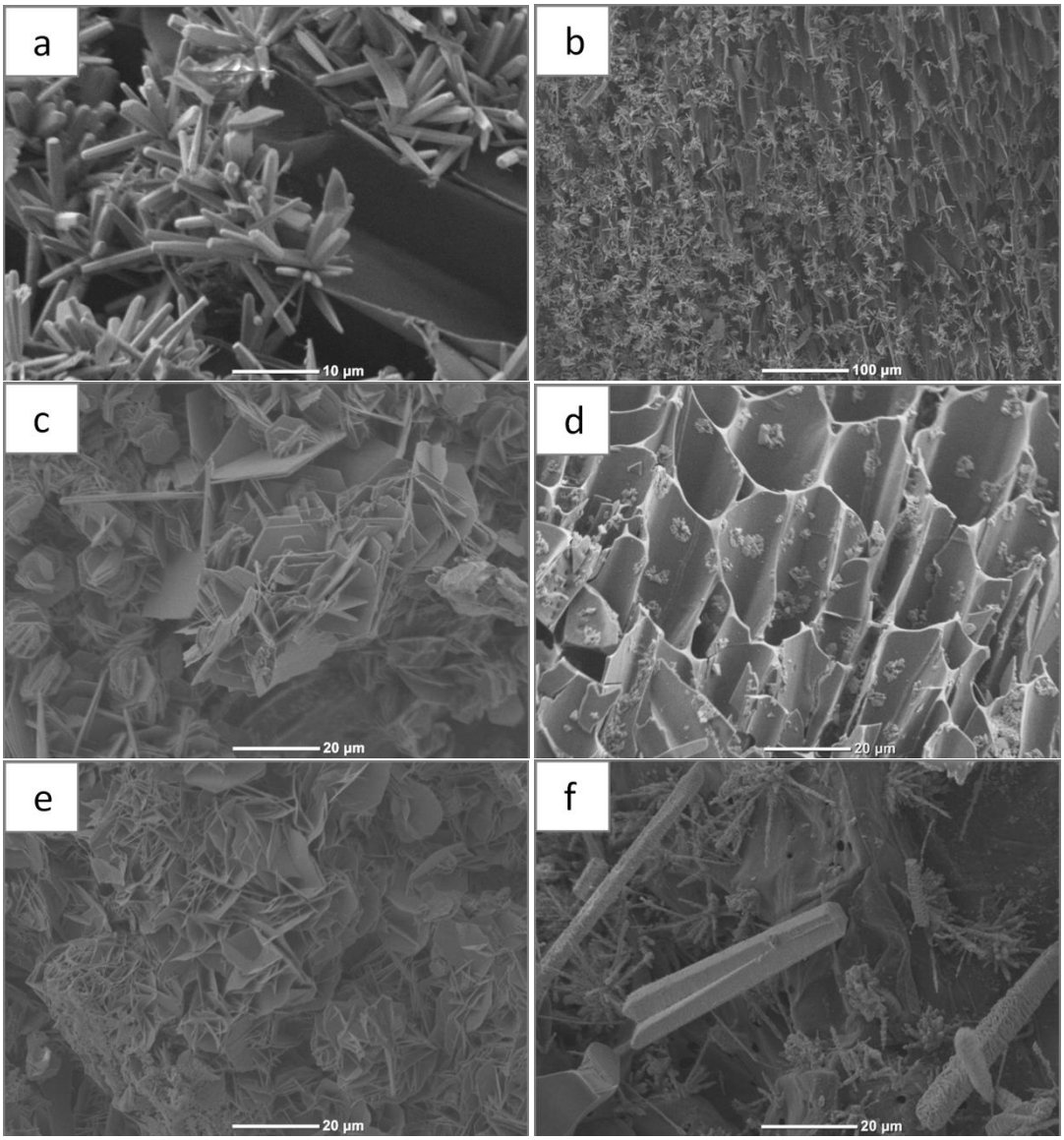

Figure 28. Activated carbon derived from retted hemp hurd in 600 °C before HCl washing (a, b) $ZnCl_2$ impregnation ratio 2:1, (c, d) $ZnCl_2$ impregnation ratio 3:1, (e, f) $ZnCl_2$ impregnation ratio 4:1.

Figure 29 shows the SEM images of activated carbons derived from retted hemp hurd by $ZnCl_2$ activation with the carbonization temperature of 700 °C at various impregnation ratios before HCl washing. Figure 29 (a, b) (c, d) (e, f) show the activated carbons with the impregnation ratio of 2:1, 3:1, and 4:1, respectively. As can be seen, at 700 °C with the impregnation ratio of 2:1, ZnO hexagonal columns and small $ZnCl_2$ drops co-exist on activated carbons. In theory, the boiling point of $ZnCl_2$ is 732 °C, but because of the nanosize effect and low partial pressure of $ZnCl_2$, it vaporizes at low temperatures as 700 °C. Other researchers also observed that the weight loss peak locations of $ZnCl_2$ were significantly reduced to lower temperature; they detected the existence of small $ZnCl_2$ by X-ray diffraction (Zhang et al., 2016). So presumably, the small white dots are particle-like $ZnCl_2$ steam condensate. At 700 °C with the impregnation ratio of 3:1 and 4:1, ZnO becomes hexagonal pyramid and hexagonal columns, and these ZnO crystals combined to spinels.

Figure 30 shows the SEM images of activated carbons derived from retted hemp hurd by $ZnCl_2$ activation with the carbonization temperature of 800 °C at various impregnation ratios before HCl washing. Figure 30 (a, b) (c, d) (e, f) show the activated carbons with the impregnation ratio of 2:1, 3:1, and 4:1, respectively. As revealed by SEM, at 800 °C, ZnO becomes hexagonal pyramid and hexagonal columns, and these ZnO crystals combined to spinels. The difference is that the amount of ZnO crystals on activated carbons increases as the impregnation rate increases.

Figure 31 shows the SEM images of activated carbons derived from retted hemp hurd by $ZnCl_2$ activation with the impregnation ratio of 2:1 on 400 °C after HCl washing. As revealed by SEM, the morphology of the bulk of activated carbons from retted hemp hurd after HCl washing keeps the original appearance of the retted hemp

hurd. As can be seen in Figure 31b, these pore channels also have high porosity on the inner wall. The ordered natural pore channels provide suitable base for the reaction of precursor and activation agent to obtain high surface area microporous activated carbons, in which the micropores are mainly formed on the surface of the channels, and the channels also act as pathways for gas molecule to enter and be adsorbed in the micropores (Yang et al., 2012).

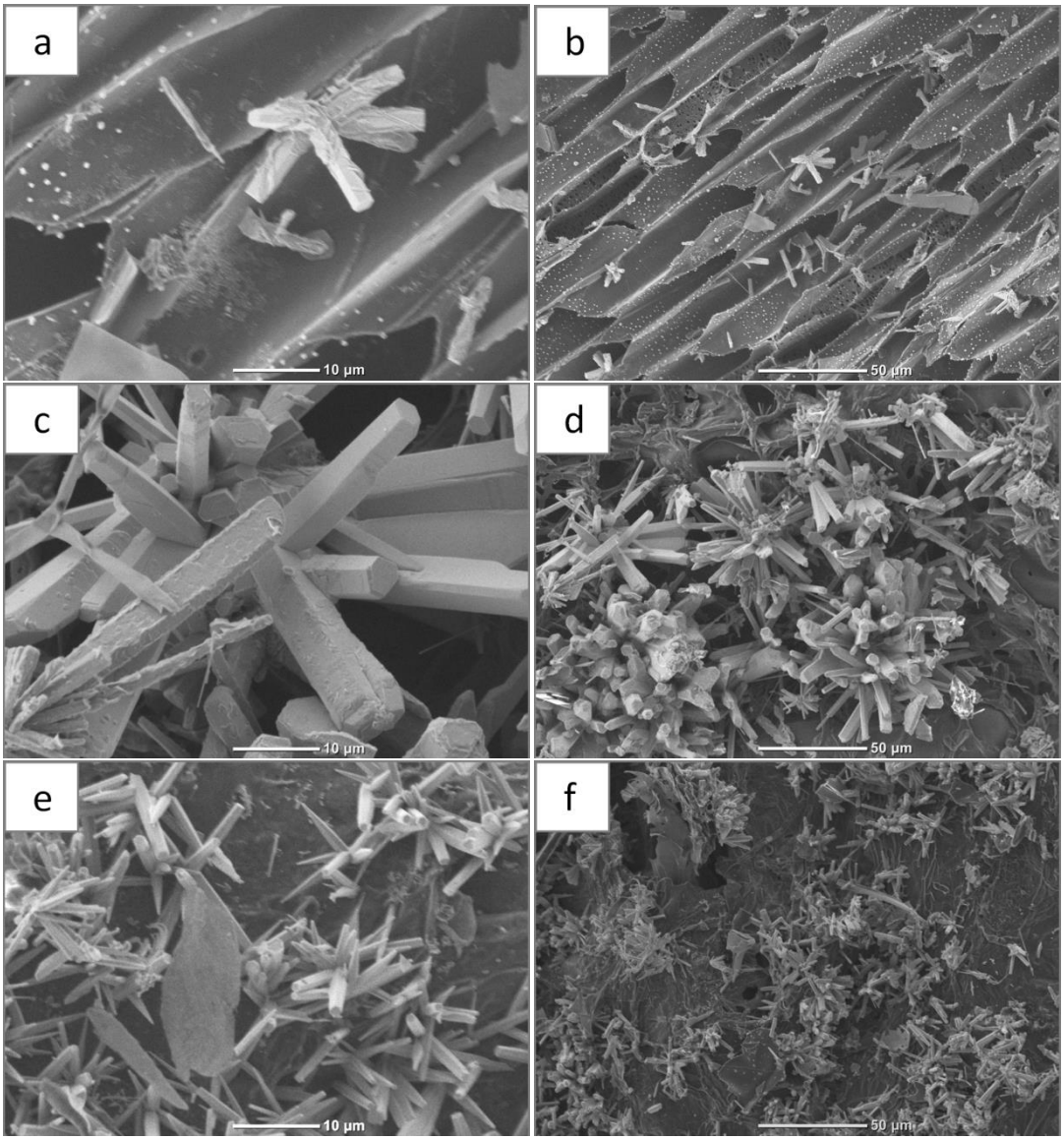

Figure 29. Activated carbon derived from retted hemp hurd in 700 °C before HCl washing (a, b) $ZnCl_2$ impregnation ratio 2:1, (c, d) $ZnCl_2$ impregnation ratio 3:1, (e, f) $ZnCl_2$ impregnation ratio 4:1.

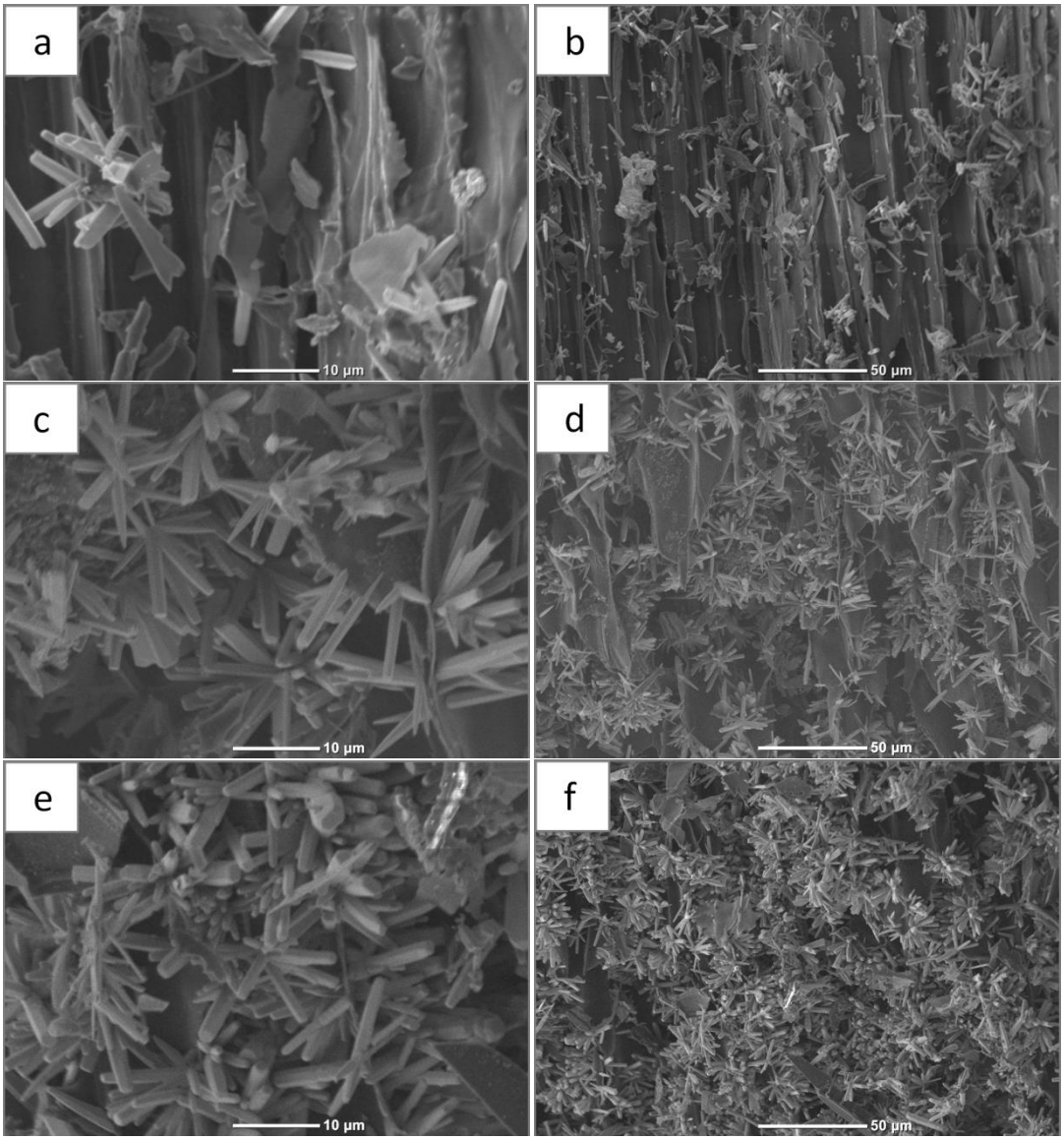

Figure 30. Activated carbon derived from retted hemp hurd in 800 °C before HCl washing (a, b) $ZnCl_2$ impregnation ratio 2:1, (c, d) $ZnCl_2$ impregnation ratio 3:1, (e, f) $ZnCl_2$ impregnation ratio 4:1.

The whole bulk and micro-morphologies of the activated carbons derived from retted hemp hurd by $ZnCl_2$ activation with other impregnation ratios and activation temperatures are similar with Figure 31a and Figure 31b, but the cross sections are quite different. The texture resulted from the decomposition of the sample matrix after the impregnation and the heat treatment in nitrogen atmosphere. The evaporation of the activation agent during the heat treatment creates spaces that were

previously occupied by activation agent for adsorption process (Arampatzidou & Deliyanni, 2016).

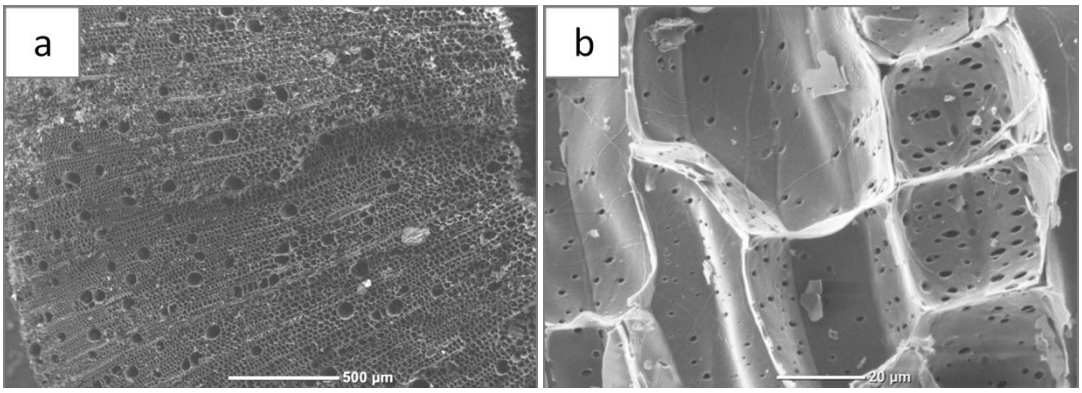

Figure 31. SEM images of full view of activated carbons from retted hemp hurd after HCl washing at different magnifications.

The cross sections of activated carbon derived from retted hemp hurd in 400 °C with different $ZnCl_2$ impregnation ratio (a) 2:1, (b) 3:1, and (c) 4:1 after HCl washing are shown in Figure 32. As can be seen in Figure 32, at 400 °C with the impregnation ratio of 2:1, there are many coil-like structures which develop from the round-like or elliptic large pore channels of retted hemp hurd. Figure 32a is the $ZnCl_2$-activated activated carbon with $ZnCl_2$ impregnation ratio of 3:1 and 4:1. The activated carbon fused together, and formed layered pore structures, clearly indicating the coil-like structures disappeared on the surfaces, as shown in Figure 32b, c.

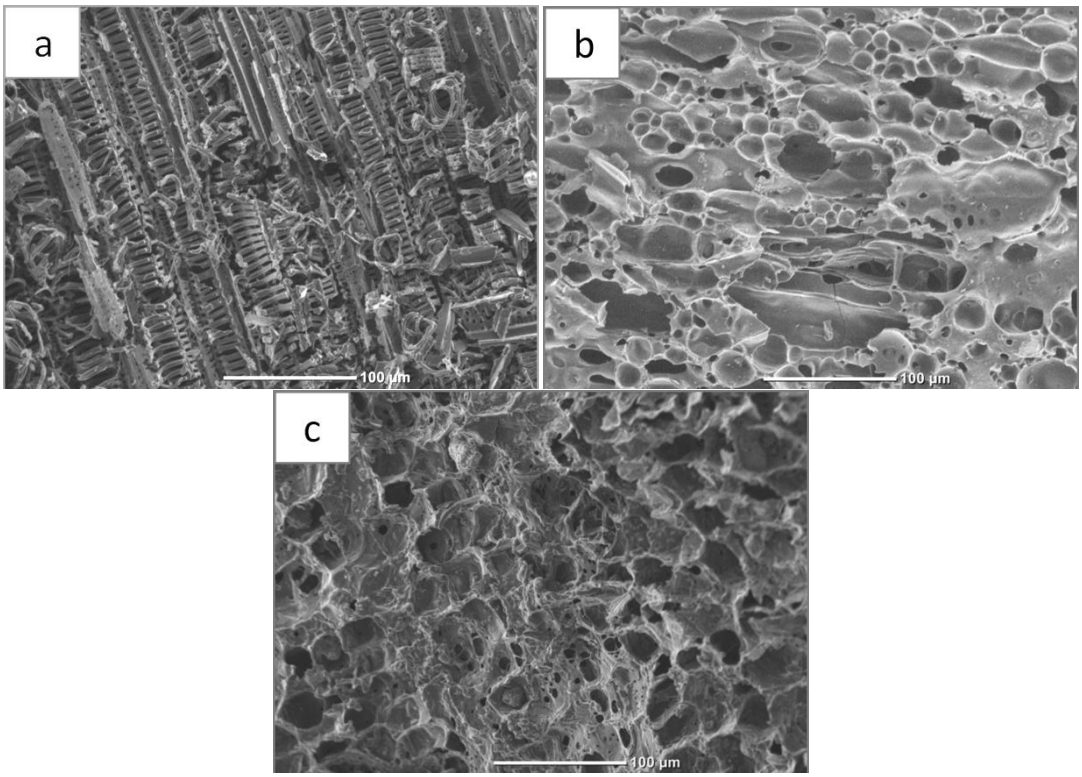

Figure 32. The cross section of activated carbon derived from retted hemp hurd in 400 °C with different $ZnCl_2$ impregnation ratio (a) 2:1, (b) 3:1, (c) 4:1 after HCl washing.

Figure 33 shows the cross sections of activated carbon derived from retted hemp hurd in 500 °C with different $ZnCl_2$ impregnation ratio (a) 2:1, (b) 3:1, and (c) 4:1 after HCl washing. As revealed by SEM, at 500 °C, the activated carbon fused together. Some of the round-like large pore channels of retted hemp hurd still exist with an impregnation ratio of 2:1. Activated carbon formed a layered pore structures with the impregnation ratio of 4:1.

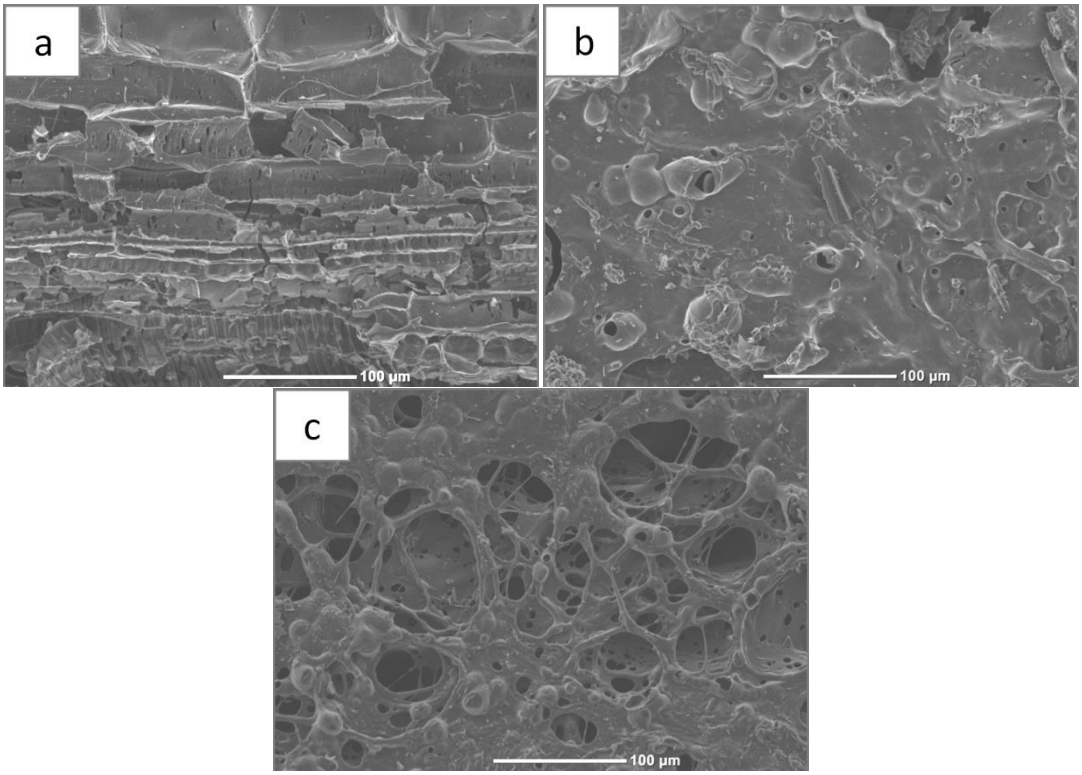

Figure 33. The cross section of activated carbon derived from retted hemp hurd in 500 °C with different $ZnCl_2$ impregnation ratio (a) 2:1, (b) 3:1, (c) 4:1 after HCl washing.

Figure 34 shows the cross sections of activated carbon derived from retted hemp hurd in 600 °C with different $ZnCl_2$ impregnation ratios of (a) 2:1, (b) 3:1, and (c) 4:1 after HCl washing. As determined by SEM, at 600 °C with the impregnation ratio of 2:1, activated carbon still retain the unique structures of retted hemp hurd, but with increased porosity of the inner walls. With the impregnation ratio of 3:1 and 4:1, the coil-like structures which come from the round like or elliptic large pore channels of retted hemp hurd coexists with fused activated carbon structures.

Figure 35 shows the cross sections of activated carbon derived from retted hemp hurd in 700 °C with different $ZnCl_2$ impregnation ratio (a) 2:1, (b) 3:1, and (c) 4:1 after HCl washing. As can be seen in Figure 35, at 700 °C with the impregnation

ratio of 2:1 and 3:1, activated carbon still keep the unique structures of retted hemp hurd with higher porosity. With the impregnation ratio of 4:1, the coil-like structures which grow from the round-like or elliptical large-pore channels of retted hemp hurd exist.

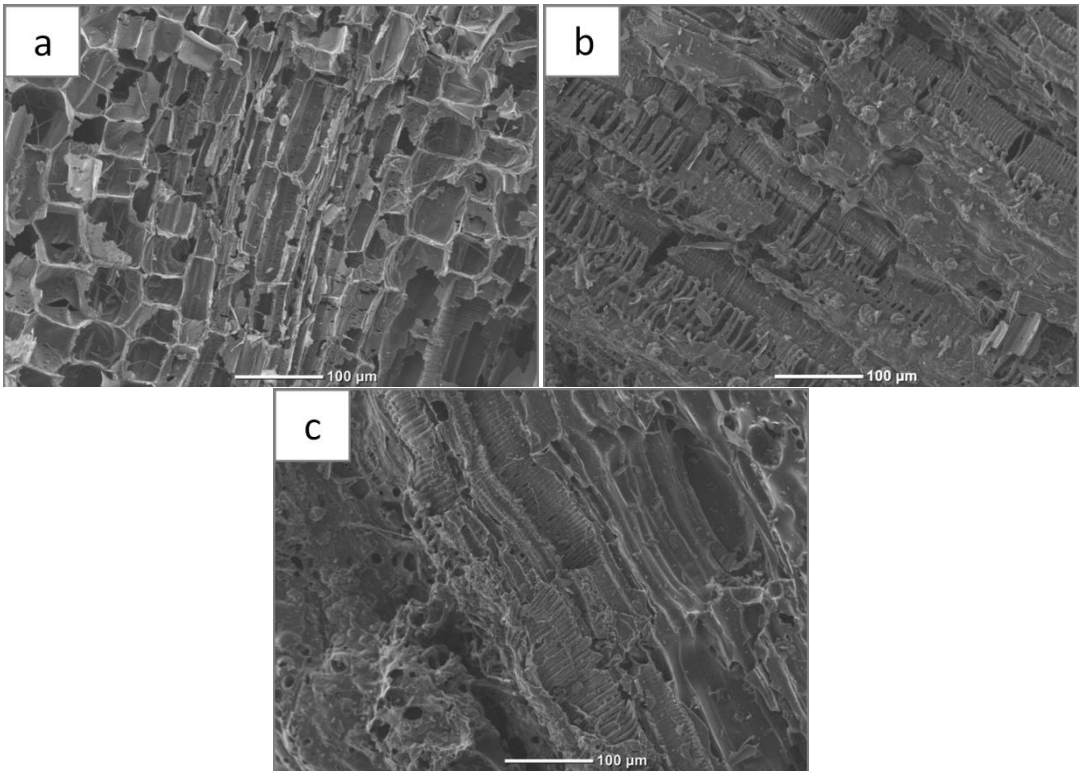

Figure 34. The cross section of activated carbon derived from retted hemp hurd in 600 °C with different $ZnCl_2$ impregnation ratio (a) 2:1, (b) 3:1, (c) 4:1 after HCl washing.

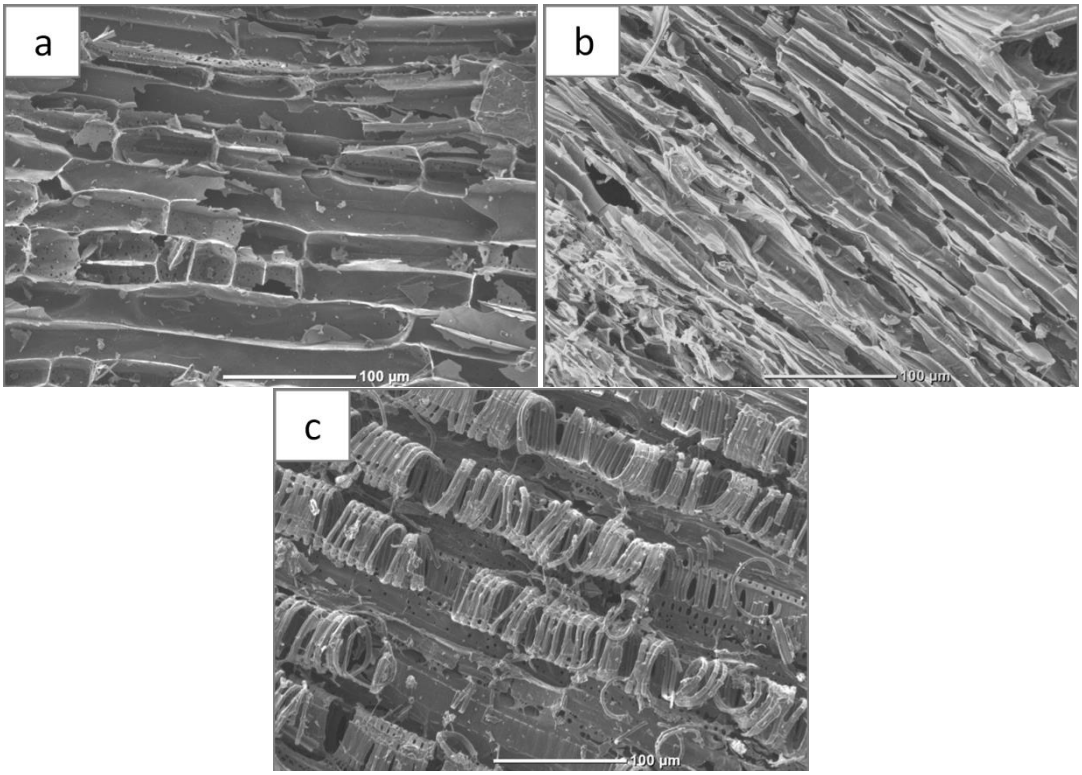

Figure 35. The cross section of activated carbon derived from retted hemp hurd in 700 °C with different $ZnCl_2$ impregnation ratio (a) 2:1, (b) 3:1, (c) 4:1 after HCl washing.

Figure 36 shows the cross sections of activated carbon derived from retted hemp hurd in 800 °C with different $ZnCl_2$ impregnation ratio (a) 2:1, (b) 3:1, (c) 4:1 after HCl washing. As revealed by SEM, at 800 °C with the impregnation ratio of 2:1 and 3:1, activated carbon still keep the unique structures of retted hemp hurd, but the porosity of the inner walls increased a lot. With the impregnation ratio of 4:1, the activated carbon fused together.

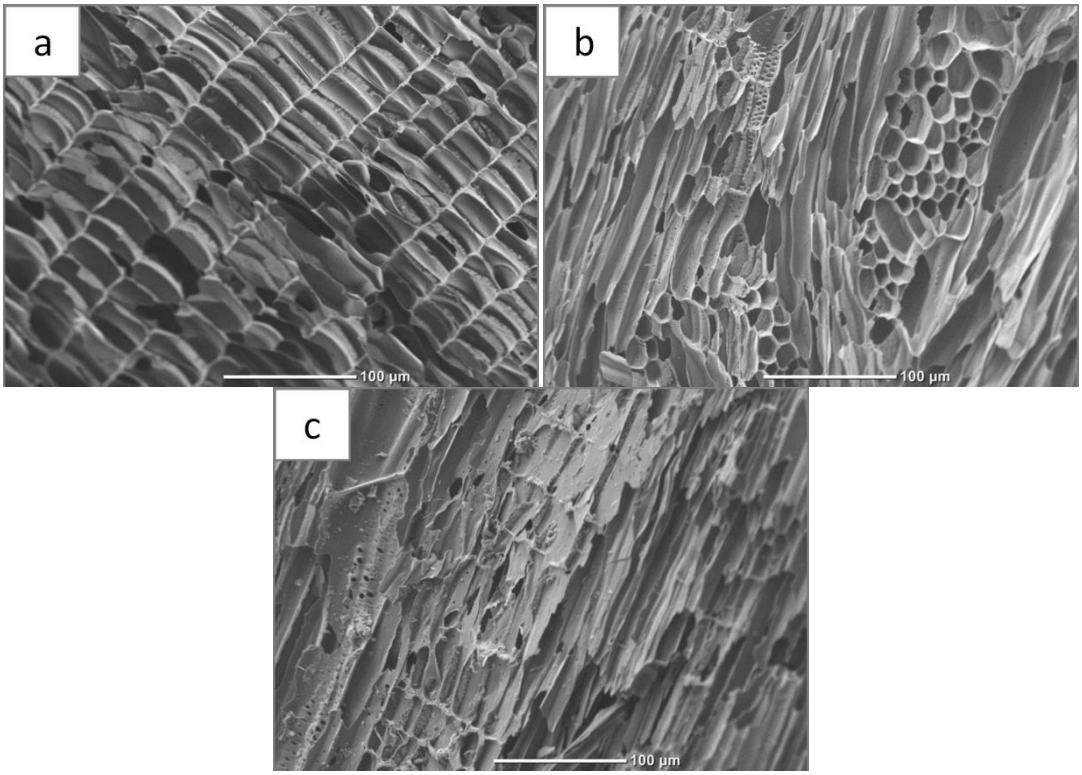

Figure 36. The cross section of activated carbon derived from retted hemp hurd in 800 °C with different $ZnCl_2$ impregnation ratio (a) 2:1, (b) 3:1, (c) 4:1 after HCl washing.

In summary, the morphologies of activated carbons derived from retted hemp hurd by $ZnCl_2$ activation with different carbonization temperature at various impregnation ratios were studied. Before HCl washing, at high temperatures (700-800 °C), Zn possesses a more stable oxide form on activated carbons including ZnO hexagonal pyramid and ZnO hexagonal columns, and some of these ZnO combined to spinels. Specially, particle-like $ZnCl_2$ steam condensate exist on activated carbons on 700 °C with the impregnation ratio of 2:1, because $ZnCl_2$ vaporized at around 700 °C. At low temperatures (400-500 °C), droplet-like $ZnCl_2$ and irregular ZnO flakes co-exist. After HCl washing, the porosity of the activated carbon inner walls increased a lot. Some activated carbons fused together and formed layered pore structures.

6.2 Retted hemp hurd

6.2.1 Yield of activated carbon

The effects of the impregnation ratio and the activation temperature on the activation process with regard to the surface chemistry and the development of the porous structure were examined.

Figure 37 shows yields of the activated carbons derived from retted hemp hurd by $ZnCl_2$ activation in relation to the influence of $ZnCl_2$ impregnation ratio and activation temperature. Table 8 presents the detailed yield data of activated carbons after washing and drying the sample. The results show that the activation temperature possessed a significant effect on the final yield of activated carbons. A higher activation temperature results in a lower yield of carbon, because of a high dehydration of the carbonaceous structure of the precursor. At the lower activation temperature (400-600 °C), there was a trend towards an increase in yield of carbon with increasing impregnation ratio. However, at the higher activation temperature (700-800 °C), the opposite tendency was observed. This trend can be attributed to higher impregnation ratios that restrict the formation of tars and volatiles, and produce a deeper dehydration at lower activation temperatures, thus increasing the carbon content, as previously observed by others (Juana M. Rosas et al., 2008). However, at the higher activation temperature, this effect is weakened.

Table 8. The yields of the activated carbons derived from retted hemp hurd by $ZnCl_2$ activation with different $ZnCl_2$ impregnation ratio and activation temperature after HCl washing.

Sample label	Activation temperature (°C)	Impregnation ratio of $ZnCl_2$ (wt. /wt.)	Yield (wt. %)
RH-400-2:1		2:1	60.8
RH-400-3:1	400	3:1	78.0
RH-400-4:1		4:1	75.7
RH-500-2:1		2:1	54.3
RH-500-3:1	500	3:1	64.4
RH-500-4:1		4:1	64.0
RH-600-2:1		2:1	41.3
RH-600-3:1	600	3:1	50.3
RH-600-4:1		4:1	50.6
RH-700-2:1		2:1	36.6
RH-700-3:1	700	3:1	34.3
RH-700-4:1		4:1	22.4
RH-800-2:1		2:1	28.6
RH-800-3:1	800	3:1	15.5
RH-800-4:1		4:1	13.2

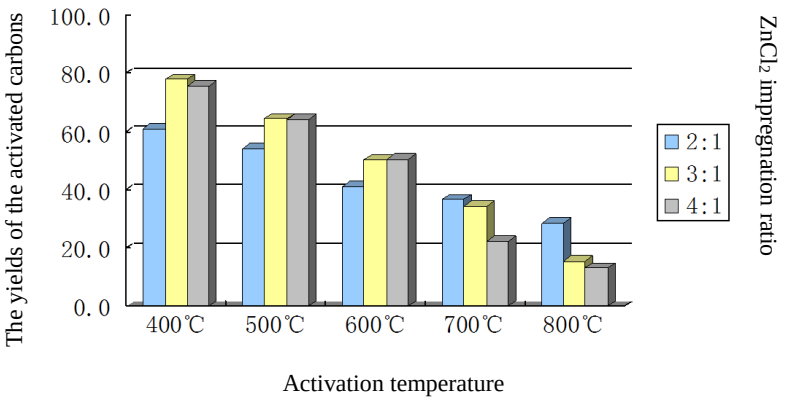

Figure 37. The yields of the activated carbons derived from retted hemp hurd by $ZnCl_2$ activation after HCl washing.

6.2.2 Surface areas and porosity of activated carbon

Activated carbon is characterized by surface areas and pore volumes. It has been reported that the high-quality activated carbons must have 800-1500 m^2/g surface area and 0.2-0.6 cm^3/g total pore volume (Erdem et al., 2016). The effect of the activation temperature and impregnation ratio on various porous characteristics such as surface area, pore volume, micropore volume and mesopore volume was investigated. Table 9 summarizes the specific surface area and pore volume of the activated carbons derived from retted hemp hurd by $ZnCl_2$ activation with different impregnation ratios (2:1, 3:1 and 4:1) and activation temperatures (400, 500, 600, 700 and 800 °C), before and after HCl washing from the N_2 isotherms at 77 K.

Specific surface area was calculated from the adsorption branch according to the BET and Langmuir method at a relative pressure in the range of the P/P_0 = (0.05-0.35). The total pore volume was calculated by converting the amount of nitrogen adsorbed at a relative pressure of 0.995 to the volume of liquid adsorbate; micropore volume using the t-plot method and the mesopore volume was determined as the difference between the total pore volume and the micropore volume (S. Liu et al., 2017).

From Table 9, the activation temperature, impregnation ratio and HCl washing significantly influence the specific surface area and pore volume of the obtained activated carbons. High-quality activated carbons were obtained from retted hemp

hurd by $ZnCl_2$ activation after HCl washing with high surface area (> 780 m^2/g) and total pore volume (> 0.3 cm^3/g).

Table 9. Specific surface area and pore volume of the activated carbons derived from retted hemp hurd by $ZnCl_2$ activation with different impregnation ratio and activation temperature before and after HCl washing obtained from N_2 isotherms at 77 K.

Sample label	S_{BET} ($m^2.g^{-1}$)		$S_{Langmuir}$ ($m^2.g^{-1}$)		V_{total} ($cm^3.g^{-1}$)		V_{micro} ($cm^3.g^{-1}$)		V_{meso} ($cm^3.g^{-1}$)	
	Before	After	Before	After	Before	After	Before	After	Before	After
RH-400-2:1	0	1089	0	1277	0	0.468	0	0.343	0	0.125
RH-400-3:1	0	1261	0	1572	0	0.590	0	0.349	0	0.241
RH-400-4:1	0	1468	0	1873	0	0.698	0	0.385	0	0.313
RH-500-2:1	0	794	0	891	0	0.318	0	0.273	0	0.045
RH-500-3:1	0	1558	0	2071	0	0.741	0	0.330	0	0.411
RH-500-4:1	0	1708	0	2411	0	0.861	0	0.278	0	0.583
RH-600-2:1	696	787	784	866	0.276	0.300	0.233	0.282	0.043	0.018
RH-600-3:1	269	1351	458	1955	0.149	0.712	0.005	0.204	0.144	0.508
RH-600-4:1	125	1781	257	2824	0.083	1.023	0.024	0.133	0.059	0.890
RH-700-2:1	474	1157	523	1326	0.177	0.468	0.169	0.384	0.008	0.084

Sample label	S_{BET} ($m^2.g^{-1}$)		$S_{Langmuir}$ ($m^2.g^{-1}$)		V_{total} ($cm^3.g^{-1}$)		V_{micro} ($cm^3.g^{-1}$)		V_{meso} ($cm^3.g^{-1}$)	
	Before	After	Before	After	Before	After	Before	After	Before	After
RH-700-3:1	566	1297	915	1520	0.307	0.539	0.035	0.412	0.272	0.127
RH-700-4:1	749	1352	977	2273	0.340	0.795	0.185	0.064	0.155	0.731
RH-800-2:1	985	1128	1134	1259	0.397	0.442	0.324	0.393	0.073	0.049
RH-800-3:1	1012	1357	1505	2199	0.546	0.785	0.144	0.075	0.402	0.710
RH-800-4:1	1128	1403	1812	2287	0.646	0.800	0.078	0.106	0.568	0.694

Figure 38 and Figure 39 are BET specific surface area and total pore volume charts of the activated carbons from retted hemp hurd by $ZnCl_2$ activation with different impregnation ratio and activation temperature before and after HCl washing obtained from N_2 isotherms at 77 K. As can be seen from Figure 38, before HCl washing, the BET specific surface area of the activated carbon seems irregular with different impregnation ratio and activation temperature. It reaches the maximum (1128 m^2/g) on 800 °C with impregnation ratio of 4:1. All of the BET specific surface areas of the activated carbons increased largely after HCl washing. The BET specific surface areas increase with the increase of impregnation ratio no matter what the activation temperature is. The optimized BET specific surface area of the activated carbon reaches 1781 m^2/g on 600 °C with impregnation ratio of 4:1. Figure 38 and Figure 39 show that the BET specific surface area and total pore volume of activated carbons from retted hemp hurd have similar trends in relation to impregnation ratio, activation temperature and HCl washing. Before HCl washing, the total pore volume

reaches the maximum (0.646 cm^3/g) on 800 °C with impregnation ratio of 4:1. However, the optimized total pore volume reaches 1.023 cm^3/g on 600 °C with the impregnation ratio of 4:1.

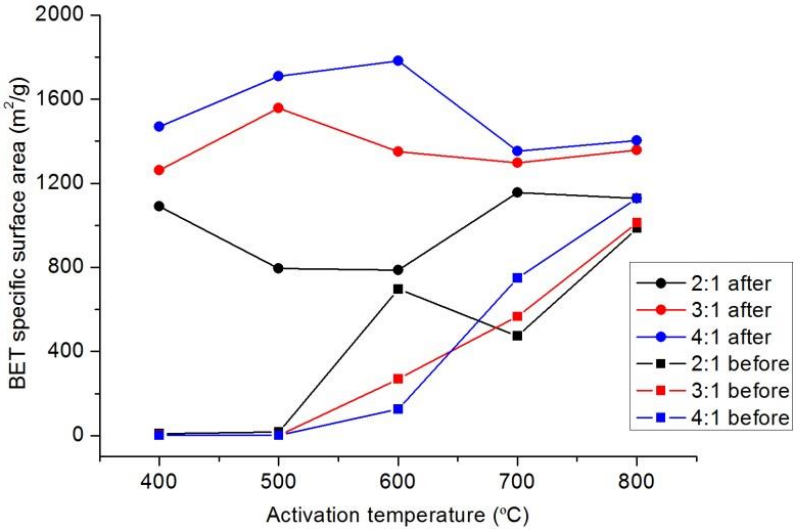

Figure 38. BET specific surface area chart of the activated carbons from retted hemp hurd by $ZnCl_2$ activation with different impregnation ratio and activation temperature before and after HCl washing obtained from N_2 isotherms at 77 K.

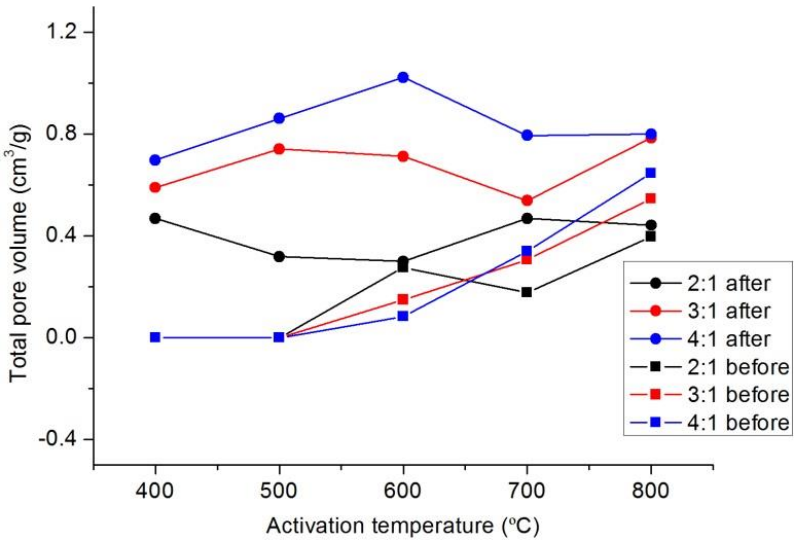

Figure 39. Total pore volume chart of the activated carbons from retted hemp hurd by $ZnCl_2$ activation with different impregnation ratio and activation temperature before and after HCl washing obtained from N_2 isotherms at 77 K.

The adsorption behaviour and pore structure of the activated carbons can be analysed using nitrogen adsorption isotherms. General properties of activated carbons can be explained by the shape of these isotherms (Demiral et al., 2016). The N_2 adsorption-desorption isotherms at 77 K on activated carbons from retted hemp hurd with impregnation ratio of 2:1 obtained at different temperatures before and after HCl washing are shown in Figure 40.

From Figure 40, RH-400-2:1 and RH-500-2:1 almost have no N_2 adsorption before HCl washing which indicate their low porosities. The other activated carbons exhibit Type I (a) isotherms which are of typical microporous solids. The adsorption branches were parallel to the pressure axis over a wide range at high relative pressure, indicating highly narrow pore size distribution of microporous solids with slit-like or plate-like pores (Erdem et al., 2016; Gottipati & Mishra, 2016). However, the small hysteresis loops seen on the adsorption–desorption isotherms of the activated carbons are due to the existence of mesopores (Demiral et al., 2016).

The major uptake on the adsorption–desorption isotherms occurs at relative pressure less than 0.1. The N_2 adsorption quantity increases sharply after HCl washing, which demonstrate that, the porosity of activated carbon by $ZnCl_2$ activation increase significantly by HCl washing. In addition, from the N_2 adsorption data, it has been determined that the RH-400-2:1, RH-700-2:1 and RH-800-2:1 after HCl washing are

high-quality activated carbons with BET surface area > 1000 m^2/g, and total pore volume > 0.4 cm^3/g.

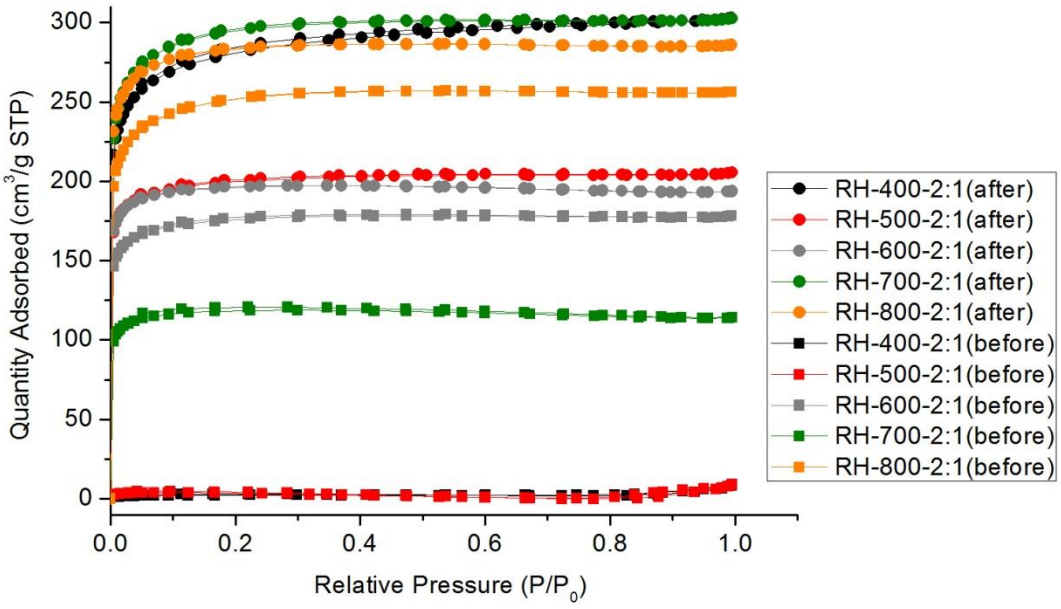

Figure 40. N_2 adsorption-desorption isotherms at 77 K on activated carbons prepared from retted hemp hurd with impregnation ratio of 2:1 on different activation temperature before and after HCl washing.

The N_2 adsorption-desorption isotherms at 77 K on activated carbons from retted hemp hurd with impregnation ratio of 3:1 obtained at different temperatures before and after HCl washing are shown in Figure 41. From Figure 41, RH-400-3:1 and RH-500-3:1 almost have no N_2 adsorption before HCl washing which indicate their low porosities. The shape of the isotherms suggest all other activated carbons exhibit Type I isotherms with an almost horizontal plateau at higher relative pressures, indicating highly microporous materials. Before HCl washing, the N_2 uptake increases with the increasing of activation temperature, and reaches a maximum at 800 °C. After HCl washing, the N_2 uptake increases with the increasing of activation

temperature, and reaches a maximum (1558 m^2/g) at 500 °C. A further increase of the activation temperature to 600, 700 and 800 °C results in decrease in the N_2 uptake.

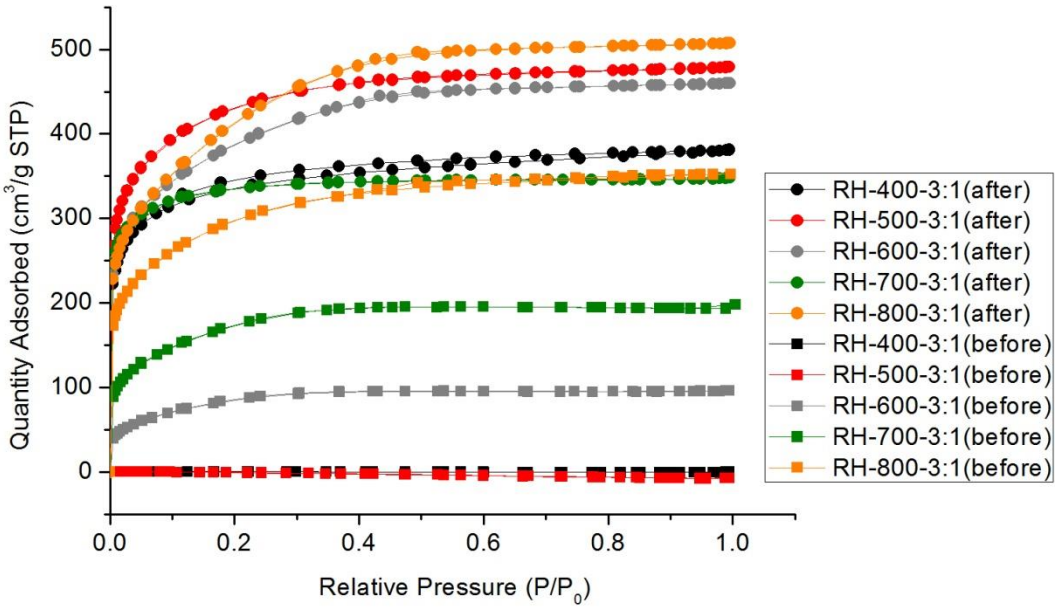

Figure 41. N_2 adsorption-desorption isotherms at 77 K of activated carbons prepared from retted hemp hurd with impregnation ratio of 3:1 on different activation temperature before and after HCl washing.

The N_2 adsorption-desorption isotherms at 77 K on activated carbons from retted hemp hurd with impregnation ratio of 4:1 obtained at different temperatures before and after HCl washing are shown in Figure 42. From Figure 42, RH-400-4:1 and RH-500-4:1 almost have no N2 adsorption before HCl washing which indicate their low porosities. The other isotherms belong to Type I (b) in the IUPAC classification, a characteristic of microporous materials. The steep rise and high N2 uptake of the initial part of the isotherms suggest the presence of a large proportion of micropores, and the fact that no obvious hysteresis is observed indicates the amount of mesopores or macropores are very small. Before HCl washing, the N_2 uptake increases with the increasing of activation temperature, and reaches a maximum at 800 °C. After HCl

washing, the N_2 uptake increases with the increasing of activation temperature, and reaches a maximum (1781 m^2/g) at 600 °C. Further rising of the activation temperature to 700 and 800 °C results in decrease in the N_2 uptake.

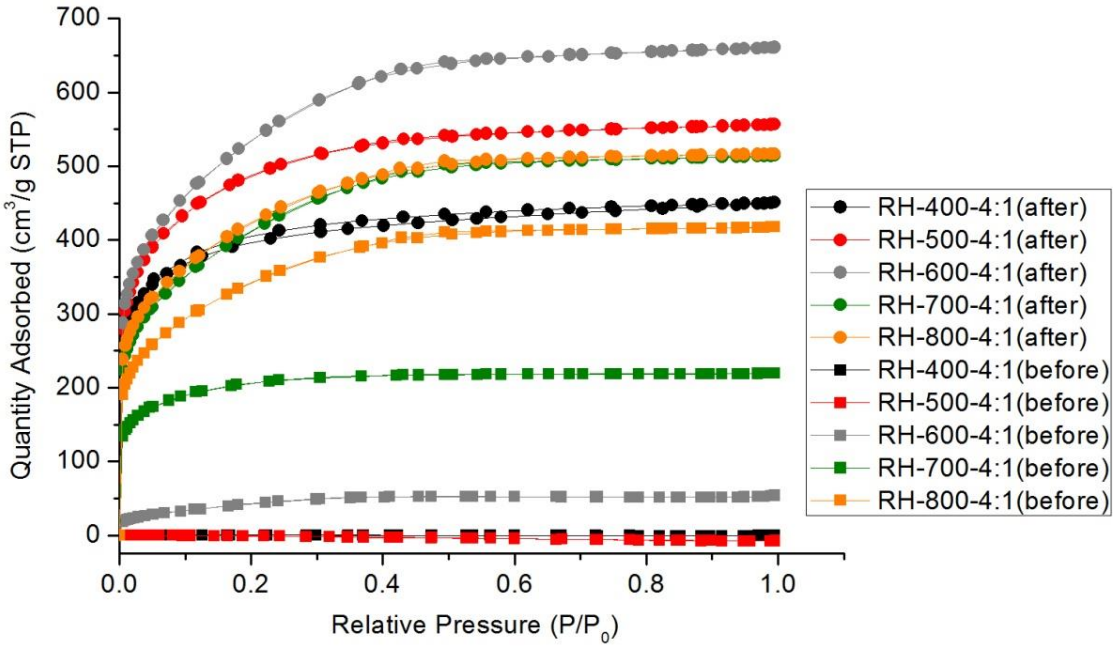

Figure 42. N_2 adsorption-desorption isotherms at 77 K of activated carbons prepared from retted hemp hurd with impregnation ratio of 4:1 on different activation temperature before and after HCl washing.

6.2.3 CO_2 adsorption capacity of activated carbon

A summary of the adsorption of CO_2 at 273 K on activated carbon from retted hemp hurd by $ZnCl_2$ activation after HCl washing is provided in Table 10. Figure 43 compares the adsorption of CO_2 at 273 K on activated carbon from retted hemp hurd with different impregnation ratio after HCl washing. From Figure 43 and Table 10, activated carbons reach maximum CO_2 adsorption capacity with activation temperature of 500 °C. The effect of the activation temperature of activated carbon from retted hemp hurd on CO_2 adsorption capacity is stronger than the effect of

impregnation rate. The adsorptions of CO_2 at 273 K reach 126, 134 and 142 cm^3/g STP with the impregnation rate of 2:1, 3:1 and 4:1 respectively.

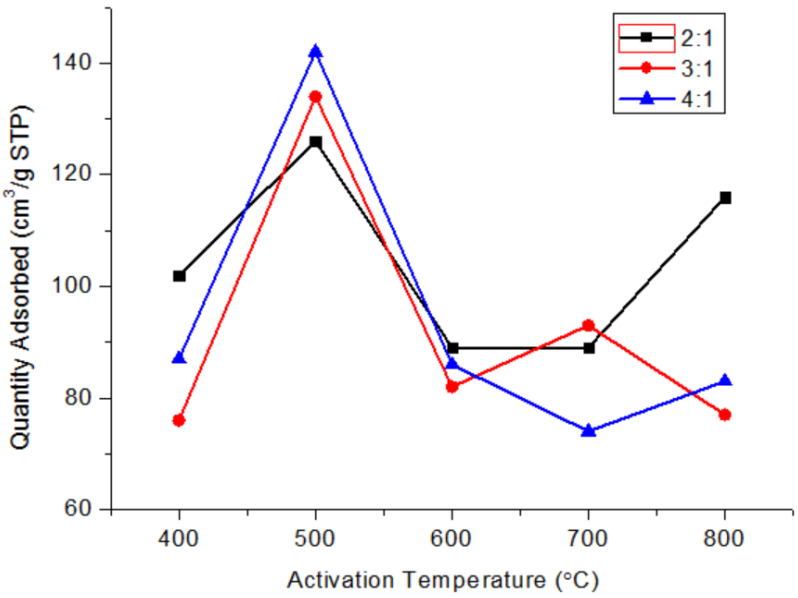

Figure 43. Adsorption of CO_2 at 273 K on activated carbon from retted hemp hurd by $ZnCl_2$ activation after HCl washing.

Table 10. Adsorption of CO_2 at 273 K on activated carbon prepared from retted hemp hurd by $ZnCl_2$ activation with different impregnation ratio and activation temperature after HCl washing.

Sample label	Activation temperature (°C)	Impregnation ratio of $ZnCl_2$ (wt. /wt.)	CO_2 adsorption after HCl washing (cm^3/g STP)
RH-400-2:1	400	2:1	102
RH-400-3:1		3:1	76
RH-400-4:1		4:1	87
RH-500-2:1	500	2:1	126
RH-500-3:1		3:1	134

RH-500-4:1		4:1	142
RH-600-2:1		2:1	89
RH-600-3:1	600	3:1	82
RH-600-4:1		4:1	86
RH-700-2:1		2:1	79
RH-700-3:1	700	3:1	81
RH-700-4:1		4:1	74
RH-800-2:1		2:1	116
RH-800-3:1	800	3:1	77
RH-800-4:1		4:1	83

6.3 Bamboo fibre

6.3.1 Yield of activated carbon

Yields of activated carbons derived from bamboo fibre with different $ZnCl_2$ impregnation ratio and activation temperature after HCl washing were given in Figure 44 and Table 11. According to the obtained data, the higher the activation temperature is, the less the yield of activated carbons derived from bamboo fibre is. At the lower activation temperature (400 °C and 600 °C), there was a trend towards an increase in yield of carbon with increasing impregnation ratio. However, at the higher activation temperature (800 °C), the opposite tendency was observed.

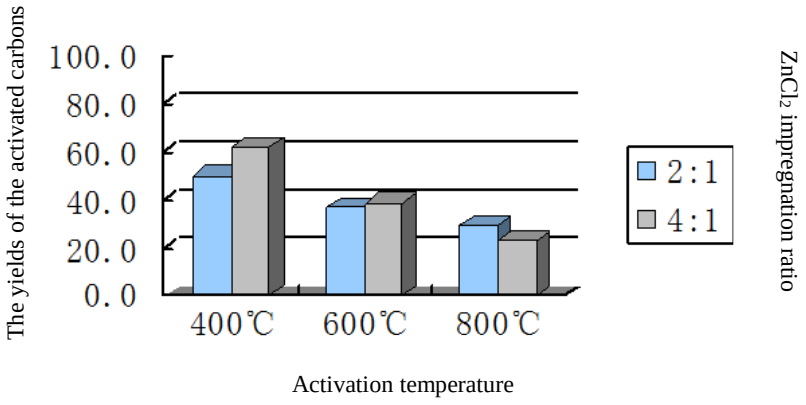

Figure 44. The yields of the activated carbons derived from bamboo fibre by $ZnCl_2$ activation after HCl washing.

Table 11. The yields of the activated carbons derived from bamboo fibre by $ZnCl_2$ activation with different $ZnCl_2$ impregnation ratio and activation temperature after HCl washing.

Sample label	Activation temperature (°C)	Impregnation ratio of $ZnCl_2$ (wt. /wt.)	Yield (wt. %)
BF-400-2:1	400	2:1	50.1
BF-400-4:1		4:1	61.5
BF-600-2:1	600	2:1	36.4
BF-600-4:1		4:1	38.8
BF-800-2:1	800	2:1	29.1
BF-800-4:1		4:1	23.0

6.3.2 Surface areas and porosity of activated carbon

Table 12 summarizes the specific surface area and pore volume of the activated carbons derived from bamboo fibre by $ZnCl_2$ activation with different impregnation ratio (2:1 and 4:1) and activation temperature (400, 600 and 800 °C) before and after HCl washing from the N_2 isotherms at 77 K. All parameters were calculated in the same way as activated carbons derived from retted hemp hurd.

Table 12. Specific surface area and pore volume of the activated carbons derived from bamboo fibre by $ZnCl_2$ activation with different impregnation ratio and activation temperature before and after HCl washing.

Sample label	S_{BET} ($m^2.g^{-1}$)		$S_{Langmuir}$ ($m^2.g^{-1}$)		V_{total} ($cm^3.g^{-1}$)		V_{micro} ($cm^3.g^{-1}$)		V_{meso} ($cm^3.g^{-1}$)	
	Before	After	Before	After	Before	After	Before	After	Before	After
BF-400-2:1	0	783	0	892	0	0.322	0	0.259	0	0.063
BF-400-4:1	0	1587	0	2176	0	0.786	0	0.334	0	0.452
BF-600-2:1	712	763	783	856	0.286	0.305	0.251	0.263	0.035	0.042
BF-600-4:1	550	1366	839	1905	0.287	0.656	0.073	0.300	0.214	0.356
BF-800-2:1	1110	1213	1286	1402	0.455	0.496	0.366	0.399	0.089	0.097
BF-800-4:1	1108	1370	1396	1761	0.505	0.641	0.304	0.363	0.201	0.278

Figure 45 and Figure 46 are BET specific surface area and total pore volume charts of the activated carbons from bamboo fibre by $ZnCl_2$ activation with different impregnation ratio and activation temperature before and after HCl washing obtained from N_2 isotherms at 77 K. As can be seen from Figure 45, before HCl washing, the BET specific surface area of the activated carbon reaches the maximum (1110 m^2/g) on 800 °C with impregnation ratio of 2:1. All of the BET specific surface areas of the activated carbons increased largely after HCl washing. The BET specific surface areas increase with the increase of impregnation ratio no matter what the activation temperature is. The optimized BET specific surface area of the activated carbon reaches 1587 m^2/g on 400 °C with impregnation ratio of 4:1. Figure 45 and Figure 46 show that the BET specific surface area and total pore volume of activated carbons from retted hemp hurd have similar trends in relation to impregnation ratio,

activation temperature and HCl washing. Before HCl washing, the total pore volume reaches the maximum (0.505 cm^3/g) on 800 °C with impregnation ratio of 4:1. However, the optimized total pore volume reaches 0.786 cm^3/g on 400 °C with the impregnation ratio of 4:1.

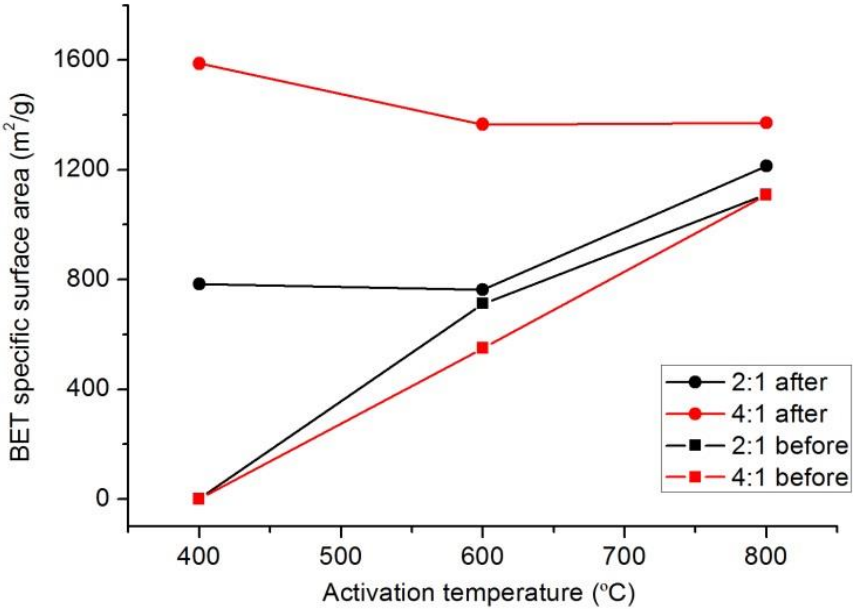

Figure 45. BET specific surface area chart of the activated carbons from bamboo fibre by $ZnCl_2$ activation with different impregnation ratio and activation temperature before and after HCl washing obtained from N_2 isotherms at 77 K.

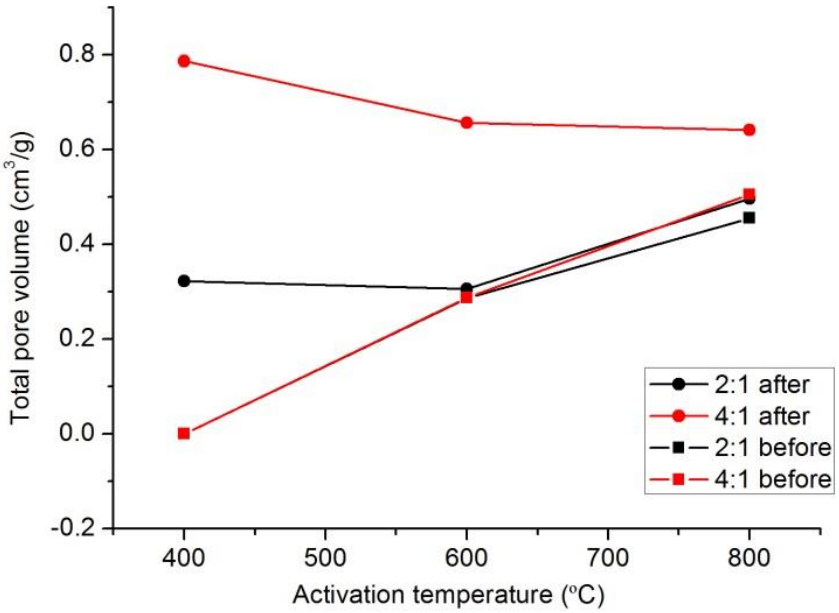

Figure 46. Total pore volume chart of the activated carbons from bamboo fibre by $ZnCl_2$ activation with different impregnation ratio and activation temperature before and after HCl washing obtained from N_2 isotherms at 77 K.

The N_2 adsorption-desorption isotherms at 77 K on activated carbons from bamboo fibre with impregnation ratio of 2:1 obtained at different temperatures before and after HCl washing are shown in Figure 47. From Figure 47, BF-400-2:1 almost have no N_2 adsorption before HCl washing, which indicate its low porosity. The other isotherms belong to Type I (a) in the IUPAC classification, a characteristic of microporous materials. The isotherms show a rapid rise in adsorbed quantity with increasing pressure up to saturation, characteristic of microporous solids. The N_2 adsorption quantity increases after HCl washing, which demonstrate that, the porosity of activated carbon by $ZnCl_2$ activation increase significantly by HCl washing. For the samples BF-600-2:1 before and after HCl washing, there is a pronounced adsorption "tail" at relative pressure approaching saturation, indicating the presence of macropores, which may be from the stack of particles. Before HCl

washing, the N_2 uptake increases with the increasing of activation temperature, and reaches a maximum (1110 m^2/g) at 800 °C. After HCl washing, the N_2 uptake also reaches a maximum (1213 m^2/g) at 800 °C.

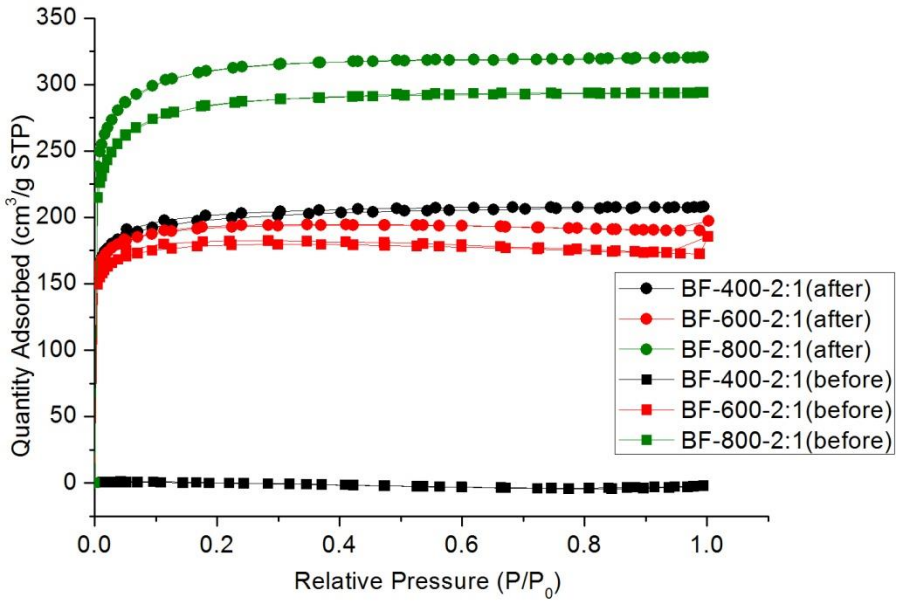

Figure 47. N_2 adsorption-desorption isotherms at 77 K of activated carbons prepared from bamboo fibre with impregnation ratio of 2:1 on different activation temperature before and after HCl washing.

The N_2 adsorption-desorption isotherms at 77 K on activated carbons from bamboo fibre with impregnation ratio of 4:1 obtained at different temperatures before and after HCl washing are shown in Figure 48. Figure 47 and Figure 48 show that the "knee" of the isotherms tend to open as the activation ratio is increased from 2:1 to 4:1, indicating the widening of microporosity. From Figure 48, BF-400-4:1 almost have no N_2 adsorption before HCl washing which indicate its low porosity. According to the IUPAC classification, the shape of the other N_2 adsorption isotherms may be considered as Type I (b). For the samples BF-800-4:1 before and after HCl washing, there is a pronounced adsorption "tail" at relative pressure

approaching saturation, indicating the presence of macropores, which may be from the stack of particles. Before HCl washing, the N_2 uptake increases with the increasing of activation temperature, and reaches a maximum at 800 °C. However, the N_2 uptake reaches a maximum (1587 m^2/g) at 400 °C after HCl washing. Further rising in the activation temperature to 600 and 800 °C provokes a decrease in N_2 uptake.

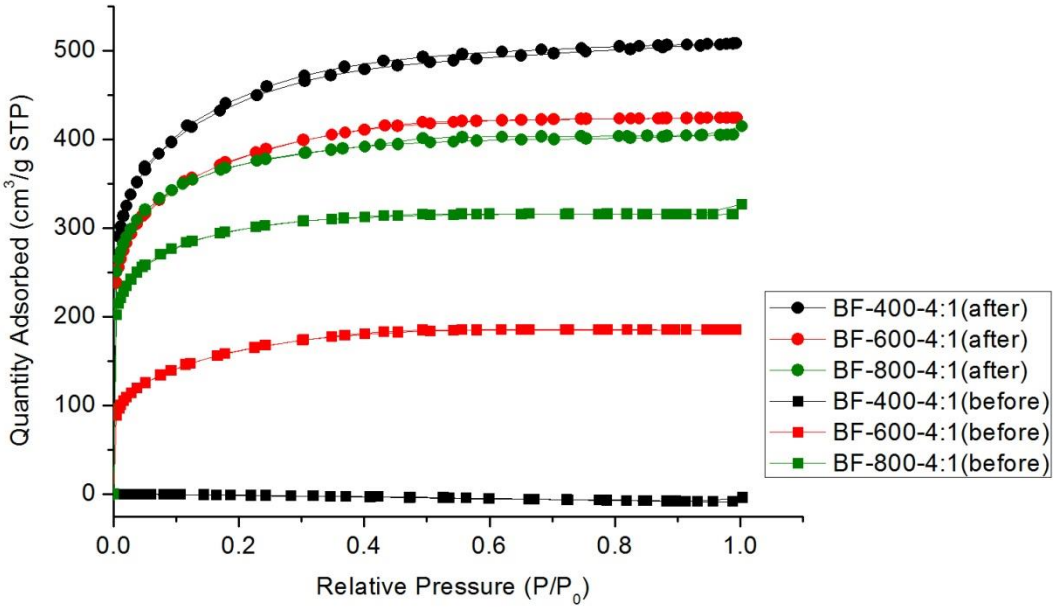

Figure 48. N_2 adsorption-desorption isotherms at 77 K of activated carbons prepared from bamboo fibre with impregnation ratio of 4:1 on different activation temperature before and after HCl washing.

6.3.3 CO_2 adsorption capacity of activated carbon

Table 13 summarizes the adsorption of CO_2 at 273 K on activated carbon prepared from bamboo fibre with different $ZnCl_2$ impregnation ratio and activation temperature after HCl washing. Figure 49 compares the adsorption of CO_2 at 273 K on activated carbon from bamboo fibre with different impregnation ratio after HCl washing. From Figure 49 and Table 13, the CO_2 adsorption capacity first increase

and then decrease with the increase of activation temperature. Activated carbons reach maximum CO_2 adsorption capacity with activation temperature of 800 °C. The adsorptions of CO_2 at 273 K on activated carbon with activation temperature of 800 °C reach 108 and 98 cm^3/g STP with the impregnation rate of 2:1 and 4:1 respectively.

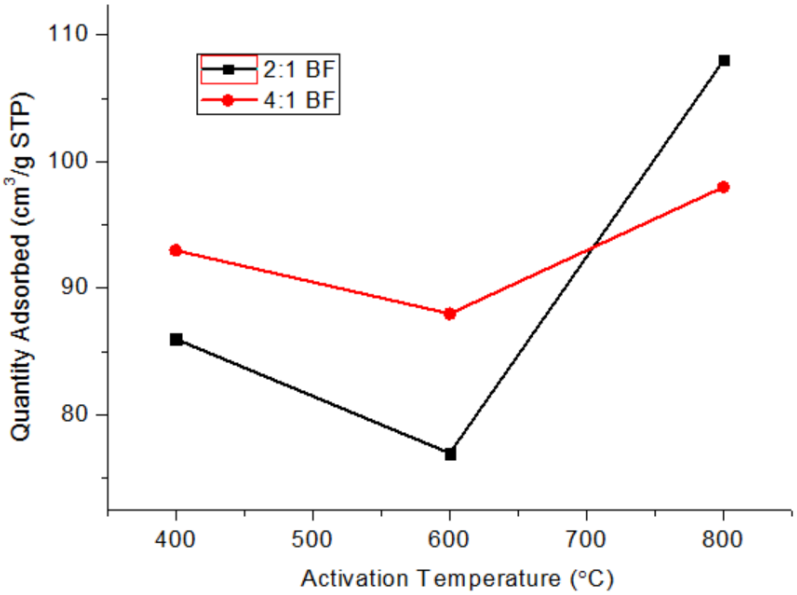

Figure 49. Adsorption of CO_2 at 273 K on activated carbon from bamboo fibre by $ZnCl_2$ activation after HCl washing.

Table 13. Adsorption of CO_2 at 273 K on activated carbon prepared from bamboo fibre by $ZnCl_2$ activation with different impregnation ratio and activation temperature after HCl washing.

Sample label	Activation temperature	Impregnation ratio of $ZnCl_2$	CO_2 adsorption after HCl washing (cm^3/g STP)
BF-400-2:1	400	2:1	86
BF-400-4:1		4:1	93
BF-600-2:1	600	2:1	77
BF-600-4:1		4:1	88
BF-800-2:1	800	2:1	108
BF-800-4:1		4:1	98

6.4 Hemp fibre

6.4.1 Yield of activated carbon

Yields of activated carbons derived from hemp fibre with different $ZnCl_2$ impregnation ratio and activation temperature after HCl washing were given in Figure 50 and Table 14. According to the obtained data, the higher the activation temperature is, the less the yield of activated carbons derived from hemp fibre. At the lower activation temperature (400 °C and 600 °C), there was a trend towards an increase in yield of carbon with increasing impregnation ratio. However, at the higher activation temperature (800 °C), the opposite tendency was observed. The yield tendency of activated carbons derived from bamboo fibre and hemp fibre are the same.

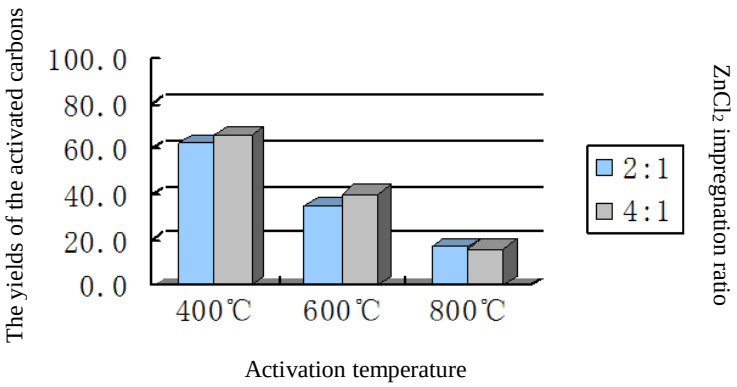

Figure 50. The yields of the activated carbons derived from hemp fibre by $ZnCl_2$ activation after HCl washing.

Table 14. The yields of the activated carbons derived from hemp fibre by $ZnCl_2$ activation with different $ZnCl_2$ impregnation ratio and activation temperature after HCl washing.

Sample label	Activation temperature	Impregnation ratio of $ZnCl_2$	Yield (wt. %)
HF-400-2:1	400	2:1	62.5
HF-400-4:1		4:1	66.3
HF-600-2:1	600	2:1	35.3
HF-600-4:1		4:1	40.2
HF-800-2:1	800	2:1	17.2
HF-800-4:1		4:1	16.4

6.4.2 Surface areas and porosity of activated carbon

Table 15 summarizes the specific surface area and pore volume of the activated carbons derived from hemp fibre by $ZnCl_2$ activation with different impregnation ratio (2:1 and 4:1) and activation temperature (400, 600 and 800 °C) before and after HCl washing from the N_2 isotherms at 77 K. All parameters were calculated in the same way as activated carbons derived from retted hemp hurd.

Table 15. Specific surface area and pore volume of the activated carbons derived from hemp fibre by $ZnCl_2$ activation with different impregnation ratio and activation temperature before and after HCl washing.

Sample label	S_{BET} ($m^2.g^{-1}$)		$S_{Langmuir}$ ($m^2.g^{-1}$)		V_{total} ($cm^3.g^{-1}$)		V_{micro} ($cm^3.g^{-1}$)		V_{meso} ($cm^3.g^{-1}$)	
	Before	After	Before	After	Before	After	Before	After	Before	After
HF-400-2:1	0	1576	0	2406	0	0.884	0	0.201	0	0.683
HF-400-4:1	0	1464	0	2169	0	0.823	0	0.201	0	0.622
HF-600-2:1	404	1368	618	2000	0.220	0.735	0.053	0.227	0.167	0.508
HF-600-4:1	213	1409	442	2270	0.151	1.026	0.010	0.088	0.141	0.938
HF-800-2:1	853	1413	1362	2289	0.553	0.941	0.070	0.124	0.483	0.817
HF-800-4:1	722	1314	976	2275	0.353	1.009	0.166	0.055	0.187	0.954

Figure 51 and Figure 52 are BET specific surface area and total pore volume charts of the activated carbons from hemp fibre by $ZnCl_2$ activation with different impregnation ratio and activation temperature before and after HCl washing obtained from N_2 isotherms at 77 K. As can be seen from Figure 51, before HCl washing, the BET specific surface area of the activated carbon reaches the maximum (853 m^2/g) on 800 °C with impregnation ratio of 2:1. All of the BET specific surface areas of the activated carbons increased largely after HCl washing. The BET specific surface areas increase with the increase of impregnation ratio no matter what the activation temperature is. The optimized BET specific surface area of the activated carbon reaches 1576 m^2/g on 400 °C with impregnation ratio of 2:1.

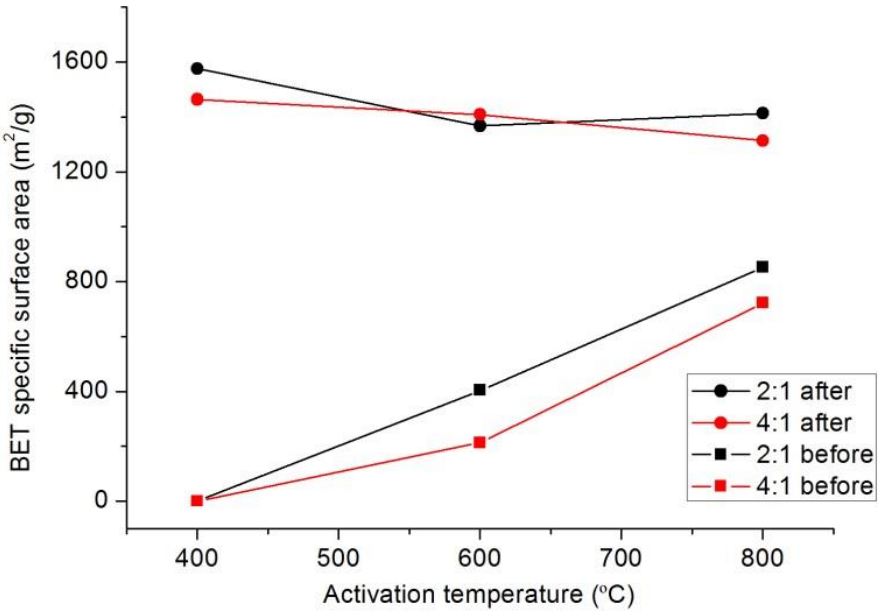

Figure 51. BET specific surface area chart of the activated carbons from hemp fibre by $ZnCl_2$ activation with different impregnation ratio and activation temperature before and after HCl washing obtained from N_2 isotherms at 77 K.

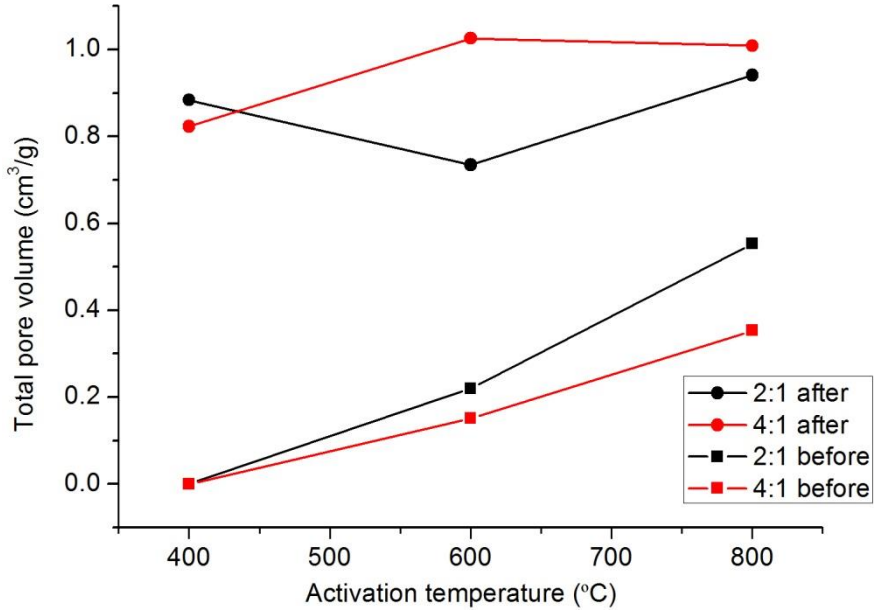

Figure 52. Total pore volume chart of the activated carbons from hemp fibre by $ZnCl_2$ activation with different impregnation ratio and activation temperature before and after HCl washing obtained from N_2 isotherms at 77 K.

The N_2 adsorption-desorption isotherms at 77 K on activated carbons from hemp fibre with impregnation ratio of 2:1 obtained at different temperatures before and after HCl washing are shown in Figure 53. From Figure 53, HF-400-2:1 almost have no N_2 adsorption before HCl washing which indicate its low porosity. The isotherms of HF-600-2:1 before HCl washing belong to Type I in the IUPAC classification. The adsorption isotherms of the other activated carbons exhibit Type IV behaviour. HF-600-2:1 after HCl washing, HF-800-2:1 before and after HCl washing have clear Type-H4 hysteresis loops, which is a typical characteristic of mesoporous materials. Type IV isotherms describe adsorption with a mixture of micropores and mesopores and an adsorption nature characterized by monolayer-multilayer adsorption of the adsorbent. A hysteresis loop can occur when the mechanism of mesopore filling by capillary condensation differs from that of mesopore emptying (Kongnoo et al., 2016).

Figure 53 shows the N_2 adsorption increasing sharply after HCl washing, which demonstrates the porosity of activated carbon from hemp fibre by $ZnCl_2$ activation increased significantly by HCl washing. Figure 53 also shows that the “knee” of the isotherm tends to open by HCl washing, indicating the widening of microporosity. After the relative pressure reaches nearly 0.1, there is still a further increase in amount adsorbed with increasing relative pressure (except HF-400-2:1 before HCl washing), which reflects a certain amount of mesopores in samples. Before HCl washing, the N_2 uptake increases with the increasing of activation temperature, and reaches a maximum at 800 °C. However, the N_2 uptake reaches a maximum (1576 m^2/g) at 400 °C after HCl washing. Further rising in the activation temperature to 600 and 800 °C caused a decrease in N_2 uptake.

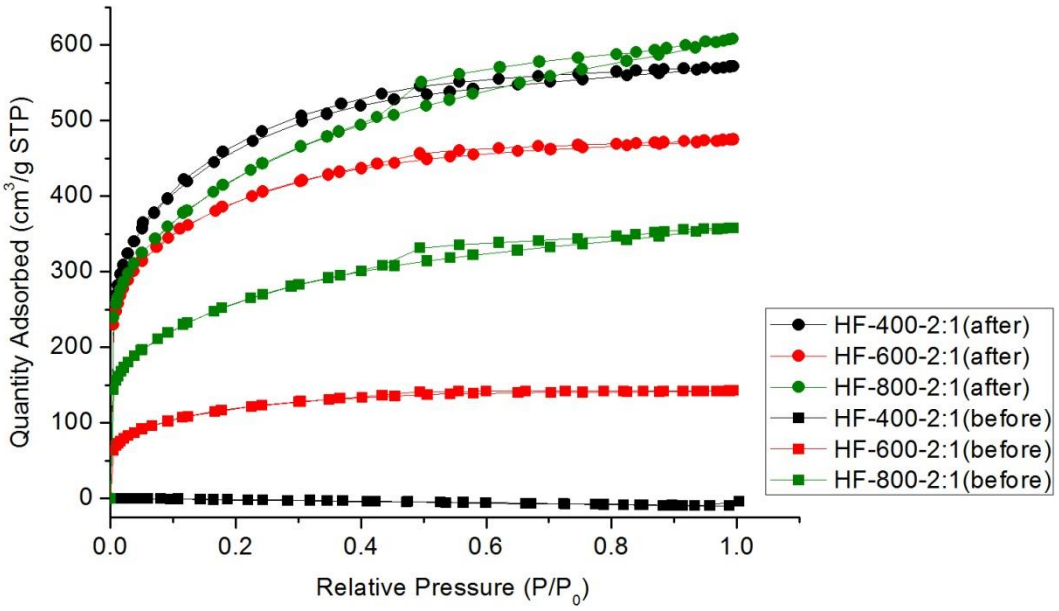

Figure 53. N_2 adsorption-desorption isotherms at 77 K of activated carbons prepared from hemp fibre with impregnation ratio of 2:1 on different activation temperature before and after HCl washing.

The N_2 adsorption-desorption isotherms at 77 K on activated carbons from hemp fibre with impregnation ratio of 4:1 obtained at different temperatures before and after HCl washing are shown in Figure 54. From Figure 54, HF-400-4:1 almost have no N_2 adsorption before HCl washing which indicate its low porosity. The isotherms of HF-600-4:1, HF-800-4:1 before HCl washing and HF-400-4:1 after HCl washing belongs to Type I in the IUPAC classification. It is clear that Type-H4 hysteresis loops emerged in the isotherms of HF-600-4:1 and HF-800-4:1 after HCl washing at a high relative pressure region between 0.4 and 1.0 and exhibited Type IV behaviour, which clearly demonstrated the wide mesopore distribution in the materials (Xia et al., 2016).

The N_2 adsorption capacities increase sharply after HCl washing, which demonstrate that the porosity of activated carbon from hemp fibre by $ZnCl_2$ activation increase

significantly by HCl washing. Figure 54 also shows that the "knee" of the isotherm tends to open by HCl washing, indicating the widening of microporosity. Before HCl washing, the N_2 uptake increased with the increasing of activation temperature, and reached a maximum at 800 °C. However, the N_2 uptake decreased with the increasing of activation temperature after HCl washing, the N_2 uptake reached a maximum (1464 m^2/g) at 400 °C after HCl washing. After the relative pressure reached nearly 0.1, there is still a further increased in amount adsorbed with increasing relative pressure, which reflects a certain amount of mesopores in samples after HCl washing.

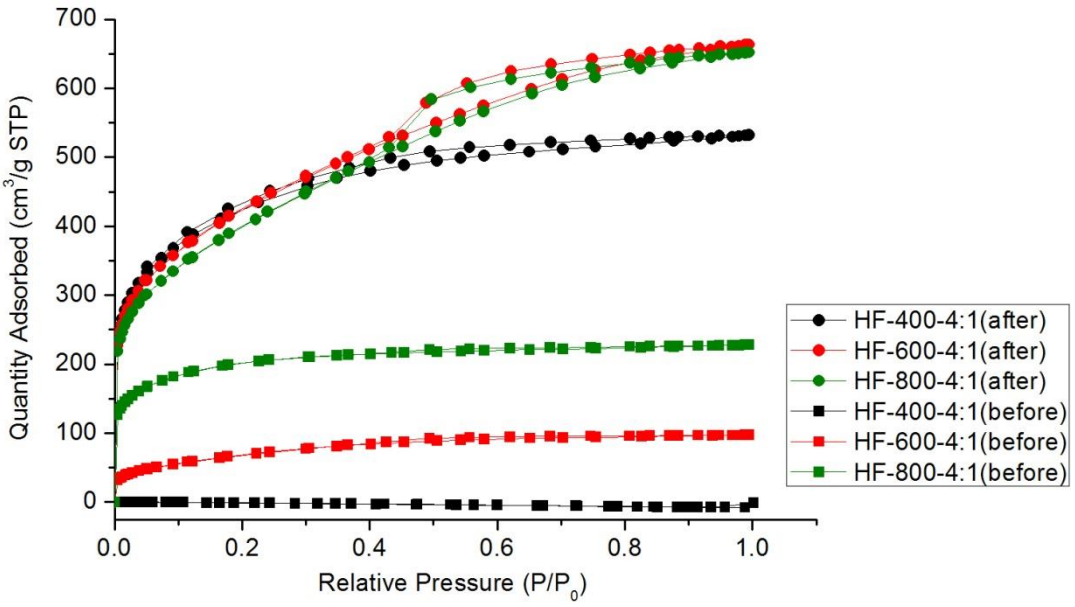

Figure 54. N_2 adsorption-desorption isotherms at 77 K of activated carbons prepared from hemp fibre with impregnation ratio of 4:1 on different activation temperature before and after HCl washing.

6.4.3 CO_2 adsorption capacity of activated carbon

Table 16 summarizes the adsorption of CO_2 at 273 K on activated carbon prepared from hemp fibre with different $ZnCl_2$ impregnation ratio and activation temperature

after HCl washing. Figure 55 compares the adsorption of CO_2 at 273 K on activated carbon from hemp fibre with different impregnation ratio after HCl washing. From Figure 55 and Table 16, both the effect of the impregnation rate and the activation temperature of activated carbon from bamboo fibre on CO_2 adsorption capacity are great. The CO_2 adsorption capacities decrease with the increase of $ZnCl_2$ impregnation ratio. The adsorptions of CO_2 at 273 K on activated carbon reach maximum (86 cm^3/g STP) with activation temperature of 400 °C and 600 °C with the impregnation rate of 2:1.

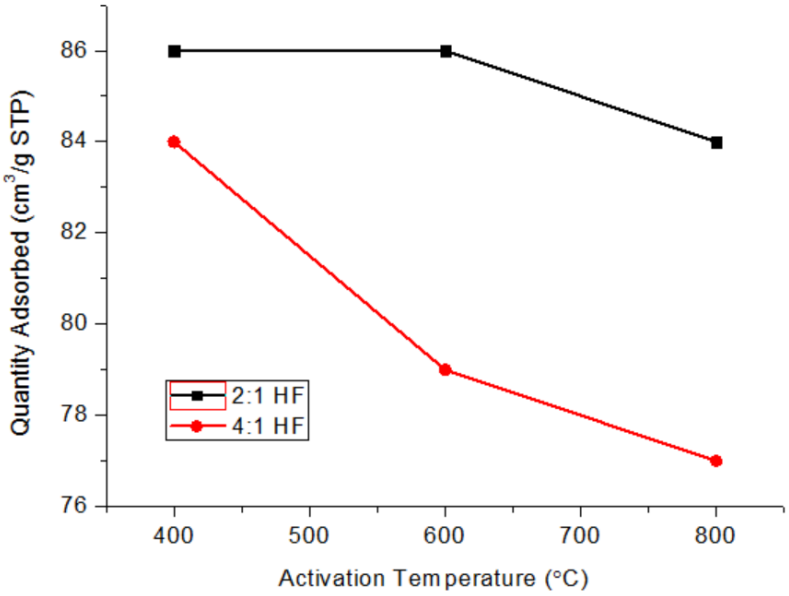

Figure 55. Adsorption of CO_2 at 273 K on activated carbon from hemp fibre by $ZnCl_2$ activation after HCl washing.

Table 16. Adsorption of CO_2 at 273 K on activated carbon prepared from hemp fibre by $ZnCl_2$ activation with different impregnation ratio and activation temperature after HCl washing.

Sample label	Activation temperature	Impregnation ratio of $ZnCl_2$	CO_2 adsorption after HCl washing (cm^3/g STP)
HF-400-2:1	400	2:1	86
HF-400-4:1		4:1	84
HF-600-2:1	600	2:1	86
HF-600-4:1		4:1	79
HF-800-2:1	800	2:1	84
HF-800-4:1		4:1	77

6.5 Comparison of activated carbon from different precursors

6.5.1 Yield of activated carbon

In this thesis, the activated carbons derived from retted hemp hurd, bamboo fibre and hemp fibre are also compared. Figure 56 shows yields of the activated carbons derived from retted hemp hurd, bamboo fibre and hemp fibre by $ZnCl_2$ activation after HCl washing. The effect of activation temperature greatly exceeds the effect of bio-precursor and impregnation rate.

Irrespective of the precursor, the effect of the impregnation ratio and the activation temperature on yield of the activated carbons was found to be similar, that is, the higher the activation temperature, the lower the yield is. At the lower activation

temperature, there was a trend towards an increase in yield of carbon with increasing impregnation ratio, while the opposite tendency was observed at the higher activation temperature.

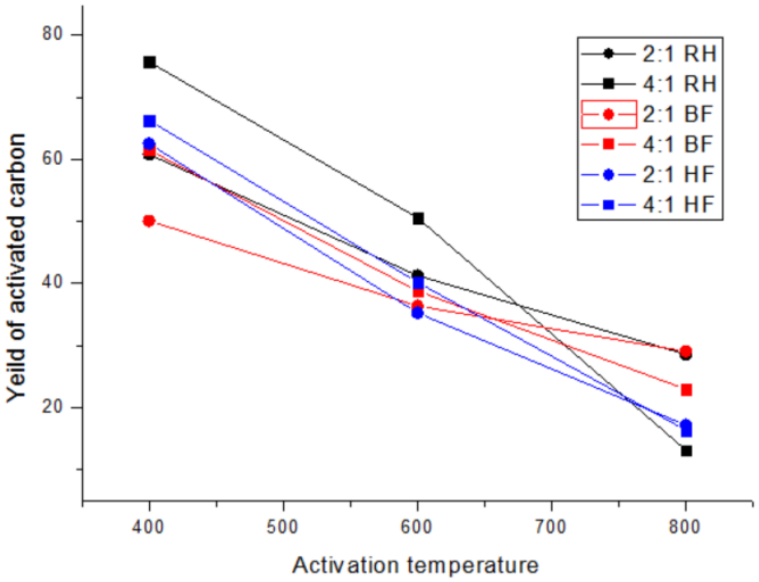

Figure 56. The yields of the activated carbons derived from retted hemp hurd, bamboo fibre and hemp fibre by $ZnCl_2$ activation after HCl washing.

6.5.2 Surface areas and porosity of activated carbon

In the previous section, the focus was primarily on the influence of the activation parameters on activated carbon performance from each precursor. In the following section, the effect of precursor on activated carbon performance is compared.

Figure 57 is the BET specific surface area, total pore volume and micropore volume chart of the activated carbons from different precursor by $ZnCl_2$ activation with different impregnation ratio and activation temperature before and after HCl washing obtained from N_2 isotherms at 77 K. As can be seen from Figure 57, the BET specific

surface area and total pore volume of the activated carbons from retted hemp hurd and bamboo fibre increased largely with high impregnation ratio.

However, the effect of impregnation ratio is not that significant on activated carbons from hemp fibre. When the impregnation ratio is 2:1, the BET specific surface area and total pore volume of the activated carbons from hemp fibre is better than those from retted hemp hurd and bamboo fibre, but its micropore volume is the least. When the impregnation ratio is 4:1, activated carbon from retted hemp hurd (RH-600-4:1) has optimized BET specific surface area (1781 m^2/g) and total pore volume (1.023 cm^3/g), but its micropore volume is relatively low. Although the BET specific surface area and total pore volume of these carbons is different, molten-salt route ($ZnCl_2$ activation) is proved to be a general way for synthesis of high quality activated carbon from biomass.

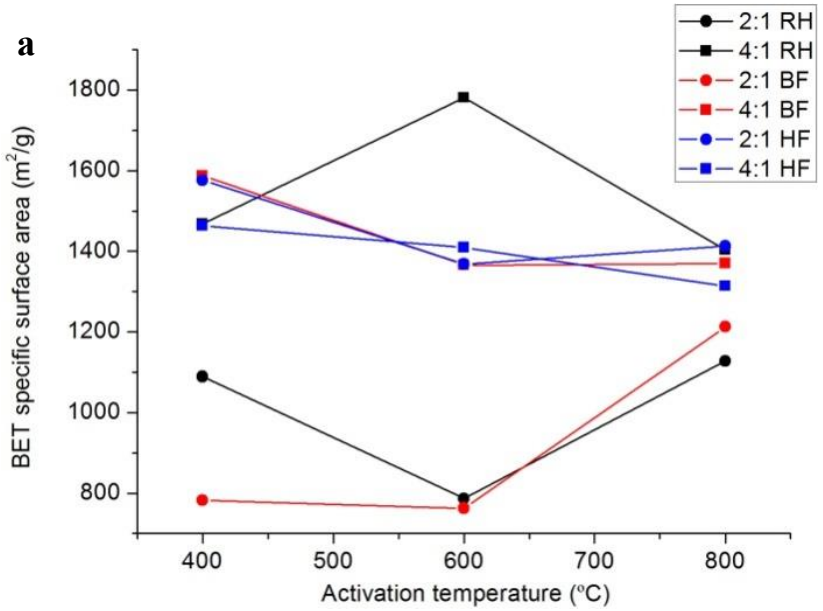

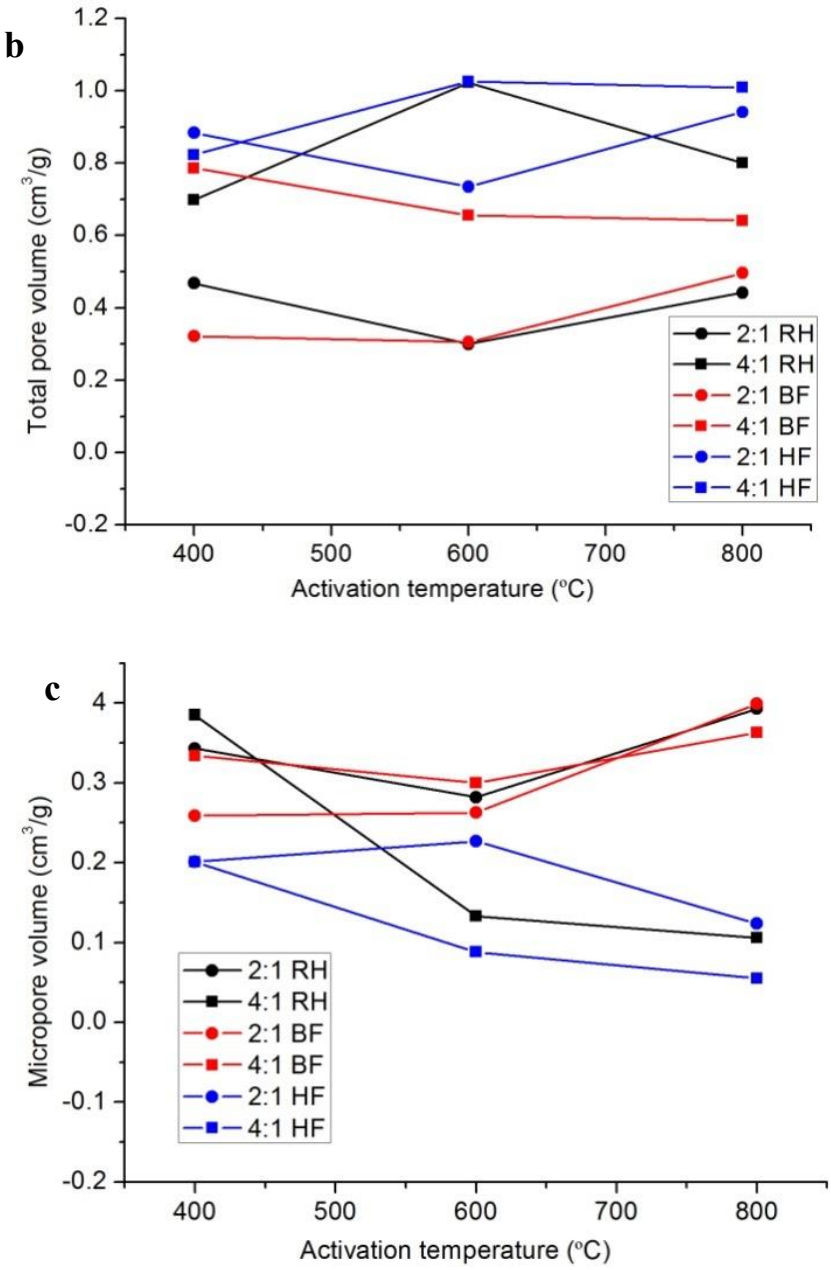

Figure 57. (a) BET specific surface area (b) total pore volume (c) micropore volume chart of the activated carbons from different precursor by $ZnCl_2$ activation with different impregnation ratio and activation temperature before and after HCl washing obtained from N_2 isotherms at 77 K.

The N2 adsorption-desorption isotherms at 77 K on activated carbons from different precursor with impregnation ratio of 2:1 after HCl washing are shown in Figure 58. From Figure 58, the N_2 adsorption-desorption isotherms on activated carbons from

retted hemp hurd and bamboo fibre are similar (Type I), which are quite different from the isotherms on activated carbons from hemp fibre (Type IV). Activated carbons from retted hemp hurd and bamboo fibre are highly micropores materials, and the fact that no obvious hysteresis is observed indicates the amount of mesopores or macropores are very small. Activated carbons from hemp fibre have mixtures of micropores and mesopores, Type-H4 hysteresis loops emerged in the isotherms at a high relative pressure region clearly demonstrated the wide mesopore distribution. The "knee" of the isotherms from hemp fibre are wider than those from retted hemp hurd and bamboo fibre, indicating the widening of microporosity.

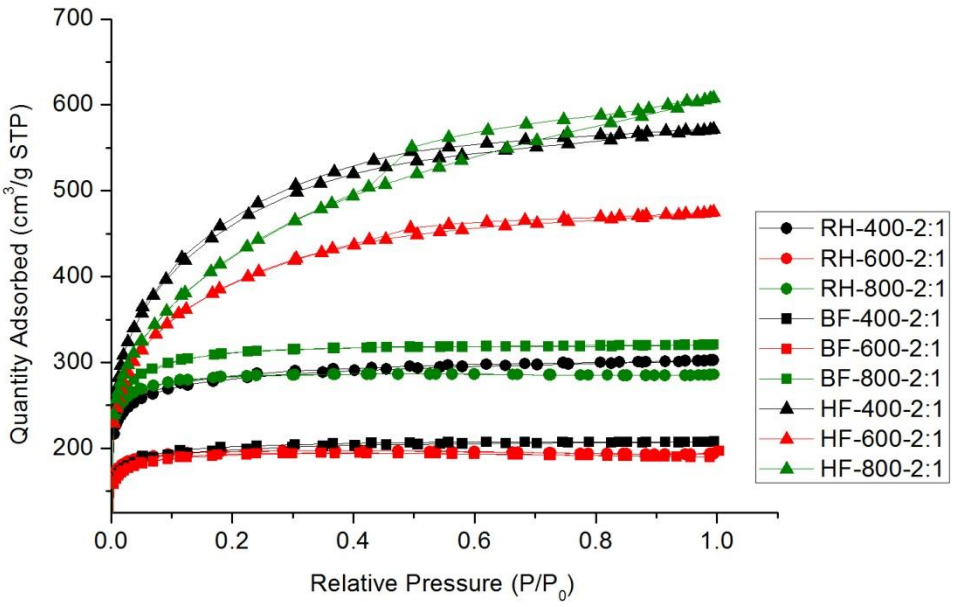

Figure 58. N_2 adsorption-desorption isotherms at 77 K of activated carbons prepared from different precursor and activation temperature with impregnation ratio of 2:1 after HCl washing.

The N_2 adsorption-desorption isotherms at 77 K on activated carbons from different precursor with impregnation ratio of 4:1 after HCl washing are shown in Figure 59. From Figure 59, the N_2 adsorption-desorption isotherms on activated carbons from

retted hemp hurd and bamboo fibre are similar (Type I (b)), which are different from some isotherms (Type IV) on activated carbons from hemp fibre (HF-600-4:1 and HF-800-4:1). Activated carbons from retted hemp hurd and bamboo fibre are highly micropores materials, and the amount of mesopores or macropores are very small. Activated carbons from hemp fibre (on 600 and 800 °C) are mixtures of micropores and mesopores and have wide mesopore distribution.

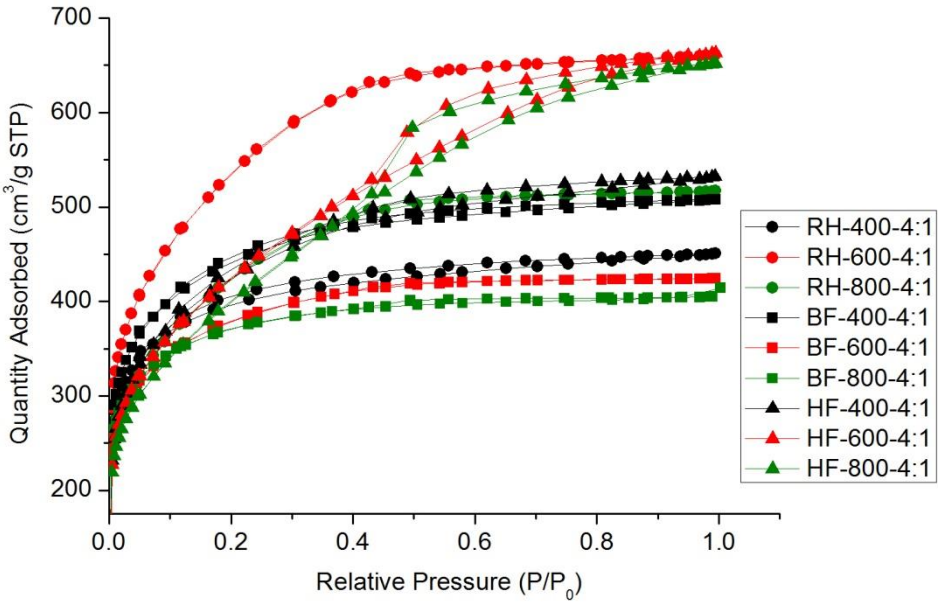

Figure 59. N_2 adsorption-desorption isotherms at 77 K of activated carbons prepared from different precursor and activation temperature with impregnation ratio of 4:1 after HCl washing.

6.5.3 CO_2 adsorption capacity of activated carbon

The physicochemical properties of activated carbon are strongly dependent on the nature of precursor and activation conditions (e.g. activation temperature and $ZnCl_2$ impregnation rate). In the previous paragraphs, the focus is primarily on the influence of the activation parameters on the adsorption of CO_2 from each precursor.

In the following paragraphs, the effect of precursor on activated carbon adsorption performance is explored.

Figure 60 compares the adsorption of CO_2 at 273 K on activated carbon prepared from different precursors with the impregnation ratio of 2:1 by $ZnCl_2$ activation after HCl washing. It shows that the precursor of activated carbon with the highest CO_2 adsorption capacity is retted hemp hurd. For activated carbons derived from retted hemp hurd and bamboo fibre, the optimal activation temperature for CO_2 adsorption is 800 °C. For activated carbons derived from hemp fibre, the activation temperature has little influence on the CO_2 adsorption capacity.

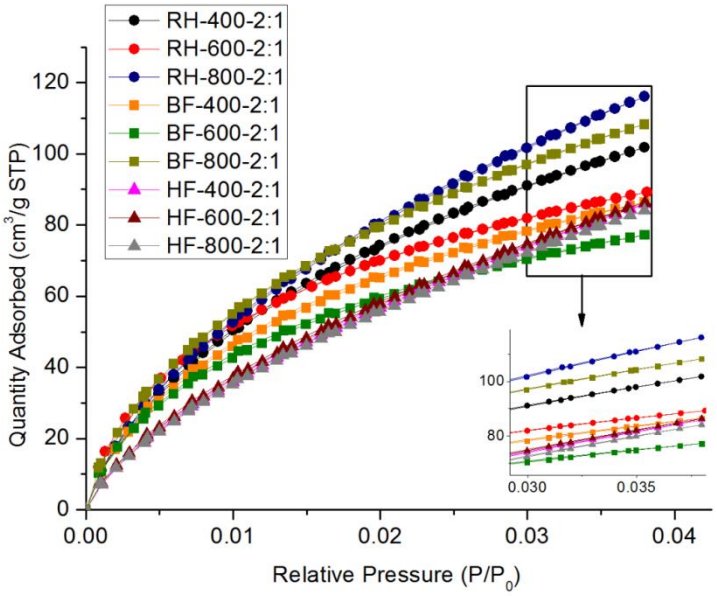

Figure 60. Adsorption of CO_2 at 273 K on activated carbon from retted hemp hurd, bamboo fibre and hemp fibre with the impregnation ratio of 2:1 by $ZnCl_2$ activation after HCl washing.

Figure 61 shows the adsorption of CO_2 at 273 K on activated carbon prepared from different precursors with the impregnation ratio of 4:1 by $ZnCl_2$ activation after HCl washing. It shows that the CO_2 adsorption capacity of activated carbon derived from

bamboo fibre is higher than that from retted hemp hurd and hemp fibre at all activation temperatures. For activated carbons derived from bamboo fibre, the optimal activation temperature for CO_2 adsorption was 800 °C. For activated carbons derived from retted hemp hurd and hemp fibre, the optimal activation temperature for CO_2 adsorption is 400 °C.

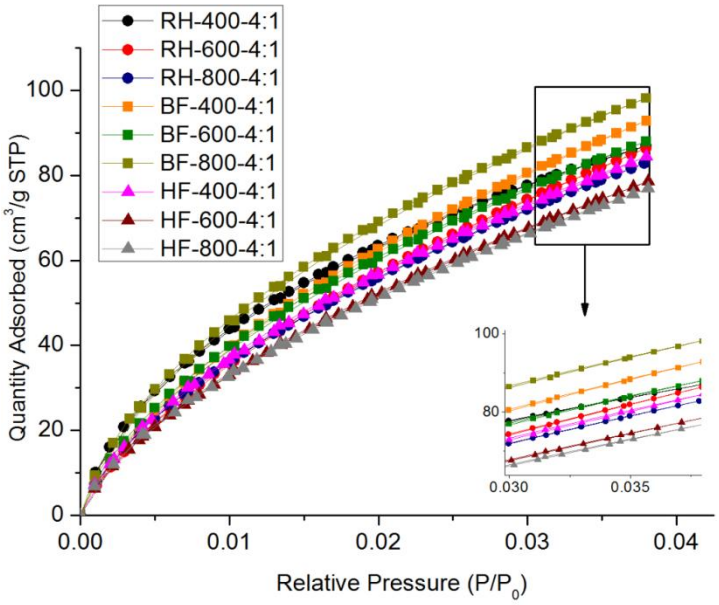

Figure 61. Adsorption of CO_2 at 273 K on activated carbon from retted hemp hurd, bamboo fibre and hemp fibre with the impregnation ratio of 4:1 by $ZnCl_2$ activation after HCl washing.

Figure 62 is the adsorption of CO_2 at 273 K on activated carbon prepared from different precursors with the activation temperature of 400 °C by $ZnCl_2$ activation after HCl washing. As shown, on activation temperature of 400 °C, the precursor of activated carbon with the highest CO_2 adsorption capacity was retted hemp hurd with the impregnation ratio of 2:1. The difference on CO_2 adsorption capacity between other activated carbons is not large.

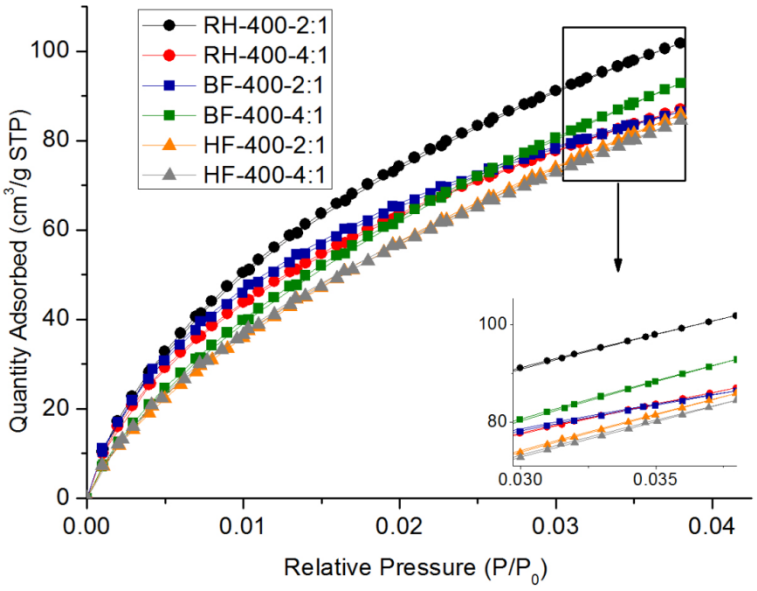

Figure 62. Adsorption of CO_2 at 273 K on activated carbon from retted hemp hurd, bamboo fibre and hemp fibre with the activation temperature of 400 °C by $ZnCl_2$ activation after HCl washing.

Figure 63 is the adsorption of CO_2 at 273 K on activated carbon prepared from different precursors with the activation temperature of 600 °C by $ZnCl_2$ activation after HCl washing. It shows that the difference of the highest CO_2 adsorption capacity from retted hemp hurd, bamboo fibre and hemp fibre (89, 88 and 86 cm^3/g STP) with the activation temperature of 600 °C is small.

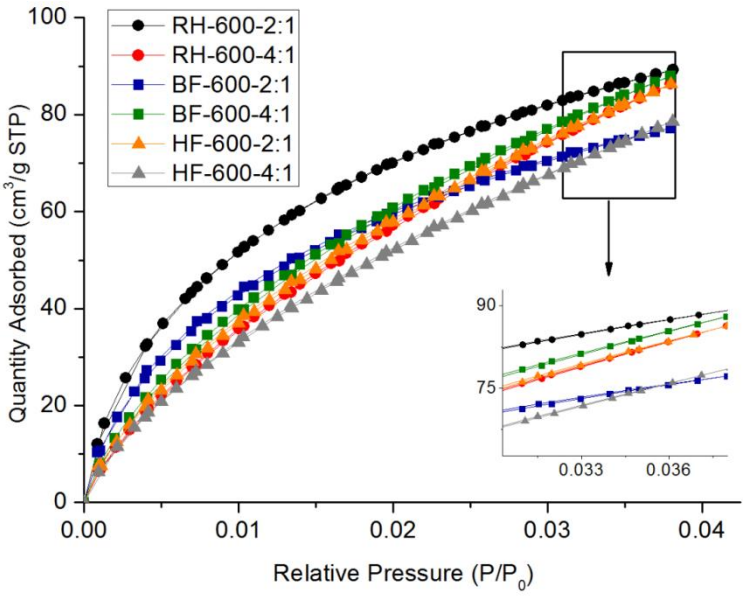

Figure 63. Adsorption of CO_2 at 273 K on activated carbon from retted hemp hurd, bamboo fibre and hemp fibre with the activation temperature of 600 °C by $ZnCl_2$ activation after HCl washing.

Figure 64 is the adsorption of CO_2 at 273 K on activated carbon prepared from different precursors with the activation temperature of 800 °C by $ZnCl_2$ activation after HCl washing. It shows the CO_2 adsorption capacity of activated carbon prepared from these three precursors with the activation temperature of 600 °C. The CO_2 adsorption capacity of activated carbon from retted hemp hurd with the impregnation ratio of 2:1 reaches 116 cm^3/g STP with the activation temperature of 800 °C. The activated carbon from hemp fibre have the least amount of CO_2 adsorption.

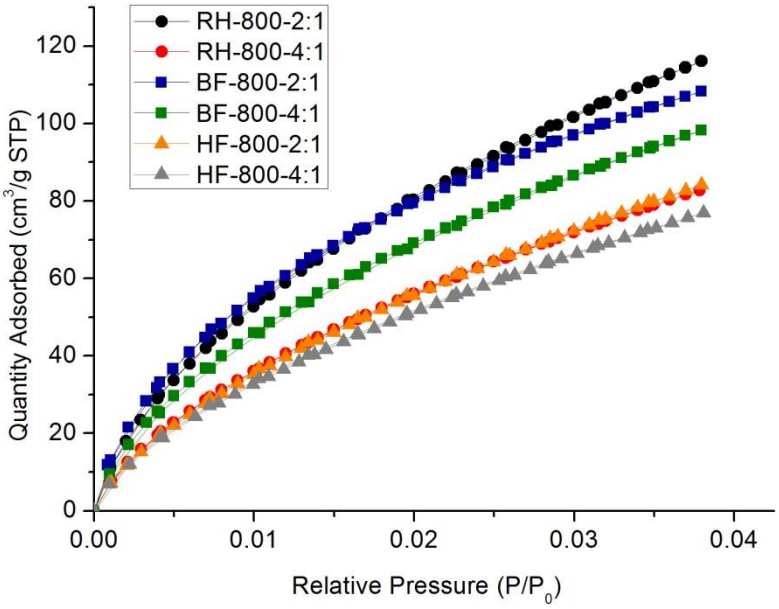

Figure 64. Adsorption of CO_2 at 273 K on activated carbon from retted hemp hurd, bamboo fibre and hemp fibre with the activation temperature of 800 °C by $ZnCl_2$ activation after HCl washing.

CHAPTER 7 CONCLUSIONS AND FUTURE WORK

7.1 Conclusions

In this work, hemp hurd and retted hemp hurd, by-products of hemp fibre industry, were used as precursors for the preparation of activated carbon by chemical activation with $ZnCl_2$ and physical activation with CO_2. Then the activated carbons derived from bamboo fibre and hemp fibre were prepared in the similar conditions for comparison. The influence of process variables such as the carbonization temperature and the impregnation ratio on morphology, porosity, chemical property and activation mechanism of the activated carbons was studied. The yields, specific surface areas, pore volumes, and pore sizes of the activated carbons were determined. The gas capture performance of the synthesized activated carbons was evaluated in adsorption of CO_2.

The results show that hemp hurd consists of two types of macropore channels of different sizes. One type is the round like or elliptic large pore channels with 40-60 μm in diameter, another type of pore channel is the polygonal or round like pores with smaller diameter, 20-30 μm. These pore channels also have high porosity on its inner wall, leading to the formation of hierarchical pore structures and connected pore geometry. Retting process caused disintegration of part of the larger pore channels and turned some of them into a coil like structure. The process of retting also improved the thermal stability of hemp hurd. The morphology of the bulk of activated carbons from hemp hurd after HCl washing retains the original appearance of the hemp hurd, and the porosity of the inner walls increased.

It has been found that the activation method significantly influences the specific surface area and pore volume of activated carbons. $ZnCl_2$ activation is proved to be a better way for synthesis of high surface area of porous carbon from biomass, and the derived activated carbons by $ZnCl_2$ activation have larger surface area compared with those using CO_2 activation. High-quality activated carbons was obtained from hemp hurd, retted hemp hurd and bamboo fibre by $ZnCl_2$ activation after HCl washing with high surface area (> 1100 m^2/g) and total pore volume (> 0.4 cm^3/g).

During CO_2 activation, porosity is developed by carbon gasification at high temperature according to the reaction "$C+CO_2 \longrightarrow 2CO$". CO_2 reacts with the carbon in hemp hurd at high temperatures. This process of gasification develops porosity and high surface area. During $ZnCl_2$ activation, $ZnCl_2$ can firstly act as a dehydrating agent, catalysing the scission of glycosidic bonds and the elimination of hydroxyl and carbonyl groups during the heating, which results in degradation of the cellulosic material and, on carbonization, produces dehydration that results in charring and aromatization of the carbon skeleton and creation of the pore structure. Secondly, the $ZnCl_2$ gas diffusion developed pathways, creating the pore structure and high surface area of the obtained activated carbon after acid washing.

The pore development was strongly dependent on the impregnation ratio of activation reagent and the subsequent carbonization temperature. HCl washing can further increase the porosity of activated carbon. All of the BET specific surface areas of the activated carbons increased largely after HCl washing. The BET specific surface area and total pore volume of the activated carbons from retted hemp hurd and bamboo fibre increased largely with high impregnation ratio. However, the effect of impregnation ratio is not that significant on activated carbons from hemp fibre. The N_2 isotherms on activated carbons from retted hemp hurd and bamboo fibre are

similar (Type I), which are quite different from the isotherms on activated carbons from hemp fibre (Type IV). Activated carbons from retted hemp hurd and bamboo fibre are highly micropores materials. Activated carbons from hemp fibre have mixtures of micropores and mesopores, Type-H4 hysteresis loops emerged in the isotherms at a high relative pressure region clearly demonstrated the wide mesopore distribution. The optimized BET specific surface area of the activated carbon from retted hemp hurd reaches 1781 m^2/g and total pore volume reaches 1.023 cm^3/g on 600 °C with impregnation ratio of 4:1. The high activation temperature results in a low yield of carbon, as a consequence of a high dehydration of the carbonaceous structure of the precursor. At the lower activation temperature, there was a trend towards an increase in yield of carbon with increasing impregnation ratio, while the opposite tendency was observed at the higher activation temperature. This may because higher impregnation ratios restrict the formation of tars and volatiles and produce a deeper dehydration at the lower activation temperature, thus increasing the carbon content. However, at the higher activation temperature, this effect is weakened.

The activated carbons by $ZnCl_2$ activation have higher CO_2 adsorption capacities compared with those by CO_2 activation. The effect of the activation temperature of activated carbon from retted hemp hurd on CO_2 adsorption capacity is greater than the effect of impregnation rate. Activated carbon from retted hemp hurd by $ZnCl_2$ activation has the highest CO_2 adsorption capacity at 273 K (142 cm^3/g STP) with the impregnation rate of 4:1 on activation temperature of 500 °C.

7.2 Future work

From the study, the morphologies of the activated carbons derived from hemp hurd and retted hemp hurd retained the unique structure and meso/macropores structure of hemp hurd, and micropores are generated during activation. These connected micro/meso/macropores geometry are highly desirable for facile electrolyte diffusion. The future work will focus on the application of activated carbons from hemp hurd and retted hemp hurd as electrode.

List of References

Abang, S., Janaun, J., Anisuzzaman, S. M., & Ikhwan, F. S. (2016). Development of carbon dioxide adsorbent from rice husk char. *IOP Conference Series: Earth and Environmental Science, 36*(1), 012022.

Ahmadpour, A., & Do, D. D. (1997). The preparation of activated carbon from macadamia nutshell by chemical activation. *Carbon, 35*(12), 1723-1732. doi:https://doi.org/10.1016/S0008-6223(97)00127-9

Altintig, E., & Kirkil, S. (2016). Preparation and properties of Ag-coated activated carbon nanocomposites produced from wild chestnut shell by ZnCl2 activation. *Journal of the Taiwan Institute of Chemical Engineers, 63*(Supplement C), 180-188. doi:https://doi.org/10.1016/j.jtice.2016.02.032

Anderson, N., Jones, J., Page-Dumroese, D., McCollum, D., Baker, S., Loeffler, D., & Chung, W. (2007). A Comparison of Producer Gas, Biochar, and Activated Carbon from Two Distributed Scale Thermochemical Conversion Systems Used to Process Forest Biomass. *Energies, 6*(1), 164.

Angın, D., Altintig, E., & Köse, T. E. (2013). Influence of process parameters on the surface and chemical properties of activated carbon obtained from biochar by chemical activation. *Bioresource Technology, 148*(Supplement C), 542-549. doi:https://doi.org/10.1016/j.biortech.2013.08.164

Angın, D., Köse, T. E., & Selengil, U. (2013). Production and characterization of activated carbon prepared from safflower seed cake biochar and its ability to absorb reactive dyestuff. *Applied Surface Science, 280*(Supplement C), 705-710. doi:https://doi.org/10.1016/j.apsusc.2013.05.046

Arampatzidou, A. C., & Deliyanni, E. A. (2016). Comparison of activation media and pyrolysis temperature for activated carbons development by pyrolysis of potato peels for effective adsorption of endocrine disruptor bisphenol-A. *Journal of Colloid and Interface Science, 466*(Supplement C), 101-112. doi:https://doi.org/10.1016/j.jcis.2015.12.003

Azargohar, R., & Dalai, A. K. (2006). Biochar As a Precursor of Activated Carbon. In J. D. McMillan, W. S. Adney, J. R. Mielenz, & K. T. Klasson (Eds.),

Twenty-Seventh Symposium on Biotechnology for Fuels and Chemicals (pp. 762-773). Totowa, NJ: Humana Press.

Azargohar, R., & Dalai, A. K. (2009). Steam and KOH activation of biochar: Experimental and modeling studies. *Microporous and Mesoporous Materials, 110*(2), 413-421. doi:https://doi.org/10.1016/j.micromeso.2007.06.047

Babel, S., & Kurniawan, T. A. (2003). Low-cost adsorbents for heavy metals uptake from contaminated water: a review. *Journal of Hazardous Materials, 97*(1), 219-243. doi:https://doi.org/10.1016/S0304-3894(02)00263-7

Balčiūnas, G., Vėjelis, S., Vaitkus, S., & Kairytė, A. (2013). Physical Properties and Structure of Composite Made by Using Hemp Hurds and Different Binding Materials. *Procedia Engineering, 57*(Supplement C), 159-166. doi:https://doi.org/10.1016/j.proeng.2013.04.023

Bamufleh, H. S. (2009). Single and binary sulfur removal components from model diesel fuel using granular activated carbon from dates' stones activated by ZnCl2. *Applied Catalysis A: General, 365*(2), 153-158. doi:https://doi.org/10.1016/j.apcata.2009.05.054

Barrett, E. P., Joyner, L. G., & Halenda, P. P. (1951). The Determination of Pore Volume and Area Distributions in Porous Substances. I. Computations from Nitrogen Isotherms. *Journal of the American Chemical Society, 73*(1), 373-380. doi:10.1021/ja01145a126

Bhatnagar, A., Ji, M., Choi, Y. H., Jung, W., Lee, S. H., Kim, S. J., . . . Kang, J. W. (2008). Removal of Nitrate from Water by Adsorption onto Zinc Chloride Treated Activated Carbon. *Separation Science and Technology, 43*(4), 886-907. doi:10.1080/01496390701787461

Bouchenafa-Saïb, N., Mekarzia, A., Bouzid, B., Mohammedi, O., Khelifa, A., Benrachedi, K., & Belhaneche, N. (2014). Removal of malathion from polluted water by adsorption onto chemically activated carbons produced from coffee grounds. *Desalination and Water Treatment, 52*(25-27), 4920-4927. doi:10.1080/19443994.2013.808845

Bouguettoucha, A., Reffas, A., Chebli, D., Mekhalif, T., & Amrane, A. (2016). Novel activated carbon prepared from an agricultural waste, Stipa tenacissima, based on ZnCl2 activation—characterization and application to the removal

of methylene blue. *Desalination and Water Treatment, 57*(50), 24056-24069. doi:10.1080/19443994.2015.1137231

Campos, J. W., Beidaghi, M., Hatzell, K. B., Dennison, C. R., Musci, B., Presser, V., . . . Gogotsi, Y. (2013). Investigation of carbon materials for use as a flowable electrode in electrochemical flow capacitors. *Electrochimica Acta, 98*(Supplement C), 123-130. doi:https://doi.org/10.1016/j.electacta.2013.03.037

Caturla, F., Molina-Sabio, M., & Rodríguez-Reinoso, F. (1991). Preparation of activated carbon by chemical activation with ZnCl2. *Carbon, 29*(7), 999-1007. doi:https://doi.org/10.1016/0008-6223(91)90179-M

Chang, B., Wang, Y., Pei, K., Yang, S., & Dong, X. (105 2014). ZnCl2-activated porous carbon spheres with high surface area and superior mesoporous structure as an efficient supercapacitor electrode. *RSC Advances, 4*(76), 40546-40552. doi:10.1039/c4ra06418f

Chang, B., Wang, Y., Pei, K., Yang, S., & Dong, X. (2014). ZnCl2-activated porous carbon spheres with high surface area and superior mesoporous structure as an efficient supercapacitor electrode. *RSC Advances, 4*(76), 40546-40552. doi:10.1039/c4ra06418f

Chen, C., Zhao, P., Li, Z., & Tong, Z. (2016). Adsorption behavior of chromium(VI) on activated carbon from eucalyptus sawdust prepared by microwave-assisted activation with ZnCl2. *Desalination and Water Treatment, 57*(27), 12572-12584. doi:10.1080/19443994.2015.1049960

Cherney, J. H., & Small, E. (2016). Industrial hemp in North America: production, politics and potential. *Agronomy, 6*(4), 58.

Cukierman, A. L. (2013). Development and environmental applications of activated carbon cloths. *ISRN Chemical Engineering, 2013*.

Dąbrowski, A., Podkościelny, P., Hubicki, Z., & Barczak, M. (2005). Adsorption of phenolic compounds by activated carbon—a critical review. *Chemosphere, 58*(8), 1049-1070. doi:https://doi.org/10.1016/j.chemosphere.2004.09.067

Daffalla, S. B., Mukhtar, H., & Shaharun, M. S. (2012). Properties of activated carbon prepared from rice husk with chemical activation. *International*

Journal of Global Environmental Issues, 12(2-4), 107-129. doi:10.1504/ijgenvi.2012.049375

Danish, M., Hashim, R., Rafatullah, M., Sulaiman, O., Ahmad, A., & Govind. (2011). Adsorption of Pb(II) Ions from Aqueous Solutions by Date Bead Carbon Activated with ZnCl2. *CLEAN – Soil, Air, Water, 39*(4), 392-399. doi:10.1002/clen.201000185

De, M., Azargohar, R., Dalai, A. K., & Shewchuk, S. R. (2013). Mercury removal by bio-char based modified activated carbons. *Fuel, 103*(Supplement C), 570-578. doi:https://doi.org/10.1016/j.fuel.2012.08.011

Demiral, İ., Aydın Şamdan, C., & Demiral, H. (2016). Production and characterization of activated carbons from pumpkin seed shell by chemical activation with ZnCl2. *Desalination and Water Treatment, 57*(6), 2446-2454. doi:10.1080/19443994.2015.1027276

Dias, J. M., Alvim-Ferraz, M. C. M., Almeida, M. F., Rivera-Utrilla, J., & Sánchez-Polo, M. (2007). Waste materials for activated carbon preparation and its use in aqueous-phase treatment: A review. *Journal of Environmental Management, 85*(4), 833-846. doi:https://doi.org/10.1016/j.jenvman.2007.07.031

dos Reis, G. S., Adebayo, M. A., Lima, E. C., Sampaio, C. H., & Prola, L. D. T. (2016). Activated Carbon from Sewage Sludge for Preconcentration of Copper. *Analytical Letters, 49*(4), 541-555. doi:10.1080/00032719.2015.1076833

Dos Santos, J. M., Felsner, M. L., Almeida, C. A. P., & Justi, K. C. (2016). Removal of Reactive Orange 107 Dye from Aqueous Solution by Activated Carbon from Pinus elliottii Sawdust: a Response Surface Methodology Study. *Water, Air, & Soil Pollution, 227*(9), 300. doi:10.1007/s11270-016-3003-z

Downie, A., Munroe, P., Cowie, A., Van Zwieten, L., & Lau, D. M. S. (2012). Biochar as a Geoengineering Climate Solution: Hazard Identification and Risk Management. *Critical Reviews in Environmental Science and Technology, 42*(3), 225-250. doi:10.1080/10643389.2010.507980

Du, X., Zhao, W., Ma, S., Ma, M., Qi, T., Wang, Y., & Hua, C. (175 2016). Effect of ZnCl2 impregnation concentration on the microstructure and electrical

performance of ramie-based activated carbon hollow fiber. *Ionics, 22*(4), 545-553. doi:10.1007/s11581-015-1571-3

Du, X., Zhao, W., Ma, S., Ma, M., Qi, T., Wang, Y., & Hua, C. (2016). Effect of ZnCl2 impregnation concentration on the microstructure and electrical performance of ramie-based activated carbon hollow fiber. *Ionics, 22*(4), 545-553. doi:10.1007/s11581-015-1571-3

Erdem, M., Orhan, R., Şahin, M., & Aydın, E. (2016). Preparation and Characterization of a Novel Activated Carbon from Vine Shoots by ZnCl2 Activation and Investigation of Its Rifampicine Removal Capability. *Water, Air, & Soil Pollution, 227*(7), 226. doi:10.1007/s11270-016-2929-5

Faraji, S., & Ani, F. N. (2015). The development supercapacitor from activated carbon by electroless plating—A review. *Renewable and Sustainable Energy Reviews, 42*(Supplement C), 823-834. doi:https://doi.org/10.1016/j.rser.2014.10.068

Fortier, H., Westreich, P., Selig, S., Zelenietz, C., & Dahn, J. R. (2008). Ammonia, cyclohexane, nitrogen and water adsorption capacities of an activated carbon impregnated with increasing amounts of ZnCl2, and designed to chemisorb gaseous NH3 from an air stream. *Journal of Colloid and Interface Science, 320*(2), 423-435. doi:https://doi.org/10.1016/j.jcis.2008.01.018

Gañán-Gómez, J., Macías-García, A., Díaz-Díez, M. A., González-García, C., & Sabio-Rey, E. (2006). Preparation and characterization of activated carbons from impregnation pitch by ZnCl2. *Applied Surface Science, 252*(17), 5976-5979. doi:https://doi.org/10.1016/j.apsusc.2005.11.011

Gaya, U. I., Otene, E., & Abdullah, A. H. (2015). Adsorption of aqueous Cd(II) and Pb(II) on activated carbon nanopores prepared by chemical activation of doum palm shell. *SpringerPlus, 4*(1), 458. doi:10.1186/s40064-015-1256-4

Gottipati, R., & Mishra, S. (2016). Preparation of microporous activated carbon from Aegle Marmelos fruit shell and its application in removal of chromium(VI) from aqueous phase. *Journal of Industrial and Engineering Chemistry, 36*(Supplement C), 355-363. doi:https://doi.org/10.1016/j.jiec.2016.03.005

Habibi, M. K., & Lu, Y. (2014). Crack Propagation in Bamboo's Hierarchical Cellular Structure. *Scientific Reports, 4*, 5598. doi:10.1038/srep05598

Hameed, B. H., Tan, I. A. W., & Ahmad, A. L. (2009). Preparation of oil palm empty fruit bunch-based activated carbon for removal of 2,4,6-trichlorophenol: Optimization using response surface methodology. *Journal of Hazardous Materials, 164*(2), 1316-1324. doi:https://doi.org/10.1016/j.jhazmat.2008.09.042

Härmas, M., Thomberg, T., Kurig, H., Romann, T., Jänes, A., & Lust, E. (2016). Microporous–mesoporous carbons for energy storage synthesized by activation of carbonaceous material by zinc chloride, potassium hydroxide or mixture of them. *Journal of Power Sources, 326*(Supplement C), 624-634. doi:https://doi.org/10.1016/j.jpowsour.2016.04.038

Hayashi, J. i., Kazehaya, A., Muroyama, K., & Watkinson, A. P. (2000). Preparation of activated carbon from lignin by chemical activation. *Carbon, 38*(13), 1873-1878. doi:https://doi.org/10.1016/S0008-6223(00)00027-0

Hong, S.-M., Choi, S. W., Kim, S. H., & Lee, K. B. (2016). Porous carbon based on polyvinylidene fluoride: Enhancement of CO2 adsorption by physical activation. *Carbon, 99*(Supplement C), 354-360. doi:https://doi.org/10.1016/j.carbon.2015.12.012

Ioannidou, O., & Zabaniotou, A. (2007). Agricultural residues as precursors for activated carbon production—A review. *Renewable and Sustainable Energy Reviews, 11*(9), 1966-2005. doi:https://doi.org/10.1016/j.rser.2006.03.013

Ioannidou, O., & Zabaniotou, A. (2013). Agricultural residues as precursors for activated carbon production—A review. *Renewable and Sustainable Energy Reviews, 11*(9), 1966-2005. doi:https://doi.org/10.1016/j.rser.2006.03.013

Jain, A., Balasubramanian, R., & Srinivasan, M. P. (2016). Hydrothermal conversion of biomass waste to activated carbon with high porosity: A review. *Chemical Engineering Journal, 283*(Supplement C), 789-805. doi:https://doi.org/10.1016/j.cej.2015.08.014

Jodeh, S., Abdelwahab, F., Jaradat, N., Warad, I., & Jodeh, W. (2016). Adsorption of diclofenac from aqueous solution using Cyclamen persicum tubers based activated carbon (CTAC). *Journal of the Association of Arab Universities for Basic and Applied Sciences, 20*(Supplement C), 32-38. doi:https://doi.org/10.1016/j.jaubas.2014.11.002

Jones, F., Tran, H., Lindberg, D., Zhao, L., & Hupa, M. (2013). Thermal Stability of Zinc Compounds. *Energy & Fuels, 27*(10), 5663-5669. doi:10.1021/ef400505u

Jutakridsada, P., Prajaksud, C., Kuboonya-Aruk, L., Theerakulpisut, S., & Kamwilaisak, K. (2016). Adsorption characteristics of activated carbon prepared from spent ground coffee. *Clean Technologies and Environmental Policy, 18*(3), 639-645. doi:10.1007/s10098-015-1083-x

Kamandari, H., Hashemipour Rafsanjani, H., Najjarzadeh, H., & Eksiri, Z. (2015). Influence of process variables on chemically activated carbon from pistachio shell with ZnCl2 and KOH. *Research on Chemical Intermediates, 41*(1), 71-81. doi:10.1007/s11164-013-1169-1

Karaçetin, G., Sivrikaya, S., & Imamoğlu, M. (2014). Adsorption of methylene blue from aqueous solutions by activated carbon prepared from hazelnut husk using zinc chloride. *Journal of Analytical and Applied Pyrolysis, 110*(Supplement C), 270-276. doi:https://doi.org/10.1016/j.jaap.2014.09.006

Karimnezhad, L., Haghighi, M., & Fatehifar, E. (2014). Adsorption of benzene and toluene from waste gas using activated carbon activated by ZnCl2. *Frontiers of Environmental Science & Engineering, 8*(6), 835-844. doi:10.1007/s11783-014-0695-4

Kong, W., Zhao, F., Guan, H., Zhao, Y., Zhang, H., & Zhang, B. (2016). Highly adsorptive mesoporous carbon from biomass using molten-salt route. *Journal of Materials Science, 51*(14), 6793-6800. doi:10.1007/s10853-016-9966-8

Kongnoo, A., Intharapat, P., Worathanakul, P., & Phalakornkule, C. (2016). Diethanolamine impregnated palm shell activated carbon for CO2 adsorption at elevated temperatures. *Journal of Environmental Chemical Engineering, 4*(1), 73-81. doi:https://doi.org/10.1016/j.jece.2015.11.015

Li, L., Wang, X., Wang, S., Cao, Z., Wu, Z., Wang, H., . . . Liu, J. (100 2016). Activated Carbon Prepared from Lignite as Supercapacitor Electrode Materials. *Electroanalysis, 28*(1), 243-248. doi:10.1002/elan.201500532

Li, L., Wang, X., Wang, S., Cao, Z., Wu, Z., Wang, H., . . . Liu, J. (2016). Activated Carbon Prepared from Lignite as Supercapacitor Electrode Materials. *Electroanalysis, 28*(1), 243-248. doi:10.1002/elan.201500532

Lin, J., & Zhao, G. (2016). Preparation and Characterization of High Surface Area Activated Carbon Fibers from Lignin. *Polymers, 8*(10), 369.

Lin, Y., Munroe, P., Joseph, S., Henderson, R., & Ziolkowski, A. (2012). Water extractable organic carbon in untreated and chemical treated biochars. *Chemosphere, 87*(2), 151-157. doi:https://doi.org/10.1016/j.chemosphere.2011.12.007

Lippens, B. C., Linsen, B. G., & Boer, J. H. d. (1964). Studies on pore systems in catalysts I. The adsorption of nitrogen; apparatus and calculation. *Journal of Catalysis, 3*(1), 32-37. doi:https://doi.org/10.1016/0021-9517(64)90089-2

Liu, B., Gu, J., & Zhou, J. (2016). High surface area rice husk-based activated carbon prepared by chemical activation with ZnCl2-CuCl2 composite activator. *Environmental Progress & Sustainable Energy, 35*(1), 133-140. doi:10.1002/ep.12215

Liu, J., Wang, S., Yang, J., Liao, J., Lu, M., Pan, H., & An, L. (2014). ZnCl2 activated electrospun carbon nanofiber for capacitive desalination. *Desalination, 344*(Supplement C), 446-453. doi:https://doi.org/10.1016/j.desal.2014.04.015

Liu, S., Ge, L., Gao, S., Zhuang, L., Zhu, Z., & Wang, H. (2017). Activated carbon derived from bio-waste hemp hurd and retted hemp hurd for CO2 adsorption. *Composites Communications, 5*(Supplement C), 27-30. doi:https://doi.org/10.1016/j.coco.2017.06.002

Liu, Y., Wang, Y., Zhang, G., Liu, W., Wang, D., & Dong, Y. (2016). Preparation of activated carbon from willow leaves and evaluation in electric double-layer capacitors. *Materials Letters, 176*(Supplement C), 60-63. doi:https://doi.org/10.1016/j.matlet.2016.04.065

Lowell, S., Shields, J. E., Thomas, M. A., & Thommes, M. (2012). Characterization of Porous Solids and Powders: Surface Area, Pore Size and Density. doi:10.1007/978-1-4020-2303-3

Lozano-Castelló, D., Cazorla-Amorós, D., Linares-Solano, A., & Quinn, D. (2002). Activated carbon monoliths for methane storage: influence of binder. *Carbon, 40*(15), 2817-2825.

Ma, Y., Wang, Q., Wang, X., Sun, X., & Wang, X. (2015). A comprehensive study on activated carbon prepared from spent shiitake substrate via pyrolysis with ZnCl2. *Journal of Porous Materials, 22*(1), 157-169. doi:10.1007/s10934-014-9882-8

Madhu, R., Veeramani, V., Chen, S.-M., Veerakumar, P., Liu, S.-B., & Miyamoto, N. (37). Functional porous carbon-ZnO nanocomposites for high-performance biosensors and energy storage applications. *Physical Chemistry Chemical Physics, 18*(24), 16466-16475. doi:10.1039/c6cp01285j

Madhu, R., Veeramani, V., Chen, S.-M., Veerakumar, P., Liu, S.-B., & Miyamoto, N. (2016). Functional porous carbon-ZnO nanocomposites for high-performance biosensors and energy storage applications. *Physical Chemistry Chemical Physics, 18*(24), 16466-16475. doi:10.1039/c6cp01285j

Mahmoudi, K., Hamdi, N., Kriaa, A., & Srasra, E. (2012). Adsorption of methyl orange using activated carbon prepared from lignin by ZnCl2 treatment. *Russian Journal of Physical Chemistry A, 86*(8), 1294-1300. doi:10.1134/s0036024412060180

Marsh, H. (1987). Adsorption methods to study microporosity in coals and carbons—a critique. *Carbon, 25*(1), 49-58. doi:https://doi.org/10.1016/0008-6223(87)90039-X

Martin, N., Mouret, N., Davies, P., & Baley, C. (2013). Influence of the degree of retting of flax fibers on the tensile properties of single fibers and short fiber/polypropylene composites. *Industrial Crops and Products, 49*(Supplement C), 755-767. doi:https://doi.org/10.1016/j.indcrop.2013.06.012

Martínez, M. B., Van der Bruggen, B., Negrin, Z. R., & Luis Alconero, P. (2012). Separation of a high-value pharmaceutical compound from waste ethanol by nanofiltration. *Journal of Industrial and Engineering Chemistry, 18*(5), 1635-1641. doi:https://doi.org/10.1016/j.jiec.2012.02.024

Martins, A. C., Pezoti, O., Cazetta, A. L., Bedin, K. C., Yamazaki, D. A. S., Bandoch, G. F. G., . . . Almeida, V. C. (2015). Removal of tetracycline by NaOH-activated carbon produced from macadamia nut shells: Kinetic and equilibrium studies. *Chemical Engineering Journal, 260*(Supplement C), 291-299. doi:https://doi.org/10.1016/j.cej.2014.09.017

Mataji, M., & Khoshandam, B. (2014). BENZENE ADSORPTION ON ACTIVATED CARBON FROM WALNUT SHELL. *Chemical Engineering Communications, 201*(10), 1294-1313. doi:10.1080/00986445.2013.808996

McHenry, M. P. (2009). Agricultural bio-char production, renewable energy generation and farm carbon sequestration in Western Australia: Certainty, uncertainty and risk. *Agriculture, Ecosystems & Environment, 129*(1), 1-7. doi:https://doi.org/10.1016/j.agee.2008.08.006

Memming, R., Tolle, H., & Wierenga, P. (1986). Properties of polymeric layers of hydrogenated amorphous carbon produced by a plasma-activated chemical vapour deposition process II: Tribological and mechanical properties. *Thin Solid Films, 143*(1), 31-41.

Mohammadi, S. Z., Hamidian, H., & Moeinadini, Z. (2014). High surface area-activated carbon from Glycyrrhiza glabra residue by ZnCl2 activation for removal of Pb(II) and Ni(II) from water samples. *Journal of Industrial and Engineering Chemistry, 20*(6), 4112-4118. doi:https://doi.org/10.1016/j.jiec.2014.01.009

Namasivayam, C., & Sangeetha, D. (2004). Equilibrium and kinetic studies of adsorption of phosphate onto ZnCl2 activated coir pith carbon. *Journal of Colloid and Interface Science, 280*(2), 359-365. doi:https://doi.org/10.1016/j.jcis.2004.08.015

Namasivayam, C., & Sangeetha, D. (2005). Kinetic studies of adsorption of thiocyanate onto ZnCl2 activated carbon from coir pith, an agricultural solid waste. *Chemosphere, 60*(11), 1616-1623. doi:https://doi.org/10.1016/j.chemosphere.2005.02.051

Namasivayam, C., & Sangeetha, D. (2006a). Recycling of agricultural solid waste, coir pith: Removal of anions, heavy metals, organics and dyes from water by adsorption onto ZnCl2 activated coir pith carbon. *Journal of Hazardous Materials, 135*(1), 449-452. doi:https://doi.org/10.1016/j.jhazmat.2005.11.066

Namasivayam, C., & Sangeetha, D. (2006b). Removal and recovery of vanadium(V) by adsorption onto ZnCl2 activated carbon: Kinetics and isotherms. *Adsorption, 12*(2), 103-117. doi:10.1007/s10450-006-0373-3

Namasivayam, C., & Sangeetha, D. (2006c). Removal of chromium(VI) by ZnCl2 activated coir pith carbon. *Toxicological & Environmental Chemistry, 88*(2), 219-233. doi:10.1080/02772240600661130

Namasivayam, C., & Sangeetha, D. (2008). Application of coconut coir pith for the removal of sulfate and other anions from water. *Desalination, 219*(1), 1-13. doi:https://doi.org/10.1016/j.desal.2007.03.008

Nelson, R. A. (1999). *Hemp Husbandry*: Rex Research Archives.

Obreja, V. V. N. (19). On the performance of supercapacitors with electrodes based on carbon nanotubes and carbon activated material—A review. *Physica E: Low-dimensional Systems and Nanostructures, 40*(7), 2596-2605. doi:https://doi.org/10.1016/j.physe.2007.09.044

Obreja, V. V. N. (2008). On the performance of supercapacitors with electrodes based on carbon nanotubes and carbon activated material—A review. *Physica E: Low-dimensional Systems and Nanostructures, 40*(7), 2596-2605. doi:https://doi.org/10.1016/j.physe.2007.09.044

Olivares-Marín, M., Fernández-González, C., Macías-García, A., & Gómez-Serrano, V. (2006). Preparation of activated carbon from cherry stones by chemical activation with ZnCl2. *Applied Surface Science, 252*(17), 5967-5971. doi:https://doi.org/10.1016/j.apsusc.2005.11.008

Özhan, A., Şahin, Ö., Küçük, M. M., & Saka, C. (2014). Preparation and characterization of activated carbon from pine cone by microwave-induced ZnCl2 activation and its effects on the adsorption of methylene blue. *Cellulose, 21*(4), 2457-2467. doi:10.1007/s10570-014-0299-y

Pandolfo, A. G., & Hollenkamp, A. F. (2006). Carbon properties and their role in supercapacitors. *Journal of Power Sources, 157*(1), 11-27. doi:https://doi.org/10.1016/j.jpowsour.2006.02.065

Park, J., Hung, I., Gan, Z., Rojas, O. J., Lim, K. H., & Park, S. (2013). Activated carbon from biochar: Influence of its physicochemical properties on the sorption characteristics of phenanthrene. *Bioresource Technology, 149*(Supplement C), 383-389. doi:https://doi.org/10.1016/j.biortech.2013.09.085

Pezoti Junior, O., Cazetta, A. L., Gomes, R. C., Barizão, É. O., Souza, I. P. A. F., Martins, A. C., . . . Almeida, V. C. (2014). Synthesis of ZnCl2-activated carbon from macadamia nut endocarp (Macadamia integrifolia) by microwave-assisted pyrolysis: Optimization using RSM and methylene blue adsorption. *Journal of Analytical and Applied Pyrolysis, 105*(Supplement C), 166-176. doi:https://doi.org/10.1016/j.jaap.2013.10.015

Pezoti, O., Cazetta, A. L., Souza, I. P. A. F., Bedin, K. C., Martins, A. C., Silva, T. L., & Almeida, V. C. (2014). Adsorption studies of methylene blue onto ZnCl2-activated carbon produced from buriti shells (Mauritia flexuosa L.). *Journal of Industrial and Engineering Chemistry, 20*(6), 4401-4407. doi:https://doi.org/10.1016/j.jiec.2014.02.007

Ramakrishnan, K., & Namasivayam, C. (2011). Zinc chloride-activated jatropha husk carbon for removal of phenol from water by adsorption: equilibrium and kinetic studies. *Toxicological & Environmental Chemistry, 93*(6), 1111-1122. doi:10.1080/02772248.2011.575073

Reed, B. E., & Matsumoto, M. R. (1993). Modeling Cadmium Adsorption by Activated Carbon Using the Langmuir and Freundlich Isotherm Expressions. *Separation Science and Technology, 28*(13-14), 2179-2195. doi:10.1080/01496399308016742

Rehman, M. S. U., Rashid, N., Saif, A., Mahmood, T., & Han, J.-I. (2013). Potential of bioenergy production from industrial hemp (Cannabis sativa): Pakistan perspective. *Renewable and sustainable energy reviews, 18*, 154-164.

Rincón-Silva, N. G., Moreno-Piraján, J. C., & Giraldo, L. (2016). Equilibrium, kinetics and thermodynamics study of phenols adsorption onto activated carbon obtained from lignocellulosic material (Eucalyptus Globulus labill seed). *Adsorption, 22*(1), 33-48. doi:10.1007/s10450-015-9724-2

Rodríguez-Reinoso, F., Molina-Sabio, M., & González, M. T. (1994). The use of steam and CO2 as activating agents in the preparation of activated carbons. *Carbon, 33*(1), 15-23. doi:https://doi.org/10.1016/0008-6223(94)00100-E

Rosas, J. M., Bedia, J., Rodríguez-Mirasol, J., & Cordero, T. (2008). Preparation of Hemp-Derived Activated Carbon Monoliths. Adsorption of Water Vapor. *Industrial & Engineering Chemistry Research, 47*(4), 1288-1296. doi:10.1021/ie070924w

Rosas, J. M., Bedia, J., Rodríguez-Mirasol, J., & Cordero, T. (2009). HEMP-derived activated carbon fibers by chemical activation with phosphoric acid. *Fuel, 88*(1), 19-26. doi:https://doi.org/10.1016/j.fuel.2008.08.004

Rouquerol, F., Rouquerol, J., Sing, K. S. W., Llewellyn, P., & Maurin, G. (2013). Adsorption by Powders and Porous Solids: Principles, Methodology and Applications.

Şahin, Ö., Saka, C., Ceyhan, A. A., & Baytar, O. (2015). Preparation of High Surface Area Activated Carbon from Elaeagnus angustifolia Seeds by Chemical Activation with ZnCl2 in One-Step Treatment and its Iodine Adsorption. *Separation Science and Technology, 50*(6), 886-891. doi:10.1080/01496395.2014.966204

Salleh, Z., Yusop, M., & Rosdi, M. MECHANICAL PROPERTIES OF ACTIVATED CARBON (Abdullah, Al.

Şencan, A., Karaboyacı, M., & Kılıç, M. (2015). Determination of lead(II) sorption capacity of hazelnut shell and activated carbon obtained from hazelnut shell activated with ZnCl2. *Environmental Science and Pollution Research, 22*(5), 3238-3248. doi:10.1007/s11356-014-2974-9

Shannon, M. A., Bohn, P. W., Elimelech, M., Georgiadis, J. G., Mariñas, B. J., & Mayes, A. M. (2008). Science and technology for water purification in the coming decades. *Nature, 452*, 301. doi:10.1038/nature06599

Stevulova, N., Cigasova, J., Estokova, A., Terpakova, E., Geffert, A., Kacik, F., . . . Holub, M. (2014). Properties Characterization of Chemically Modified Hemp Hurds. *Materials, 7*(12), 8131.

Subha, R., & Namasivayam, C. (2010). ZnCl2-Modified Activated Carbon from Biomass Coir Pith for the Removal of 2-Chlorophenol by Adsorption Process. *Bioremediation Journal, 14*(1), 1-9. doi:10.1080/10889860903455360

Supplemental Material: A Practical Guide to Isotherms of Adsortion on Heterogeneous Surfaces. Retrieved from See Supplemental Material at http://hektor.umcs.lublin.pl/~awmarczx/awm/ads/t-plot.htm.

Supplemental Material: BJH. Retrieved from See Supplemental Material at http://eng.thesaurus.rusnano.com/wiki/article1157.

Supplemental Material: ELGA Lab activated carbon. Retrieved from See Supplemental Material at https://www.elgalabwater.com/technologies/activated-carbon.

Supplemental Material: Kuraray Chemical Co., Ltd. Retrieved from See Supplemental Material at http://kuraray-c.ofdesign.co.jp/en/business/study/.

Supplemental Material: Surface area Analysis Using BET. Retrieved from See Supplemental Material at https://www.coursehero.com/file/13512492/Surface-area-Analysis-Using-BET/.

Supplemental Material: Surface Area and Pore Size Distribution.

Supplemental Material: Tam Dinh Co. Ltd. Retrieved from See Supplemental Material at http://tamdinh.com/.

Tay, T., Ucar, S., & Karagöz, S. (2009). Preparation and characterization of activated carbon from waste biomass. *Journal of Hazardous Materials, 165*(1), 481-485. doi:https://doi.org/10.1016/j.jhazmat.2008.10.011

Thakur, V. K., & Thakur, M. K. (2014). Processing and characterization of natural cellulose fibers/thermoset polymer composites. *Carbohydrate Polymers, 109*(Supplement C), 102-117. doi:https://doi.org/10.1016/j.carbpol.2014.03.039

Uçar, S., Erdem, M., Tay, T., & Karagöz, S. (2008). Preparation and characterization of activated carbon produced from pomegranate seeds by ZnCl2 activation. *Applied Surface Science, 255*(21), 8890-8896. doi:https://doi.org/10.1016/j.apsusc.2009.06.080

Uçar, S., Erdem, M., Tay, T., & Karagöz, S. (2009). Preparation and characterization of activated carbon produced from pomegranate seeds by ZnCl2 activation. *Applied Surface Science, 255*(21), 8890-8896. doi:https://doi.org/10.1016/j.apsusc.2009.06.080

Vargas, D. P., Giraldo, L., & Moreno-Piraján, J. C. (2016). Accessible area and hydrophobicity of activated carbons obtained from the enthalpy characterization. *Adsorption, 22*(1), 3-11. doi:10.1007/s10450-015-9721-5

Vedoy, D. (2013). *Development of Methodologies for Improving Thermal Stability of Plant Fiber for Application in Thermoplastic Composites.* UWSpace. Retrieved from http://hdl.handle.net/10012/7201

Walton, K. S., & Snurr, R. Q. (2007). Applicability of the BET Method for Determining Surface Areas of Microporous Metal−Organic Frameworks. *Journal of the American Chemical Society, 129*(27), 8552-8556. doi:10.1021/ja071174k

Wang, H., Xu, Z., Kohandehghan, A., Li, Z., Cui, K., Tan, X., . . . Mitlin, D. (2013). Interconnected Carbon Nanosheets Derived from Hemp for Ultrafast Supercapacitors with High Energy. *ACS Nano, 7*(6), 5131-5141. doi:10.1021/nn400731g

Wang, T., Tan, S., & Liang, C. (2009). Preparation and characterization of activated carbon from wood via microwave-induced ZnCl2 activation. *Carbon, 47*(7), 1880-1883. doi:https://doi.org/10.1016/j.carbon.2009.03.035

Williams, P. T., & Reed, A. R. (2003). Pre-formed activated carbon matting derived from the pyrolysis of biomass natural fibre textile waste. *Journal of Analytical and Applied Pyrolysis, 70*(2), 563-577. doi:https://doi.org/10.1016/S0165-2370(03)00026-3

Williams, P. T., & Reed, A. R. (2004). High grade activated carbon matting derived from the chemical activation and pyrolysis of natural fibre textile waste. *Journal of Analytical and Applied Pyrolysis, 71*(2), 971-986. doi:https://doi.org/10.1016/j.jaap.2003.12.007

Xia, D., Tan, F., Zhang, C., Jiang, X., Chen, Z., Li, H., . . . Wang, Y. (2016). ZnCl2-activated biochar from biogas residue facilitates aqueous As(III) removal. *Applied Surface Science, 377*(Supplement C), 361-369. doi:https://doi.org/10.1016/j.apsusc.2016.03.109

Xu, X., Gao, B., Jin, B., & Yue, Q. (2016). Removal of anionic pollutants from liquids by biomass materials: A review. *Journal of Molecular Liquids, 215*(Supplement C), 565-595. doi:https://doi.org/10.1016/j.molliq.2015.12.101

Yang, R., Liu, G., Li, M., Zhang, J., & Hao, X. (2012). Preparation and N2, CO2 and H2 adsorption of super activated carbon derived from biomass source hemp

(Cannabis sativa L.) stem. *Microporous and Mesoporous Materials, 158*(Supplement C), 108-116. doi:https://doi.org/10.1016/j.micromeso.2012.03.004

Yang, R., Liu, G., Xu, X., Li, M., Zhang, J., & Hao, X. (2011). Surface texture, chemistry and adsorption properties of acid blue 9 of hemp (Cannabis sativa L.) bast-based activated carbon fibers prepared by phosphoric acid activation. *Biomass and Bioenergy, 35*(1), 437-445. doi:https://doi.org/10.1016/j.biombioe.2010.08.061

Yang, R., Wang, Y., Li, M., & Hong, Y. (2014). A New Carbon/Ferrous Sulfide/Iron Composite Prepared by an in Situ Carbonization Reduction Method from Hemp (Cannabis sativa L.) Stems and Its Cr(VI) Removal Ability. *ACS Sustainable Chemistry & Engineering, 2*(5), 1270-1279. doi:10.1021/sc500092z

Yu, L., Tu, C., & Luo, Y. (2015). Fabrication, characterization and evaluation of mesoporous activated carbons from agricultural waste: Jerusalem artichoke stalk as an example. *Frontiers of Environmental Science & Engineering, 9*(2), 206-215. doi:10.1007/s11783-014-0631-7

Zhang, G., Luo, H., Li, H., Wang, L., Han, B., Zhang, H., . . . Sun, X. (2016). ZnO-promoted dechlorination for hierarchically nanoporous carbon as superior oxygen reduction electrocatalyst. *Nano Energy, 26*(Supplement C), 241-247. doi:https://doi.org/10.1016/j.nanoen.2016.05.029

Zhou, L., Wang, Y., Huang, Q., & Liu, Z. (2008). Preparation and Optical Properties of ZnO Nano-and Micro-crystals with Different Morphologies. *The Chinese Journal of Process Engineering, 02*(8), 5.

Zhu, S., Chen, Q., Shi, Y., Chen, Z., Bao, R., Zhou, L., . . . Yuan, C. (102 2016). Lignite-derived mesoporous N- and O-enriched carbon sheet: a low-cost promising electrode for high-performance electrochemical capacitors. *Journal of Solid State Electrochemistry, 20*(3), 713-723. doi:10.1007/s10008-015-3100-8

Zhu, S., Chen, Q., Shi, Y., Chen, Z., Bao, R., Zhou, L., . . . Yuan, C. (2016). Lignite-derived mesoporous N- and O-enriched carbon sheet: a low-cost promising electrode for high-performance electrochemical capacitors. *Journal of Solid State Electrochemistry, 20*(3), 713-723. doi:10.1007/s10008-015-3100-8

Zhu, Z., Li, A., Yan, L., Liu, F., & Zhang, Q. (2007). Preparation and characterization of highly mesoporous spherical activated carbons from divinylbenzene-derived polymer by ZnCl2 activation. *Journal of Colloid and Interface Science, 316*(2), 628-634. doi:https://doi.org/10.1016/j.jcis.2007.09.016

Zyoud, A., Nassar, H. N. I., El-Hamouz, A., & Hilal, H. S. (2015). Solid olive waste in environmental cleanup: Enhanced nitrite ion removal by ZnCl2-activated carbon. *Journal of Environmental Management, 152*(Supplement C), 27-35. doi:https://doi.org/10.1016/j.jenvman.2015.01.001